POLITECNICO DI TORINO

Master of Science
in Mechanical Engineering

Master's thesis

3D printing of bio-based soybean oil epoxy acrylate resin

Sebastiano Fattoruso, 263674

Supervisor
Prof. Massimo Messori

Co-supervisor
Prof. Giovanna Colucci

A.Y.2023

Summary

List of Tables

1. Introduction

The research for more eco-friendly and sustainable production methods and materials is pushed in recent decades by the need to reduce the environmental impact of human activities and to develop alternatives in all industrial areas. The massive and sometimes misguided use of plastics is one of the most worrying elements since the impact of the cycle life of this material in terms of production, use, and disposal is seriously dangerous for the climate, the environment, and the living species health [1].

The wide variety of fields of application due to the simplicity of processing, the high strength-density ratio, the high resistance to physic-chemical degradation, and the low price of polymers have quickly made these materials one of the widely used in manufacturing [1]. According to the Organization for Economic Co-operation and Development (OECD) report "Global Plastics Outlook Economic Drivers, Environmental Impacts and Policy Options", annual plastics production has reached 460 million tonnes in 2019, and the amount of plastic waste has been 353 million tonnes. To get an idea of the growth of these figures, it is useful to compare them with the annual production and waste in 2000, which were 234 million tonnes and 156 million tonnes, respectively. Much of this waste is poorly managed, again according to the OECD report, in the 2019 year 22 Mt of plastic waste was dumped in the environment and 6.1 Mt of these wastes have been leaked into rivers, lakes and the Ocean. Obviously plastic pollution in the waters is a very serious and visible consequence of plastic disposal and misuse but it is not the only one, the OECD report explains that greenhouse gas emissions from the life cycle of polymeric materials are worth 3.4 percent of global emissions and quantifies 2019 polymer materials life cycle emissions of 1.8 gigatonnes (Gt) of which 90 percent come from production and conversion from fossil fuels [2].

This scenario has directed environmental policies towards waste reduction and increasing recycling and reuse, however highly valued and very used materials with good physical stability and strength characteristics like thermosetting polymers are also more difficult to recycle and indeed their recycling is a point on which research is focusing [3]. Therefore, also considering the need to lower the consumption of fossil resources in polymeric materials production, simultaneously reducing gas emissions, in addition to reuse, another target is to find alternatives to conventional polymers. In this regard among the most promising solutions there are bio-based plastics as confirmed by the European Environment Agency, a UE delegacy that included the market of these products as one of the six identified for "A lead market initiative for Europe" [4]. Paul Anastas and John Warnern already included the use of renewable raw materials in their 12 principles of green chemistry in 1998 [5], but today a complete replacement of fossil-based plastics is unthinkable in the short to medium

term, due to the higher costs and less availability and processability of bio-based polymers. It is therefore desirable to contribute to the technological and scientific research improving production and applications of these alternatives, in fact the topic now follows an upward trend. This is confirmed by the dates of bio-based plastics production in 2014 amounting to 1.48 million tonnes, 70% durable and 30% degradable [6] and from the rising number of publications and citation about bio-based polymers between 1988 and 2023 resulted by consulting the scientific citation indexing service "Web of science" as shown in the graphic of Figure 1, "Times Cited and Publications Over Time about Bio-based polymers".

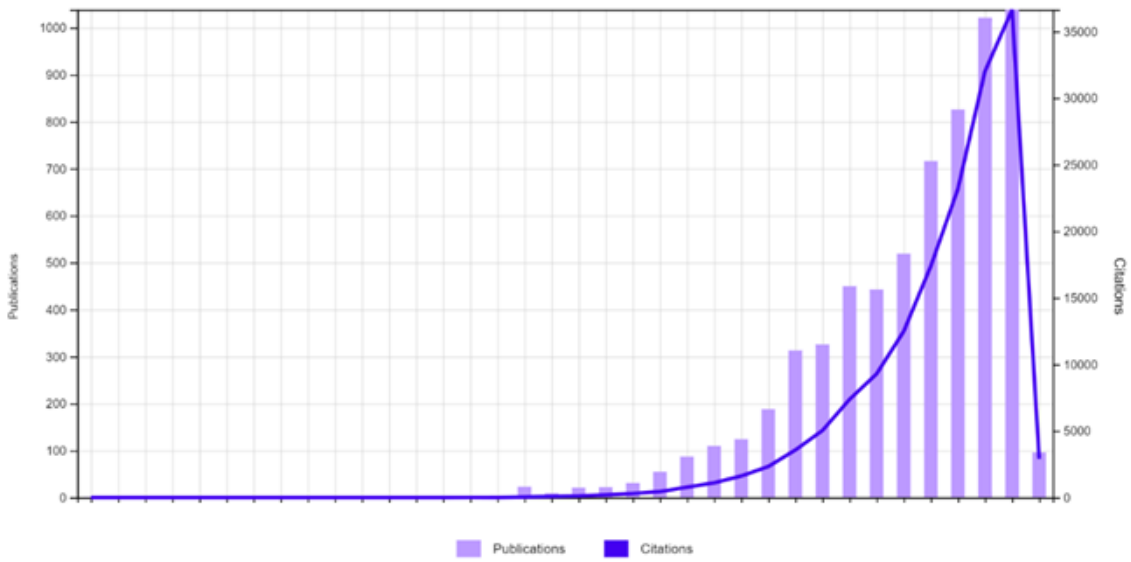

Figure 1. Times cited and publications from 1988 to 2023 about bio-based polymers

Among the most innovative technologies to produce objects and parts made of polymeric materials is additive manufacturing (AM), but even in this field, most of the polymers used are of fossil origin [7], [8]. Research in the field of bio-based plastics is now also concerned with proposing them as materials for additive manufacturing and this possibility is of considerable interest [9]. If bio-based materials are already an important opportunity for pursuing the goal of making human activity more environmentally sustainable, also additive manufacturing has several aspects that make it a potentially eco-friendly technology. Firstly, it is based on layer-by-layer building approach, it is less wasteful than traditional subtractive manufacturing processes, if well exploited [10]. Additionally, using AM, it is possible to redesign in a completely different and flexible way since some functional limitations typical of other manufacturing technologies are not imposed, improving resource exploitation efficiency [11]. The absence of certain constraints together with the fast and direct transition from virtual model to physical object and the automated production process, make AM highly effective in the production of customised and on-demand objects, leading also to a supply chain shortening and a manufacturing sites delocalization [12].

1.1. Polymers

Polymers are large molecules, also named macromolecules, long chains made of many smaller molecules, called monomers, linked together through the polymerization chemical reactions [13], [14].

Macromolecular structures can have natural origin like natural rubber or cotton, or they can arise via synthetic routes, in any case, they are characterized by high molecular weight, typically polymers contain hundreds of thousands or millions of monomers [14].

The characteristics of polymeric substances are closely tied to the molecular weight of the polymer. For instance, polystyrene, a synthetic polymer, exhibits rigidity and fragility at room temperature when its degree of polymerization, the average number of monomer units in a polymer molecule, is 1,000, whereas it becomes soft when the degree of polymerization is 10 [13].

The nomenclature "plastics" designates a composite of polymers materials and a variety of fillers, reinforcing agents, and additives [13]. Plastics are fundamental materials applied in many fields due to their lightweight nature, excellent optical properties, electric and thermal insulating features, and lower cost and production time, furthermore their great variety is reflected in the differentiation of the characteristics that different types of polymer can provide hence in the diverse applications for design engineers, varying for example from soft to hard, brittle to ductile, and weak to tough [13], [15].

1.1.1. Classification of polymers and thermomechanical properties

Polymers are classified based on their behaviour when subjected to heating or cooling. The first category includes the so-called thermoplastics, they can be remelted several times through heating and can pass from liquid to solid by cooling, without undergoing any substantial chemical alteration or degradation, so these processes are reversible [16]. Thermoplastics are composed of long and flexible molecular chains that are held together by weak intermolecular van der Waals forces [17]. Increasing temperature, kinetic energy proper of each molecule is higher, causing interferences between intermolecular interactions, reducing the effectiveness of the binding forces between the molecules [18]. For this reason, the molecular chains tend to become more mobile, resulting in the ability for the macromolecules to slide each other and consequentially in the flowing viscous liquid behaviour of the thermoplastic polymer at higher temperatures. Due to these secondary intermolecular interactions at lower temperatures the long molecules are no longer allowed to move freely, instead, at higher temperatures interactions are weaker and flowing is possible, these two situations are reversible, so thermoplastics can repeatedly soften when heated and harden when cooled without degradation[17].

The other category is thermoset polymers, they solidify starting from monomers or oligomers, when subjected to a chemical reaction (also called curing process) by means of heating or light irradiation and this irreversible process leads to the formation of a cross-linked network.
Cross-linking is a chemical process that involves forming primary valence bonds between polymer molecules, so density of cross-linking refers to the number of covalent bonds between polymer chain, a high number of covalent bonds means higher cross-linking density resulting in chain mobility reduction. Cross-linking, additionally, does not allow the polymer to exhibit flow behaviour, as chains are no able to slip past each other also at higher temperatures.
Another important characteristic of polymers is their structural morphology, they can have an amorphous structure, with molecules solidified in a random arrangement, or semicrystalline structure, with ordered three-dimensional structure along with the amorphous parts, since during solidification some molecules stay aligned [13-17]. A grade of crystallinity can be identified individuating the percentage of crystalline phase present in the polymer and this grade can be maximum around 90% [16].
Thermoset polymers are characterized by an amorphous morphology instead thermoplastic can be amorphous or semicrystalline [13].
Amorphous thermoplastics are characterized by molecular disorder that persists during cooling, below their so defined glass transition temperature (T_g), they solidify or becomes a vitreous substance.
Conversely, semi-crystalline thermoplastics solidify by establishing a certain molecular structure order as they cool and begin to harden below their melting temperature (T_m). In semi-crystalline polymers, molecules that do not transform into ordered regions remain in small amorphous regions, which lose their ability to flow below their glass transition temperature. These amorphous regions exist within the semi-crystalline domains.
The glass transition temperature (T_g) is defined as the temperature at which a glassy rigid solid that is heated reach a softer and more rubbery state, while the melting temperature (T_m), still considering the heating of a polymer, is the temperature to eliminate the intermolecular forces holding of the ordered regions transitioning to the liquid phase. The degree of crystallinity has no significant effect on the T_g instead its increase generally results in higher melting temperature [16]. Considering the cooling of a melted polymer, the crystallization does not occur at Tm but for a lower temperature that is defined crystallization temperature, additionally crystallization occurs if cooling is not too quick, because the polymer structure would not have the time to create an ordered structure [19].
This difference in cooling and heating for semicrystalline polymers is simply shown in the Figure 2 [19], with specific volume trend of a polymer respect to the temperature in a process of cooling and in a process of heating.

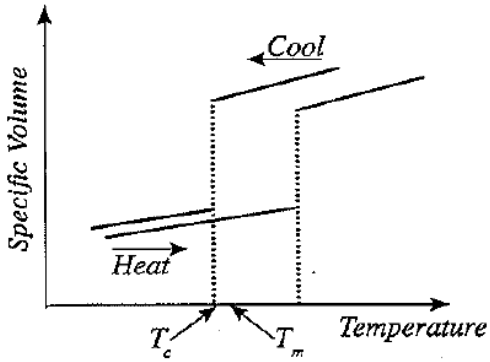

Figure 2. Schematic trend of specific volume as temperature varies for a semicrystalline polymer

In Figure 3 [20] the specific volume of polymers respect to temperature is represented in a qualitative way, highlighting the difference between the amorphous polymers and semicrystalline polymers, it is also represented an ideal totally crystalline behaviour [20].

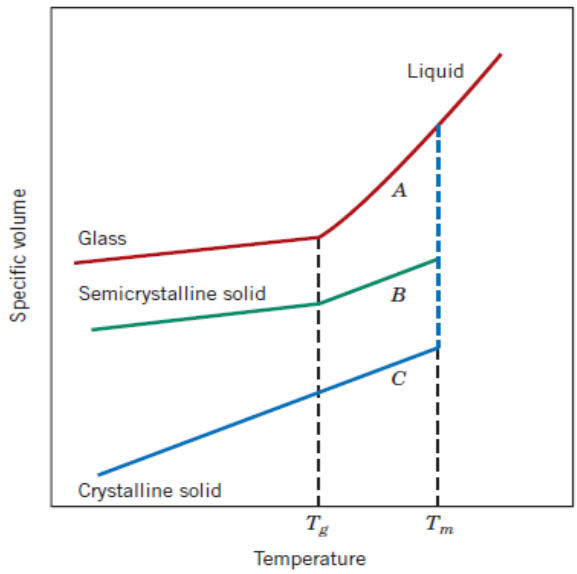

Figure 3. Specific volume as varing of temperature for semicrystalline, amorphous and ideal cristalline polymer

For amorphous polymer when T_g occurs during heating, expansion is faster and the hard glassy solid became a rubbery material. As the temperature continues to increase, the polymer changes from a rubbery state to a viscous liquid, gradually viscosity decreases and if heat is still provided, decomposition occurs. In contrast, for semicrystalline polymers, the velocity of the expansion and so the change of trend slope at T_g is less significant because in this temperature range the crystalline structures have not disintegrated and they are dispersed in a rubbery amorphous matrix. At the melting temperature, the crystallites melt, resulting in a viscous state, which persists above T_m until degradation. An ideal fully crystalline polymer would not show any physical change, and neither would the slope of its curve change at T_g,

only a phenomenon would occur at the Tm, the break of all the bonds of the crystalline structure meaning direct passage from solid to liquid phase [20].
In Figure 4 [13], a trend for shear Modulus for polypropylene respect to temperature is reported and it is clear the behaviour respect to the various crystallization grades.

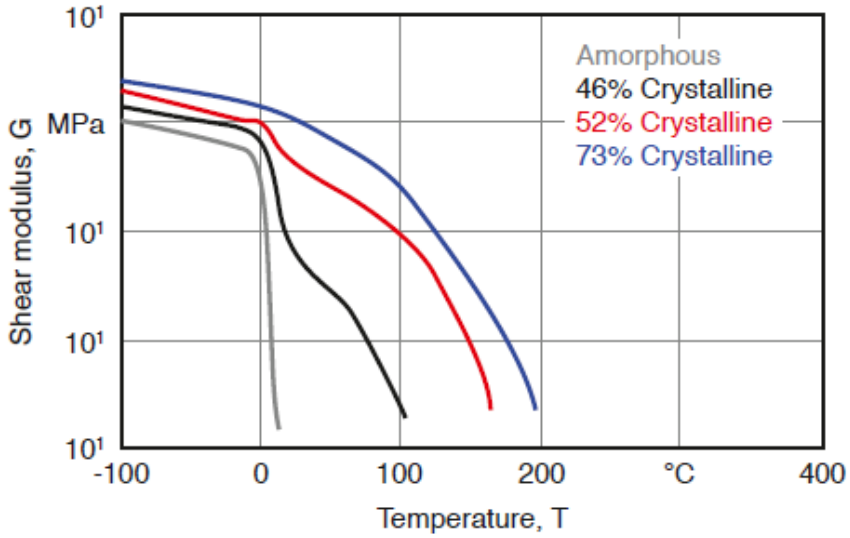

Figure 4. Shear modulus-temperature curve for polypropylene with various degrees of crystallinity

In Figure 5 and Figure 6 [13] the tensile strength (in red) and the strain at failure (in grey and in black) for a thermoplastic amorphous and for a semi-crystalline are shown. Below its glass transition temperature, the amorphous thermoplastic is brittle and reaches failure under low strains, however, as the temperature rises, the amorphous thermoplastic's strength diminishes, and it becomes more flexible. Once the temperature exceeds T_g, the strength progressively decreases, and the maximum strain continues to increase until the material reaches its flow properties and mechanical strength is negligible, marked in the diagram with the temperature at which polymer can flow T_f. Instead, semi-crystalline thermoplastics has a T_m, melting temperature, is after this last that the polymer is a flowing viscous fluid, and respect to the amorphous there is has an increase in toughness between the glass transition temperature and the T_m, due to the crystalline regions not yet broken up [13].

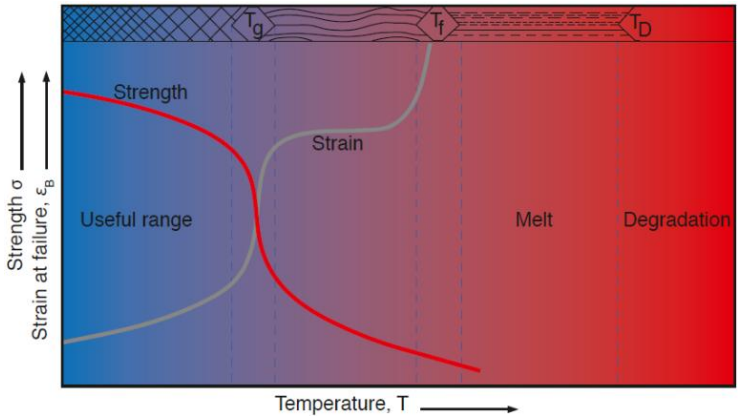

Figure 5. Tensile strength and strain at failure typical for amorphous thermoplastic

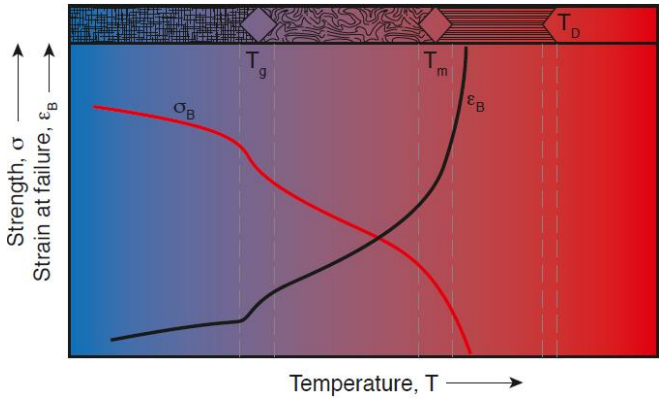

Figure 6. Tensile strength and strain at failure typical for semi-crystalline thermoplastic

There is indeed another type of polymers classified as elastomers, they exhibit the characteristic property to have a glass transition temperature significantly lower than room temperature. Consequently, crosslinked elastomers exhibit a highly compliant and soft elastic solid behaviour at room temperature. The lower density of chemical bonds between polymer chains allows them to stretch and retract easily to a large extent make elastomers deform significantly and reversibly returning to their original shape [13]. Elastomers are non-crosslinked if un-vulcanized, but after crosslinking process, obtained through vulcanizing agents and called vulcanization, the ability to flow is lost, new cross-links between polymer chains are created and chain mobility is reduced while cohesion between them increased. Vulcanized elastomers are less deformable but mechanical properties like resistance are improved [21].

In polymers with cross-linked structure, density of cross-linking is an important feature in their behaviour during heating, due to the irreversibility and the elimination of the transformation into a viscous fluid, and for the mechanical properties. By analysing Figure 7 [13], the difference in shear modulus between highly crosslinked, crosslinked, and non-crosslinked polymers, it can be noticed that in the glassy region, cross-linking has less effect on the modulus, instead in the rubbery region, a higher cross-linking density leads to higher modulus. Elastomers, lightly crosslinked systems, display a low modulus above the glass transition temperature, typically below -50 °C, resulting in softness and flexibility at room temperature. In contrast, highly

crosslinked systems, found in thermosets, show a smaller decrease in stiffness as the temperature is raised above the glass transition temperature, the reduction in properties becomes less significant as the degree of crosslinking increases as can be seen from Figure 8 [13], the strength, and the strain at failure of a thermoset which indicates that the strength maintains a relatively constant level until it reaches its thermal degradation temperature.

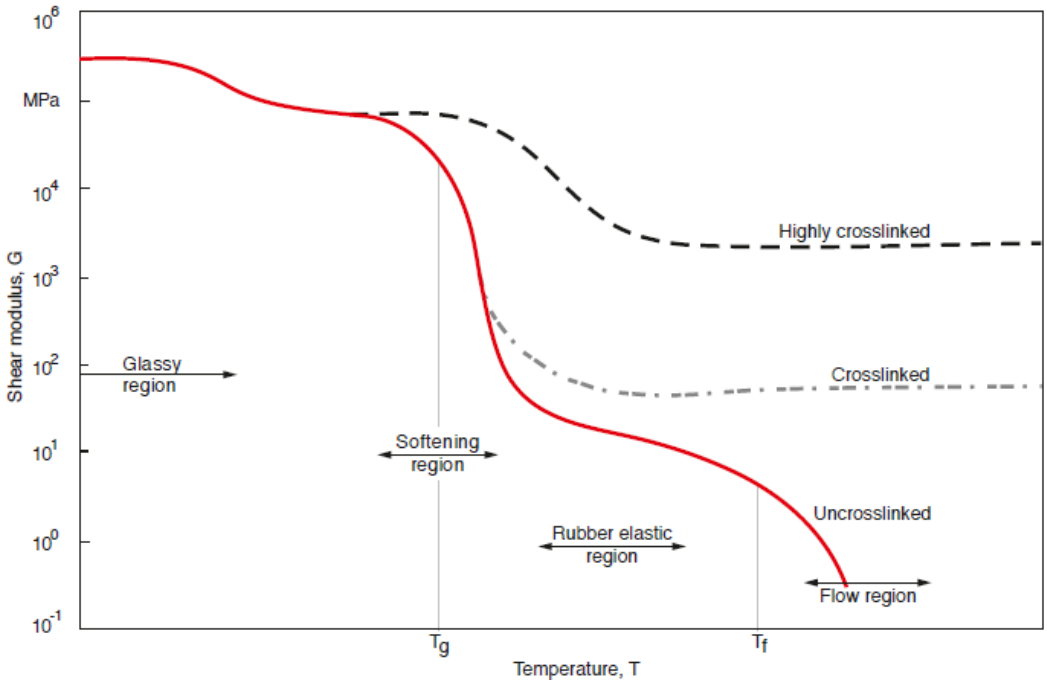

Figure 7. Shear modulus of a polymer with different cross-linking density as Temperature increases

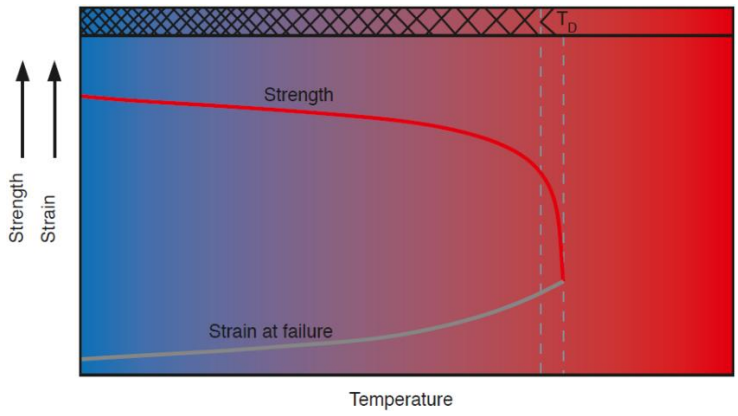

Figure 8. Typical trend of strength and strain at failure respect to Temperature of a thermoset

Figure 9 [13] illustrates shear modulus curves for low molecular weight and high molecular weight amorphous, semi-crystalline and cross-linked polystyrene, it is highly useful in summarizing the differences that various structures and morphologies of polymers exhibit, such as the presence of T_m for semicrystalline polymers and a less significant decrease in the shear modulus after T_g, which would also be evident for other properties. Additionally, in the zone after T_g it shows the more pronounced

descent of properties for a lower molecular weight polymer, and finally, the absence of degradation in the properties of a crosslinked polymer.

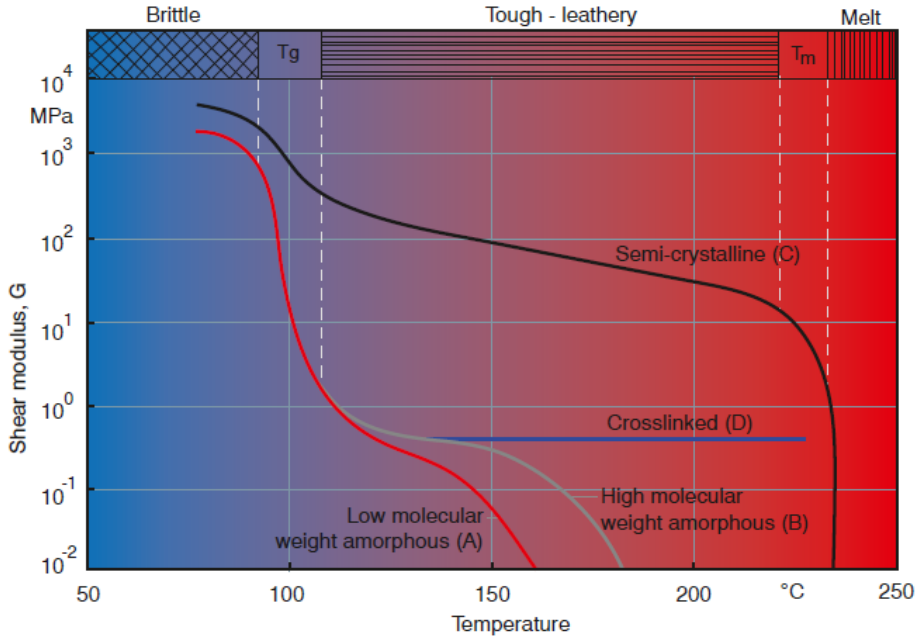

Figure 9. Shear modulus respect to Temperature of polystyrene with different structures

Many of polymers and plastics most used are in the table in Figure 10 [13], where it is possible to also notice their general shear modulus exemplificative of others mechanical properties too, versus the reduced temperature that take in account T_g of all the materials.

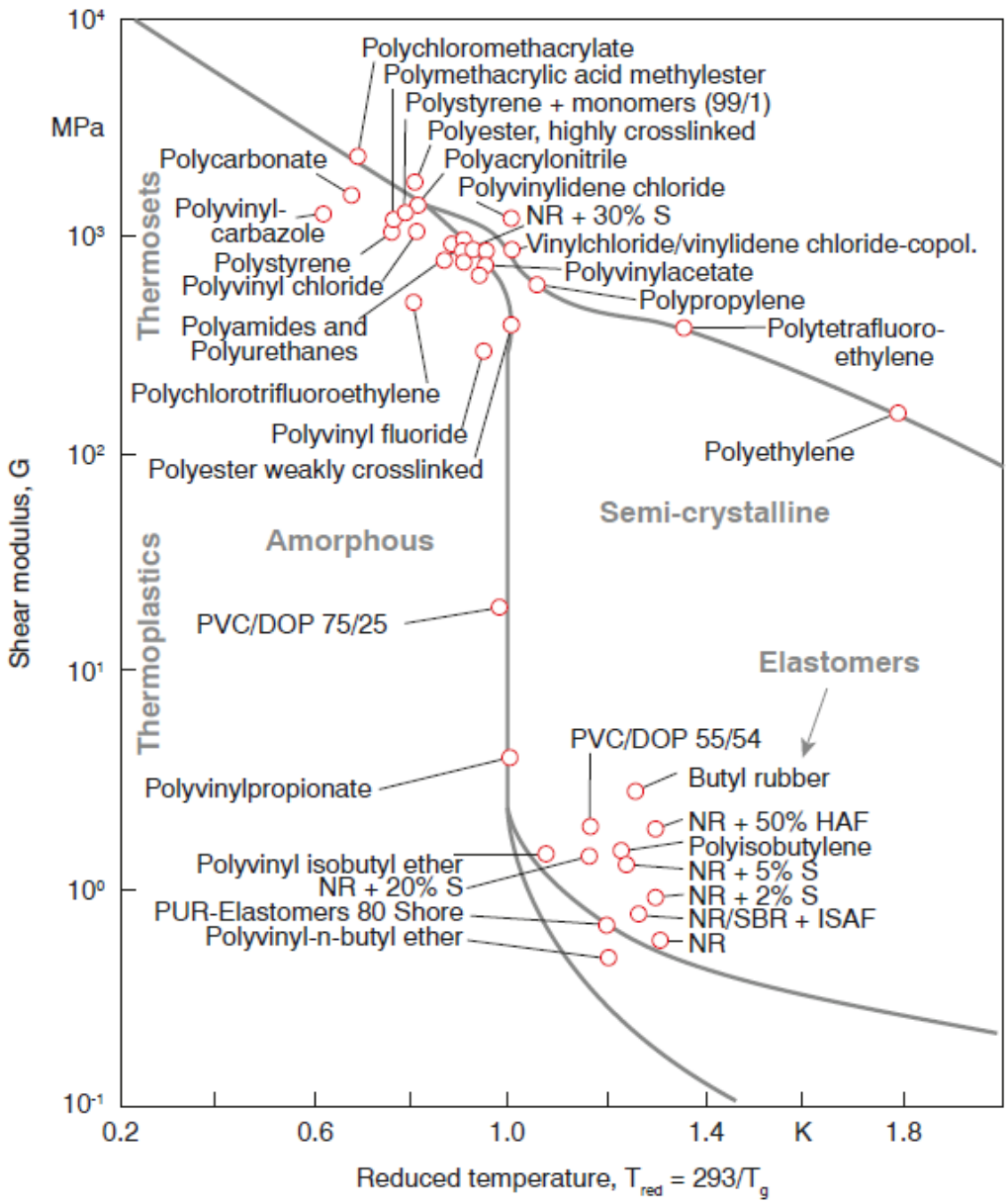

Figure 10. Shear modulus for various polymers respect to Temperature

Interesting examples of application and characteristics materials in the graph of Figure 10 are Polyamides, thermoset synthetic polymers with good mechanical properties, there are polyamides with strength about 140 MPa but also high abrasion resistance and toughness comparable to those of aluminium [22], but with density of a half lower, in fact also having a low friction coefficient they are used in bearings and gears productions [23]. Between the thermosets there is Polyurethane, very interesting because it is an extremely versatile material that offers a wide range of properties depending on its structure, this allows for a great deal of customization for manufacturers, from soft coatings to rigid construction materials [24].

1.2. Bio-based polymers

The term "bio-based" refers to substances that are derived completely or in large part from biomasses, which are organic materials of biological origin, such as plants, trees, algae, marine organisms, micro-organisms, animals, etc. These substances include bulk chemicals, platform chemicals, solvents, polymers, and bio-composites. Therefore, bio-based substances are sourced from feedstock obtained from organic waste, rather than from geological formations or fossil materials. [25].

The conversion of biomass into value-added products and fuels can occur through various processes, including biochemical, thermochemical, or biotechnological methods. In the case of bio-based polymers, the process may involve polymerizing a monomer that has been synthesized conventionally or using bacterial processes from biomass or starting from natural bio-based polymers and then modify them to meet specific requirements [25], [26].

In terms of biodegradability, bio-based materials, like all polymers, possess this property only if they can be transformed into natural substances, such as water, carbon dioxide, and compost, through processes carried out by various organisms, such as microbiological biodegradation. The biodegradability of a material is not solely determined by its bio-based composition, but also by its chemical structure and the conditions in which micro-organisms can degrade the material, such as in water or soil and in the presence or absence of oxygen. Therefore, the fact that a material is bio-based does not necessarily imply its biodegradability, and vice versa [27].

One approach to produce bio-based plastics is to use natural bio-based polymers, including proteins, nucleic acids, and polysaccharides [26] the first generation of bio-based polymers derived from agricultural feedstocks like corn and potatoes [26].

These bioplastics are part of the “Old Economy” bioplastics and include materials like rubber, cellophane, celluloid, linoleum and cellulose acetate, materials commonly utilized before fossil-based plastics explosion in the market but still used today. Today vegetable oils are between the most investigated in scientific literature as bio-resources, interesting is their application as starting substance to obtain bio-based polymers due to their abundance and the presence of triglycerides that can be directly polymerized or modified to add functional groups to polymerize [28].

New types of bioplastics, known as “New Economy”, bioplastics, have been developed over the past 30 years, which include the so called “novel bioplastics” and “drop-ins” [6]. Novel bioplastics have a unique chemical structure and properties, whereas drop-ins have the same chemical structure as existing fossil plastics but are derived from different feedstocks [6].

A clear classification of bioplastics divides them in these three categories, also Figure 11 [29] schematically represents the three categories. In addition, here explained the division:

- Renewable-resource-based bioplastics are either naturally synthesized from plants and animals or entirely synthesized from renewable resources like starch, cellulose, proteins, and lignin. Recent breakthroughs in technology have also allowed for the synthesis of traditional petroleum-derived polymers like polyethylene and nylon from biological resources [29].
- Petroleum-based bioplastics are synthesized from petroleum resources but are biodegradable [29].
- Bioplastics from mixed sources are made from combinations of biobased and petroleum monomers, like poly(trimethylene terephthalate) and some bio-thermosets [29].

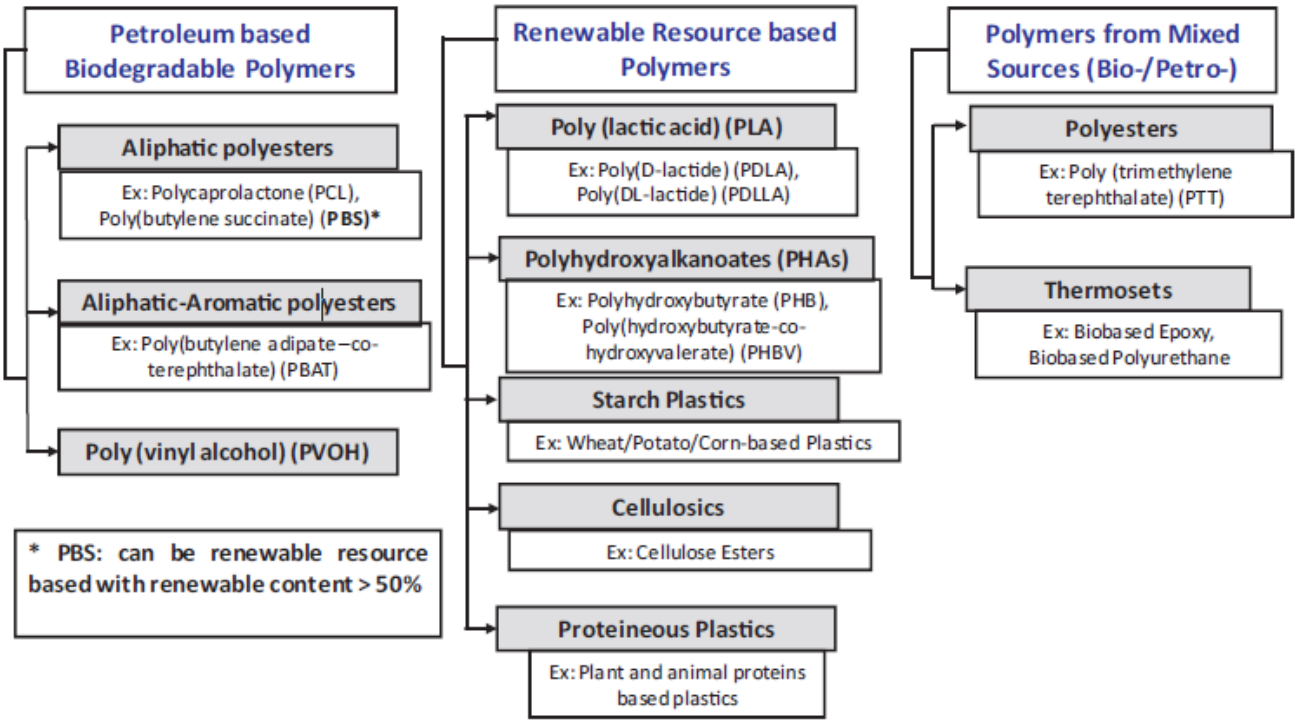

Figure 11. Classification of Bio-based polymers

Various biobased polymers can be found on the market and are now widely used, between those completely synthesized from plants animals, or from renewable resources there are Poly (lactic acid) (PLA) or Polyhydroxyalkanoates (PHA) [26], [29]. Poly(lactic acid) (PLA) origins from lactic acid and is a widely used biocompatible and biodegradable polymers. Its thermomechanical properties are not comparable to those of traditional thermosetting polymers. Despite these limitations, PLA offers the advantages of low cost and easy availability, and is predominantly utilized in the packaging, textile, and biomedical fields. Current research is focused on developing PLA-based copolymers and composites to improve the materials' mechanical strength and properties [26], [29].

Polyhydroxyalkanoates (PHA) have become increasingly popular in research as environmentally friendly and attractive alternative to non-biodegradable synthetic

materials due to their biodegradability, biocompatibility, piezoelectricity, microbial origin, and non-toxic nature [30].
Examples of Polymers made from mixing biobased and petroleum-based monomers are Poly(trimethylene terephthalate) (PTT) and Biobased Polyurethane [26], [29].
Finally, there are also biodegradable polymers derived from fossil resources like Polycaprolactone (PCL) and Poly (butylene-adipate-co-terephthalate) (PBAT) [29].
PLA and PCL based polymers are very diffused in applications with 3D printing, they have excellent processability and good mechanical properties [31], [32]. Others various mixed bio-/petrol- polymers are used as resins or as diluents in 3D printing, and there are several studies that try to find materials to replace especially the classical non-bio-based thermosetting polymers with more environment friendly materials in the field of additive manufacturing [32]–[34].

1.2.1. Vegetable oil-based polymers and Soybean oil in polymers

In scientific literature, there are numerous studies exploring the use of materials derived from natural oils, also known as vegetable oils [28], [35]–[38].

The use of natural or vegetal oils as a substitute for polymers derived from petroleum has gained significant attention among researchers, various insights are about their use in materials industry since they are not expensive, but abundant and renewable natural resources available in large quantities from oilseeds or fruits.

Vegetable oils are liquid triglycerides at regular room temperatures that are products of plants and insoluble in water. Triglycerides are ester compounds that are produced by combining one glycerol molecule with three fatty acid molecules [39]. Figure 12 [39] represents schematically a triglyceride molecule, R_1, R_2 and R_3 are three fatty acid chains.

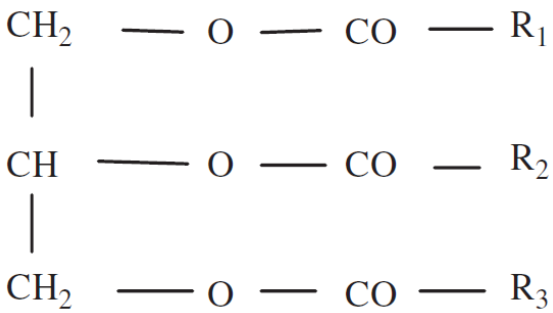

Figure 12. Scheme of a triglyceride molecule

Using triglycerides as the main building block polymers can be produced because they contain a high number of chemically reactive positions such as ester groups, C=C double bonds, allylic positions, and the α-position of ester groups. All of them are directly curable, for example the C=C double bonds through free radical or cationic mechanism could form growing chains, but the internal double bonds and the other groups in the triglyceride structure are used to be transformed in more reactive functional groups to finally obtain chemical compounds like photocurable thermosets [38], [35].

The difference between the oils in their application as basis for a polymer is given by the fatty acids in their structure, each type of triglyceride oil possesses a unique fatty acid distribution which is precisely what determines the presence of different functional groups in triglycerides [39]. In fact, fatty acids vary from each other in having hydroxyl, epoxy or oxo groups, or triple bonds and for their C=C double bonds distribution, this last is displayed in Figure 13 [39], where they can be seen the saturated (a), unsaturated (b), isolated (c), and conjugated (d) fatty acid chain.

(a) $-CH_2-CH_2-CH_2-CH_2-$

(b) $-CH_2-CH=CH-CH_2-$

(c) $-CH_2-CH=CH-CH_2-CH=CH-CH_2-$

(d) $-CH_2-CH=CH-CH=CH-CH_2-$

Figure 13. Type of fatty acid chains

An important feature is the presence of C=C double bonds being reactive, linseed oil for example has a lot of unsaturated fatty acids that can be cured with atmospheric oxidation and it is used in paint binder. Furthermore, epoxidation reaction is one of the most effective modifications of triglycerides in which the C=C double bonds are converted to oxirane (epoxide) rings, very reactive and exploitable to produce important chemical compounds for polymer synthesis or for curable thermoset [38], [40]. Acrylate is another highly reactive group and acrylate triglycerides can be polymerized for thermoset polymer production [38] and copolymerized easily with other commercial comonomers, and even to obtain acrylate double bonds it is necessary to convert the triglyceride double bonds to an epoxide and after to open the epoxy groups with acrylic acid [41].

Studies and applications of polymers from vegetable oils demonstrate respect to other biomaterials specific characteristics and qualities, for example good cytocompatibility and degradation properties of phosphoester cross-linked vegetable oils and their metabolites that make them suitable biomaterials for implantation [37] or soybean oil based resin to fabricate dental scaffold due to cytotoxicity analysis resulting in better results than traditionally used polyethylene glycol diacrylate (PEGDA) [37], [42].

Another aspect is the excellent compatibility with certain natural fillers, fibres, henequen, cellulose, bamboo, carbon black particles and carbon nanotubes [43]. Since triglycerides are composed of aliphatic chains, the resulting triglyceride-based materials may lack the necessary rigidity and strength required for some applications [35], but the possibility to produce composites with additives could bring them closer to mechanical and thermal properties of petroleum-based polymers or to improve specific characteristics for specific applications [43].

Soybean oil is an exemplary model of production of polymers and polymer composites, it contains an average of 11% palmitic acid, 4% stearic acid, 23% oleic acid that has 1 double bond, 54% linoleic acid that has 2 unsaturated chains, and 8% linolenic acid that has 2 unsaturated chains [43]. Soybean oil contains an average of 4.5 double bonds per triglyceride molecule, making it quite reactive compared to other vegetable oils such as palm oil, which contains only 1.4. Soybean oil mainly consists of unsaturated fatty acids such as oleic, linoleic, and linolenic acids. This gives it good reactivity in polymerization processes [43].

In the past soybean oil have already been utilized in printing inks and paints [43], furthermore considerable research has been devoted to transforming soybean oils

into solid polymeric materials with viable mechanical properties [44], but epoxidized soybean oil (ESO) is a significantly more used compared to pure oil, it is a good plasticizer of PVC products alternative for example to phthalates [45] for this purpose. Compared to raw soybean oil ESO suffers less thermal and oxidative deterioration due to the absence of allyl hydrogens, in fact its potential application is as high-temperature lubricant [46].

Another particularly interesting derived of soybean oil is Acrylated epoxidized soybean oil (AESO), already used in plastic and coating industry, it displays excellent characteristics such as flow and levelling properties, as well as enhancing flexibility [43], [47] and is currently being evaluated for its potential as the primary monomer of a resin for 3D printing. A 3D printing resin for a photopolymerization process must be highly reactive at certain wavelengths and must also be easily processable. AESO is a monomer rich in functional groups and highly reactive [47], making it an ideal candidate for additive manufacturing. Additionally, its biocompatibility and bio-based nature are also being studied [42]. Numerous studies have explored the use of AESO as a primary monomer for 3D printing, demonstrating its suitability for various types of printing on different dimensional scales [48]. However, a critical issue regarding its application is its high viscosity, which is around the interval 18000 - 32000 cps at 25 °C and makes printing difficult [47], [49].

To overcome this issue, synthetic reactive diluents are commonly used, but these diluents are not bio-based or biodegradable [38], [43], [50]. There are studies proposing the use of bio-based diluents as an alternative to conventional reactive diluents [47]. To improve the processability of AESO in 3D printing, bio-based diluents such as IBOMA and THFA are being investigated [47]. The aim is to obtain a completely bio-based polymer that can replace traditional polymers in the field of 3D printing, thus contributing to the reduction of the environmental impact of the manufacturing industry.

1.3. Additive Manufacturing

Additive manufacturing, also known as 3D printing, is a process of creating three-dimensional objects from a digital model by adding layer upon layer of material, such as plastics, metals, or ceramics [51].

Additive manufacturing has many applications in various fields, including aerospace, automotive, healthcare, and consumer products to create prototypes, customized products, and even replacement body parts, such as dental implants [52]–[54].

This is attributable to the remarkable capability of generating intricate geometries that would be challenging or unfeasible to manufacture using conventional production methods [55]. Additionally, additive manufacturing can be used to create objects with unique properties, such as lightweight structures with high strength-to-weight ratios [56].

The first patent about a layer manufacturing production process was registered by Charles Hull, consisting in a stereolithography system, in 1984, was a primary example of rapid prototyping, using the CAD softwires it was possible to build layer by layer physical objects [57]. The name rapid prototyping is referred to the creation of a prototype directly from the CAD file in few hours but the progress in this field brought process to became already a commercial reality in 1987, and in 1990 pieces built with layer-by-layer manufacturing technology were used as casting patterns, in 1995 as tools and in 2000 as production parts. Since these years it has been possible to create directly end usable parts with these manufacturing processes and this approach has broadened its scope from rapid prototyping to the definition of additive manufacturing or 3D printing.

Not surprisingly, the market of this manufacturing process, products and services is growing in last years as all the predictions anticipated [58], form “Statista” research about Global 3D printing products and services market size it is noticed that in 2020 it was valued at around 12.6 billion U.S. dollars, the results are in Figure 14.

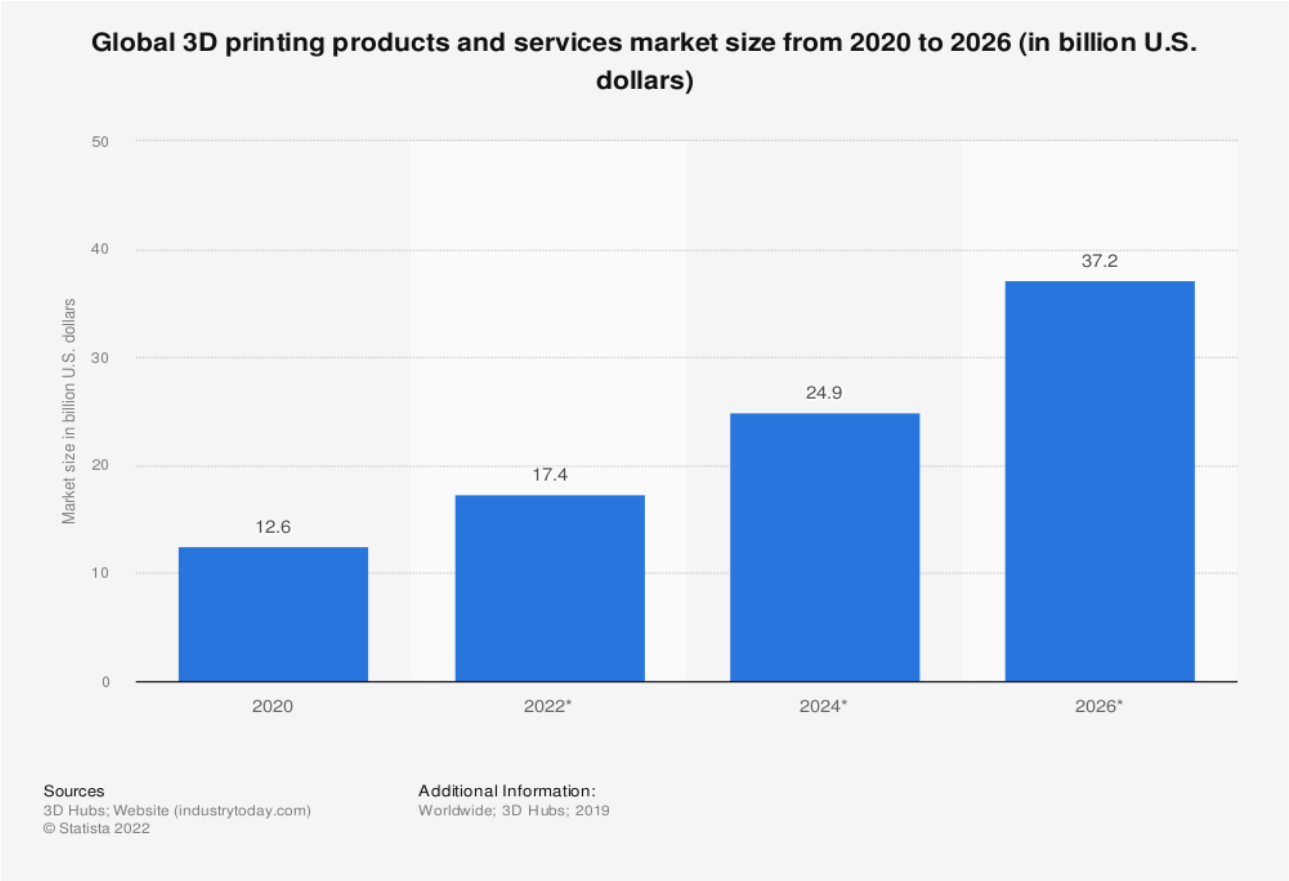

Figure 14. Global 3D printing products and services market size from 2020 to 2026

In 2020 3D printing devices for design amounted to 550,000, they are based on a lot of different technologies invented from the 1980s to today as reported on the graph in Figure 15 showing the most used 3D printing technologies, from the research on the portal to provide statistical data “Statista”.

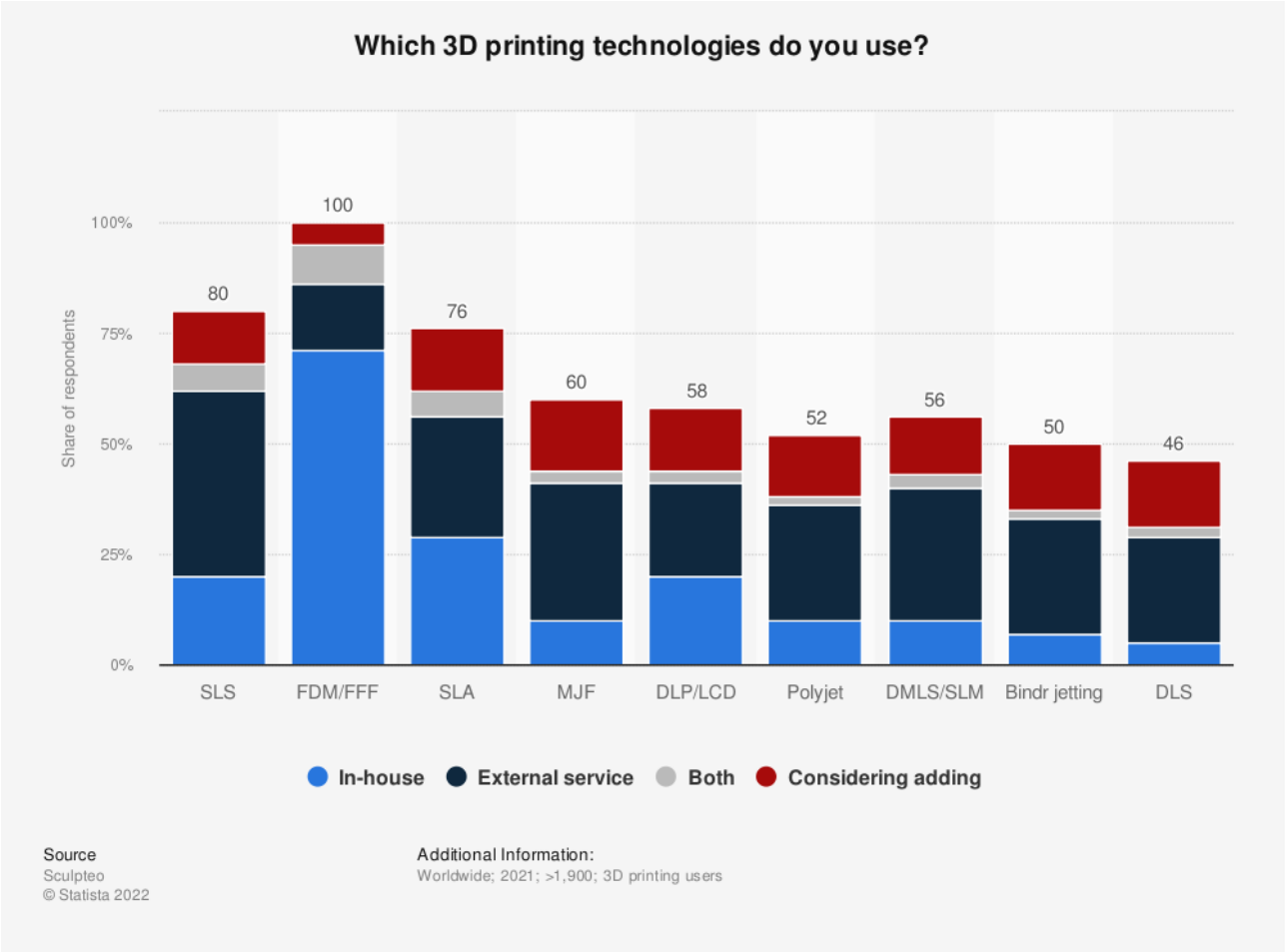

Figure 15. Most used 3D printing technology in 2021

Thus, the first technology to be invented was stereolithography, in the following years the other techniques have been developed, in 1991 were commercialized three 3D printing processes [59]:

- fused deposition modelling (FDM) technology in which thermoplastics are extruded in filament form [60];
- solid ground curing (SGC) based on UV-light to solidify entirely one layer of the liquid polymer;
- laminated object manufacturing (LOM) technology with cutting and sticking of the starting material that is in form of sheets [61].

A scheme of the technique for FDM and for LOM process are reported in Figure 16 [60], [61].

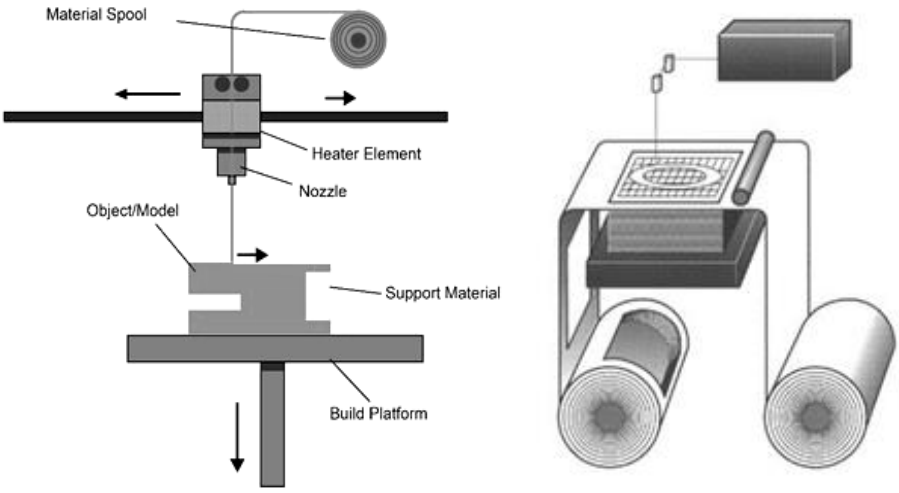

Figure 16. FDM 3D printing and LOM 3D printing schemes

In 1992 was born Selective laser sintering (SLS), as can be observed from Figure 17 [62] the process uses material in form of powder fused by heat from a laser obtaining the part layer by layer. In 2001 was presented digital light processing (DLP) technology to polymerize an entire layer at once [59].

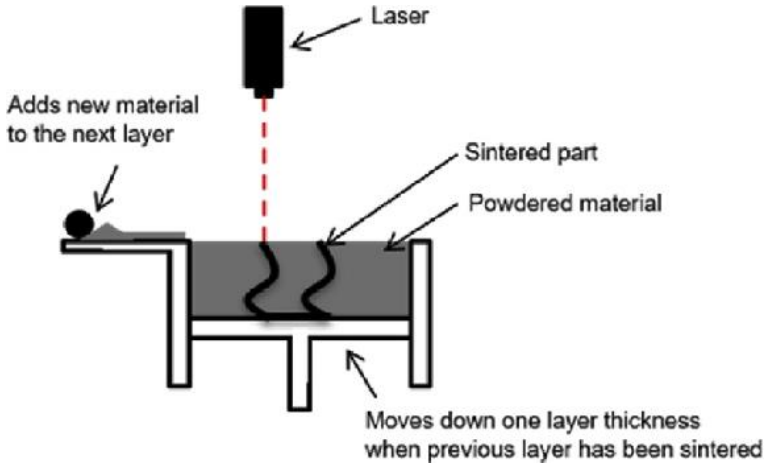

Figure 17. SLS 3D printing scheme

These are some of the discoveries that have expanded the range of possibilities for additive manufacturing technologies. Today, there are many techniques available and classifying them into distinct categories can aid in comprehending their applications and enable informed decisions for production requirements or for the material being processed. There are various methods to distinguish them and one of the first classifications, in 1998 was by type and condition of the raw materials: particles, laminated solid films, and liquid/molten materials [63]. It's possible to classify the technologies as well as by materials also by the type of machine used and the transformation of the material during the process. Today the standard for the

terminology about the AM techniques and their classification is defined by the ISO/ASTM 52900 [64], according to the technical regulation the processes are:

- Material Extrusion (EXTR) which works by means of a heated nozzle, selectively depositing material in form of plastic filament onto a platform where it cools and solidifies to build the solid object layer, in this category falls the FDM [65];
- Powder Bed Fusion (PBF), also SLS is one of the techniques in this category in which particles of thermoplastic powders, metal powders or ceramic powders placed on a print bed are selectively fused together via a heat source to create the part layer by layer, each layer of material is subsequently deposited and in turn fused until the process is complete [66];
- Directed Energy Deposition (DED) schematized in Figure 18 [67], a 3D printing process in which the material, is in the form of wire or powder and is deposited and simultaneously melted by a powerful thermal energy, such as a laser or electron beam [68];

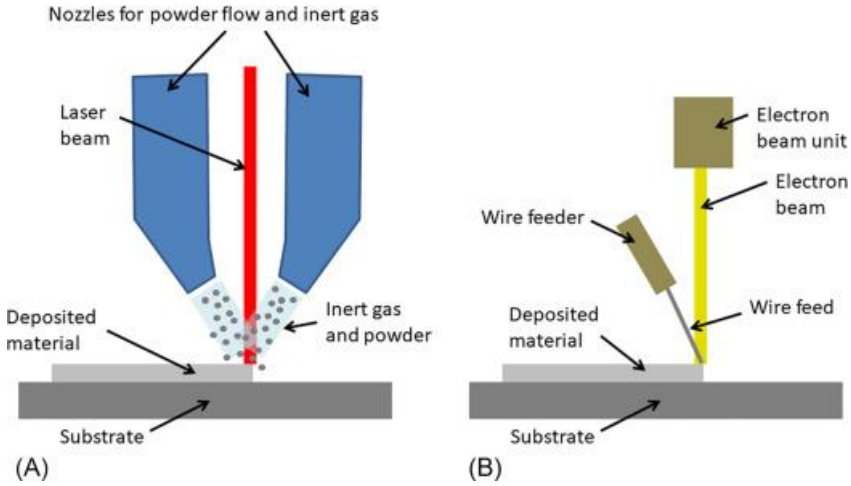

Figure 18. DED systems schemes: (A) based on laser and with powder feedstock; (B) based on electron beam and with wire feedstock.

- Sheet Lamination (SHL), one of the processes in this category is LOM. SHL involves the use of very thin sheets of materials like paper, polymer, or metal, that are placed on top of each other and cut one at a time and fused together using heat or binders [69];
- Vat Photopolymerization (VPP) uses liquid photopolymer, this in a vat or tank is selectively subject to curing, polymerisation is activated by a light source, curing is repeating layer by layer until the 3D object is formed. Two examples are Stereolithography (SLA) that selectively irradiates polymers with a mobile laser and DLP, that selectively irradiate one whole layer at a time [70], [71];
- Material Jetting (MJET) in which droplets of material such as photopolymers or wax are deposited in a controlled manner and polymerised by light on a printing plate forming the final object, like schematized in Figure 19 [72];

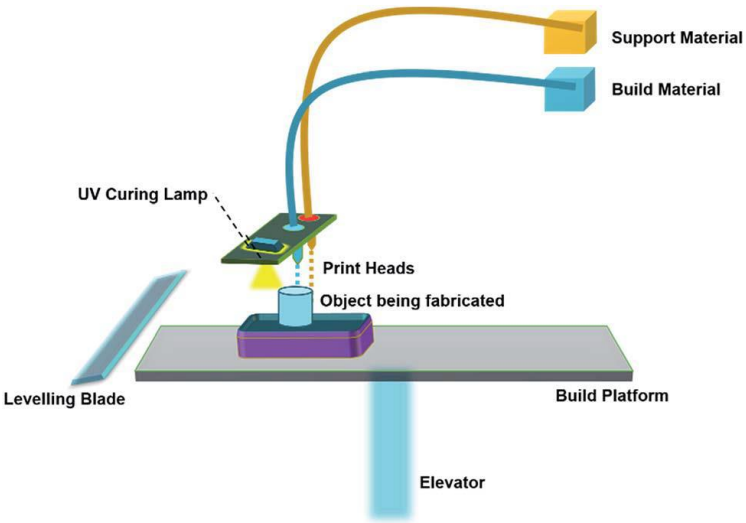

Figure 19. MJET 3D printing process scheme

- Binder Jetting (BJET), a process with a printhead that moves across the surface of a bed covered by material like sand, polymer, or metal powder. Binder droplets are deposited by the head to bond together the powder particles and generate the layer of the object [73]. BJET functioning is in Figure 20 [74].

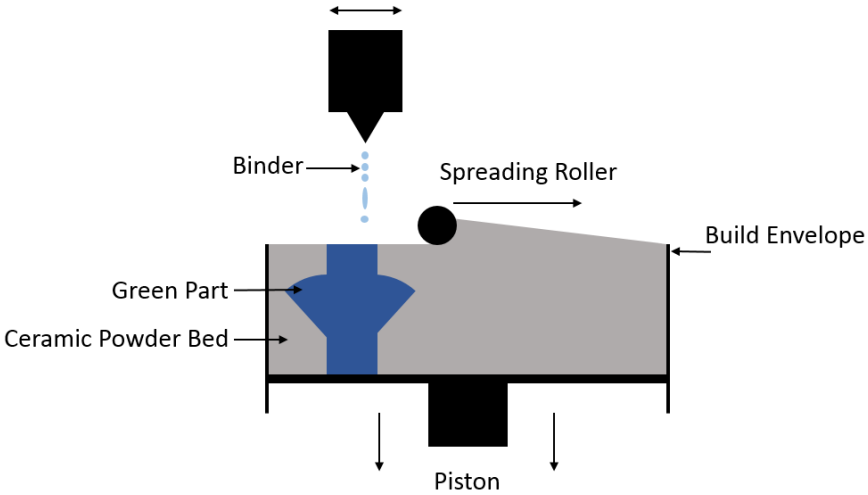

Figure 20. Scheme of BJET3D printing process

Each of these technologies offers unique characteristics, for example Vat polymerization methods offer a key advantage over other 3D printing techniques in the fact that the starting liquid material, the photopolymer, can be customized by adjusting its chemical composition and this opens a wide range of possibilities for producing parts with tailored properties. By fine-tuning these primary elements, functional 3D printed objects can be obtained with precise, application-specific properties [75], [76].

Additive manufacturing processes are automated systems that employ 2D layers of computer data, derived from a 3D object file created in a CAD environment, to construct 3D solid objects layer by layer. The layer-by-layer characterizes all the types of process, the difference lies in their specific modes of final object construction. The

entire process of manufacturing starts from the 3D CAD software to design the 3D CAD model and to transform it into the tessellated model, saved in the STL file form [77]. STL format has been developed by 3D Systems, which named the file format 'Standard Triangulation Language' and put it in the public domain, it is a standard format that can be found in almost all solid modelling CAD systems [59]. To construct an STL file, the surface of the object is divided into triangles, three sided planar facets, each triangle is described by three points and a vector with a direction normal to the face of the triangle and positive sense towards the outside of the surface [78]. This topological information constitutes the STL file in two different ways, it is stored in binary form as 32-bit single floating-point format as per IEEE standard 754, or in ASCII strings. The second storage method is larger and human readable, the arrangement of the STL file in ASCII format initiates with the term "solid", proceeded by the appellation of the document, then the triangles are delineated by specifying the facet normal and the vertices' coordinates and concludes with "endsolid" [77], [78].
In additive manufacturing, the use of tessellated representation has some critical issues, including the first-order approximation of the original CAD model. There is always a so-called chordal error, like shown in Figure 21 [79] it is the difference between the points on the surface of the original CAD model and the tessellated one, in the image, P_{CAD} is the point on the CAD file surface, while P_{STL} is the point on the tessellated model, especially when the surface of the part is curved, the two point are not coincident. Increasing the number of triangles would make the surface more accurate and smoother, approximating the original one with sides and faces of triangles that are closer to it, however this leads to much larger data files [77].

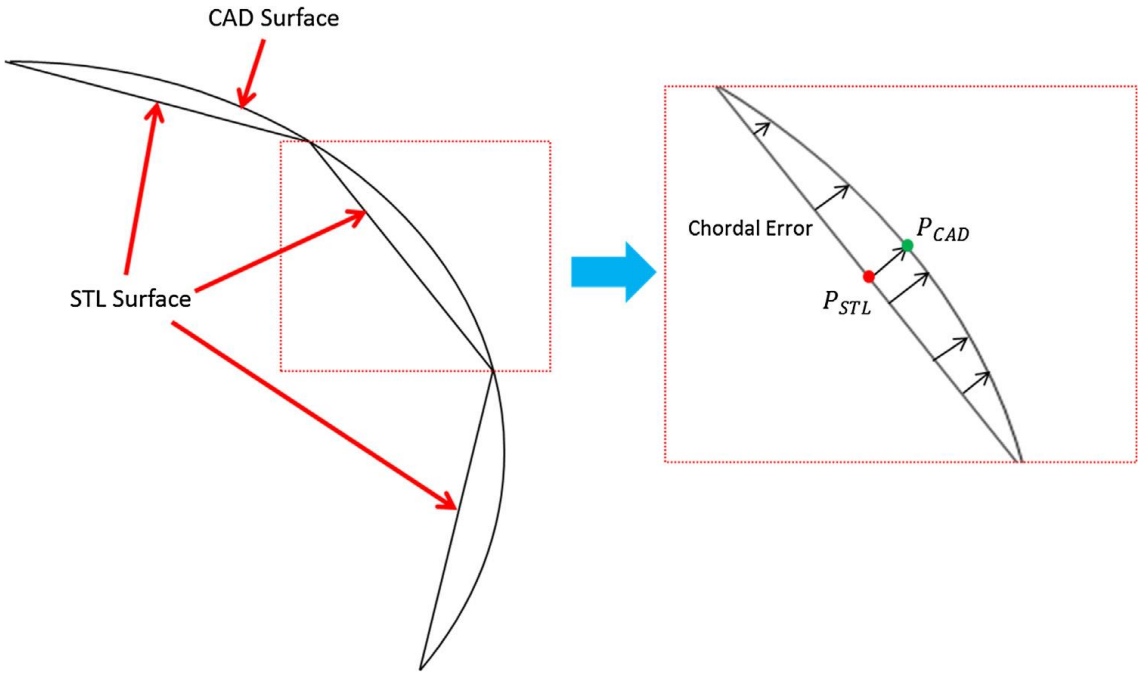

Figure 21. Chordal error between CAD and STL model

Once the STL file is generated using CAD software, the latter can be transferred to the machine software for 3D printing, by now all additive manufacturing machines have adopted the STL format. This makes possible to print any object regardless of the software that was used to design it and regardless of which machine will be used to print it [77].
The next phase is slicing, which is the intersection of the CAD model with a plane to determine 2D contours. The software creates the slicing of the STL model, a sequence of 2D parallel slicing planes which are the layers that one at a time will be built by the printer. An important parameter is the thickness of the slicing, and it can be chosen by the users, a smaller thickness permits achieving better surface quality and a more detailed shape, in some cases the slicing can also be adaptive, varying layer thickness along the vertical axes of the model, high-curvature surfaces are sliced with less thickness while low-curvature surfaces with more thickness [77], [80]. From Figure 22 [81] it can be noticed the difference between the curve surface quality using thicker or thinner layer, in the first case the printed part surface will exhibit a more evidently the so called "staircase effect" [80].

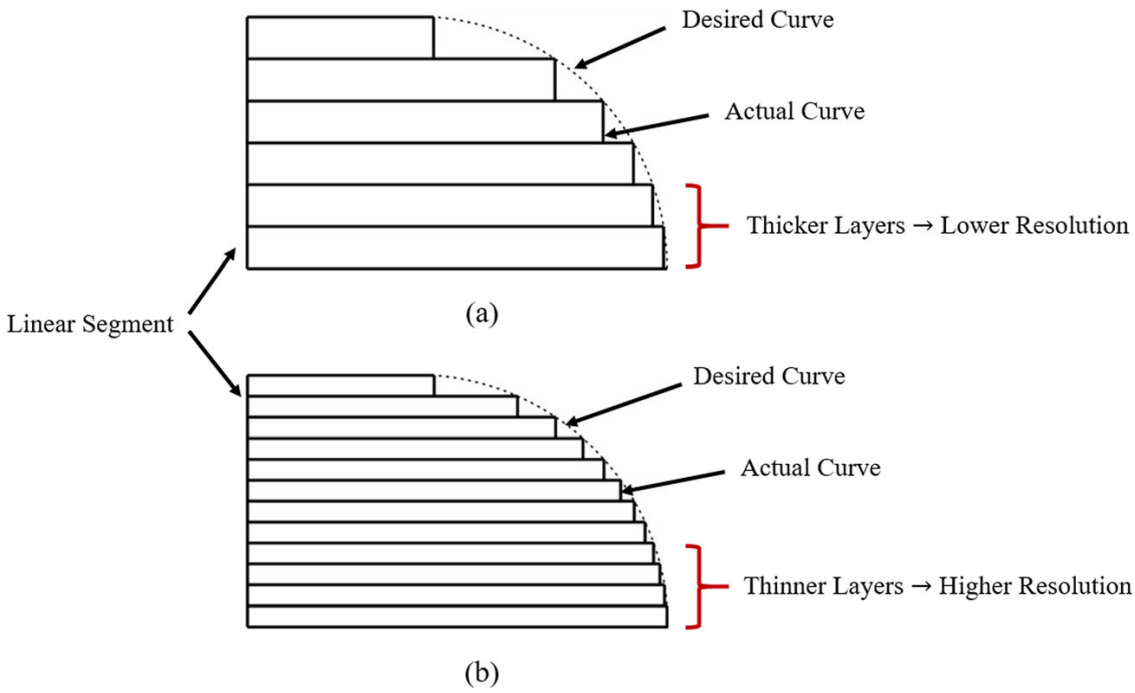

Figure 22. Difference in quality surface varying slicing thickness

In the AM machine software is also possible to orient the piece in the building area of the printer and to generate the supports, after that, once entered layer thickness Δs, is generated the slicing of the STL model [82]. Then, it is possible to pass this file processed from the printer's software to the printer itself. When the file is available for the printer, only its settings and parameters must be chosen, depending on the model and the materials used and by starting the process it will form each layer one after the other overlapping them and obtaining the final object. Once the final part is ready, it is collected from the machine and supports and material in excess are

removed, the very last passage is post-processing, consisting in different passages, some of them are cleaning, post-curing, polishing, painting.
The sequence of all the passages is illustrated in Figure 23.

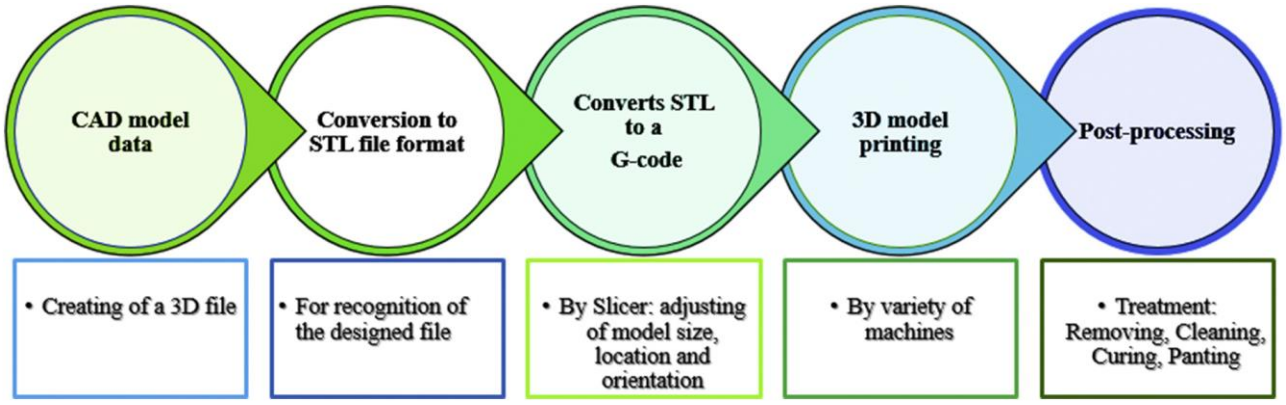

Figure 23. Steps of Additive Manufacturing production

1.3.1. Additive Manufacturing Sustainability and Cost-effectiveness

3D printing has a completely different setting from traditional manufacturing, the possibility to produce parts of various forms and with different materials with a single machine and a single process is very interesting especially in fields in which the scope of the product imposes an exclusivity of the shape, like dental or biomedical areas where is needed anatomical personalization, or when it is required ergonometric design or customization and individualization [83], [84].

In addition, moulds, tools, and special equipment are not needed to print 3D objects, and no personnel or operators are required during production; finally, the complexity of the object does not affect the cost of production, and shapes that are not envisaged in traditional production, such as undercuts, are allowed at the design stage [83]–[85]. In Figure 24 [85] a graph compares the cost of additive manufacturing and traditional manufacturing respect to the complexity of the piece, there is a breakeven point, consisting in a level of complexity at which producing with 3D printing is more convenient because this technology is not affected by shape complexity, in fact its trend is a horizontal line.

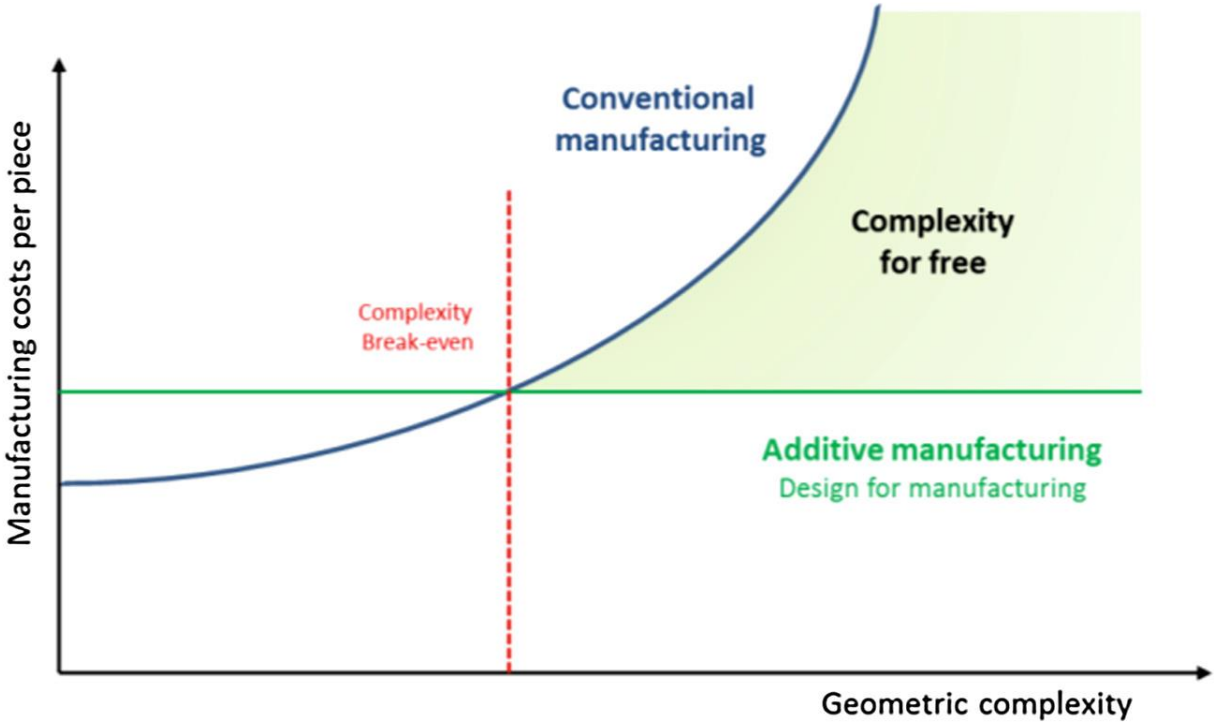

Figure 24. Costs of manufacturing processes respect to geometry complexity of the product

The graph before is referred to costs per piece but the convenience of usage of one approach over the other, depending on production volume too, in fact a large volume of production of identical pieces is a typical approach for conventional manufacturing. Conventional and additive manufacturing are not mutually exclusive, but they can also be used on different specific stage of the product development and production

[83], [84]. To summarize additive technologies are generally better suited for small parts and very complex or intricate designs, instead with larger batches, larger objects, and less complex parts, subtractive processes become more competitive.
The certain freedom of design inherent in this technology also opens others interesting scenarios, for example a particular approach has developed thanks to the possibility of producing objects with 3D printing, the topology optimisation [56]. Objects can be lightened of certain parts that would only be needed for production reasons in traditional manufacturing and nowadays various software packages allow components to be topology optimised at the design stage [86]. In this approach material is removed in areas where it is not structurally or functionally necessary, permitting to reduce the number of parts in the initial design and at the same time ensuring an improvement in minimum weight achievement, static strength, dynamic behaviour, and thermal performance [56], [87].
Through this software for topology optimization, it is possible to specify the types and values of the loads that undergo each part to stress, the functional use of the part and the requirements for thermal resistance or dynamic behaviour, software will process this incoming data and intersect all the designer's requirements to return a part with a shape optimized based on the inputs [86]. An example of Topology optimization application is presented in Figure 25 [87].

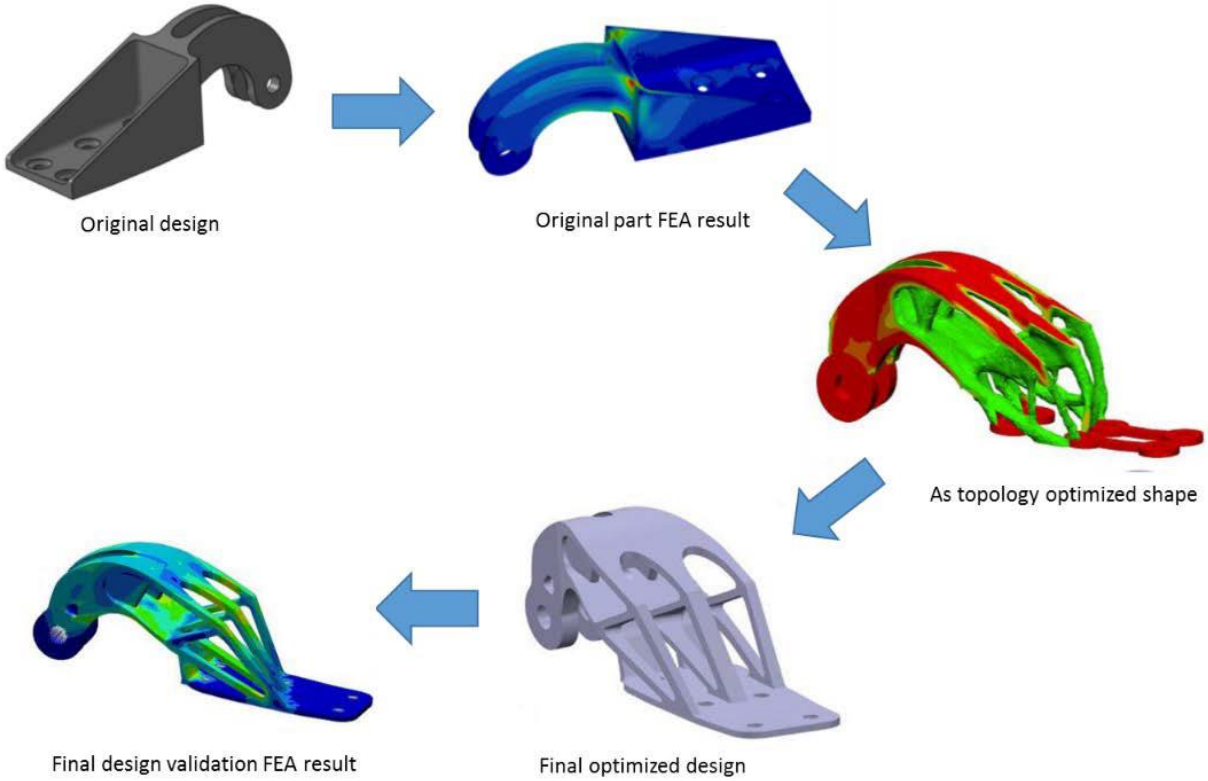

Figure 25. Example of Topology optimization steps on a mechanical component

From the point of view of sustainability, additionally to the possibility to produce pieces on demand, avoiding overproduction, to decentralize production centres also

shortening supply chain and to consider ad hoc repairs [12], the logic of the production of parts with additive manufacturing processes can be exploited to produce smaller amounts of waste material respect to classical manufacturing processes [10]. Additive manufacturing technology or 3D printing is based on the layer-by-layer concept and if used smartly makes possible savings in raw material consumption, costs, and energy, especially as the complexity of the object to be produced increases [88]. Considering the processes and the workflows of traditional manufacturing, in some cases they may not be very efficient from the point of view of material utilization, in fact the process is subtractive, starting from an initial block of material some portions are removed by machining such as grinding, milling, rolling, turning, and drilling [84]. In contrast, 3D printing is an 'additive' process in which the machine realizes the design coming from CAD software and, working layer by layer, spaces can be leaved where no material is needed. The volume of initial material used is almost equal to the volume of the final product since the only waste would be the supports which, however, are still placed by the designer who can try at the design stage to minimize them [11].

Anyway, with additive manufacturing it can be possible to have the tendency to reduce waste due to machining but at the same time obtaining parts that meet the requirements of the sector of use, especially for customized and unique part and this trend can be aimed to contribute to environmental sustainability[88].

Of course, the designer must consider the limitations of the additive manufacturing since the size of the product is imposed by the size of the machine, just as the materials or colours of the object are limited to those that the printer can handle, and the speed of the machine strongly defines and limits the production time of the part [56].

Also, to be included in the assessment of the criticalities of additive manufacturing processes are the issues related to the limited number of materials available on the market and thus the limited functionality and high cost in the field of polymers, for example, which still drive research to find new ones and make them more functional and environmentally and economically sustainable [8].

1.4. Vat polymerization 3D printing

Vat polymerization (VP) 3D printing is a process where a liquid photopolymer in a vat undergoes photopolymerization upon light irradiation, resulting in the selective curing of the material. The part is built sequentially layering polymerized on a movable platform along the z-axis [64], [89].

There are two types of possible configurations for VP printers, the top-down configuration and bottom-up configuration like it can be seen from Figure 26 [90], [91].

In the top-down configuration, the print platform is located above the vat containing the liquid resin. A lifting system of the print platform positions the working surface of the platform itself in the liquid, and UV light is emitted from a source placed above the tank, polymerizing the resin on the platform surface. The platform is then slightly lifted, and the process is repeated to create the next layer. This process continues until the finished object is complete [90]–[92].

In the bottom-up configuration, the print platform is located inside the vat, completely immersed in the liquid resin. UV light is emitted from the bottom of the tank, polymerizing the resin on the platform surface. When one layer is complete, the platform is slightly lifted, and the process is repeated to create the next layer. Also in this case, the process continues until the finished object is complete [92].

The top-down configuration can produce more precise objects, but it may require more time for the preparation and positioning of the printing platform, on the other hand, the bottom-up configuration is generally faster but may be subject to layer adhesion issues to the printing platform [90]–[92].

During the process, the plate is re-immersed or remains immersed into the resin together with already polymerised material, in general a partially printed part meets the not yet polymerised resin and immerses itself in it, during the process [77]. Thus, cured photopolymer repeatedly meets the still liquid resin, therefore, the solid material obtained from photopolymerization must be insoluble in the liquid resin, it is necessary that cross-linkable photopolymers which irradiated by sufficient light energy reach the gel point, the state in which the liquid undergoes a sudden change in its fluidity due to the formation of a three-dimensional matrix, the so called gel with mechanical properties similar to solid material [77], [93].

When the production of a part with a specific material is established, the printing process must be set up and there are several parameters to evaluate and to choose because they are fundamental for the printability [94], [95]:

- printing platform velocity during the downward run diving into the tank;
- printing platform velocity during the upward run to return in rest position;
- plate tank distance in phase of rest position;
- time during which the plate is stationary in the resting position;
- time before the irradiation start when the plate is the tank;
- time after the irradiation, before to upward run;
- Various irradiation times for specific positions in the part to print.

The printing parameters must be adjusted according to the type of resin used. The viscosity of the resin affects the exposure times and the speed of movement of the printing platform, as well as the rest times of the platform both inside and outside the printing tank before and after light exposure [96]. In the presence of a highly viscous resin, the time required for the resin to flow under the platform or for droplets to fall from the platform increases. This can be addressed by adjusting the speed of the platform and increasing the rest times. On the other hand, the light exposure times depend on the reactivity of the resin: a highly reactive resin will require a longer exposure time[96]–[98].

There are various vat polymerization technologies, the specific light source used for irradiation, as well as the technique employed for directing this light to selectively cure the liquid material at desired locations while leaving the surrounding material in a liquid state, differentiates the various types: stereolithography (SLA), digital light processing (DLP) and LCD printing, also called Mask stereolithography (MSLA) [82], [89], [99].

- The SLA was the first technology to be invented in the field of the additive manufacturing in 80's years [57], [59], it uses a mobile laser to induce localised polymerization irradiating selectively point by point each layer. The laser beam is focused on the liquid photopolymer contained in the vat and trace the shape of the layer planned by the STL sliced model to implement selective photopolymerization, by using a computer-controlled mobile mirror to control the laser pattern [100]. The optical arrangement of SLA devices is schematized in Figure 26 [91];

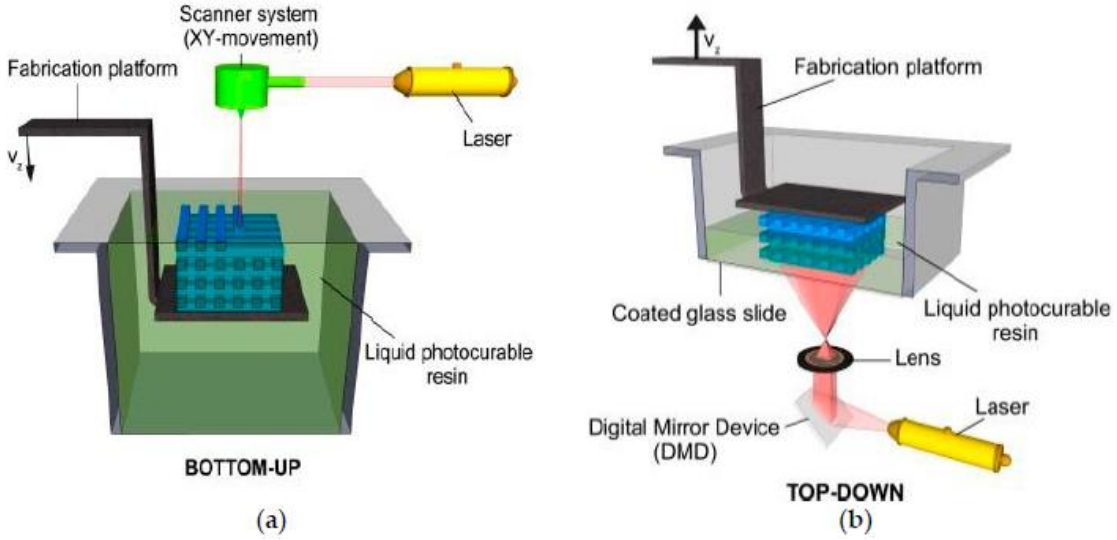

Figure 26. SLA 3D Printing schemes: a) Bottom-up configuration; b) Top-down configuration

- DLP technology differs from SLA from the way to irradiate the layer, the former illuminates and polymerizes entirely and not point by point. DLP 3D printers are based on direct irradiation of the whole surface and its envisaged shape through a projector with micromirrors in its lens to control the light pattern. Micromirrors represents one pixel in the digital image and each micromirror can be turned by the printer control to polymerise where foreseen in the layer to be built [101]. In Figure 27 the projector is in the lower part of the image, coloured in grey, it irradiates the entire surface. In the lower part of the Figure 27 and grey-coloured there is the printing platform with the polymerized resin attached while rising from the vat like typically occurring in top-down configuration [102];

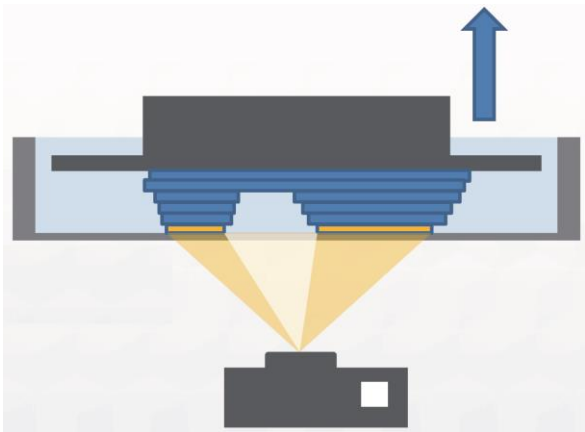

Figure 27. Optical arrangement of DLP 3D printer

- The last type is LCD printing, again as with DLP the resin in each layer is struck by light entirely, however the light source used is an LED lamp and is conveyed by an LCD screen. The pixels of the LCD screen are switched on or off as needed to block the light or let it through by irradiating the resin to selectively polymerise the layer to be built, basically the LCD screen acts as a mask for the

light source (hence the name Masked SLA) [103]. In the image in Figure 28 an LCD printer is reported, it is possible to notice the LED source selectively irradiating the vat, passing through the LCD screen mask [104].

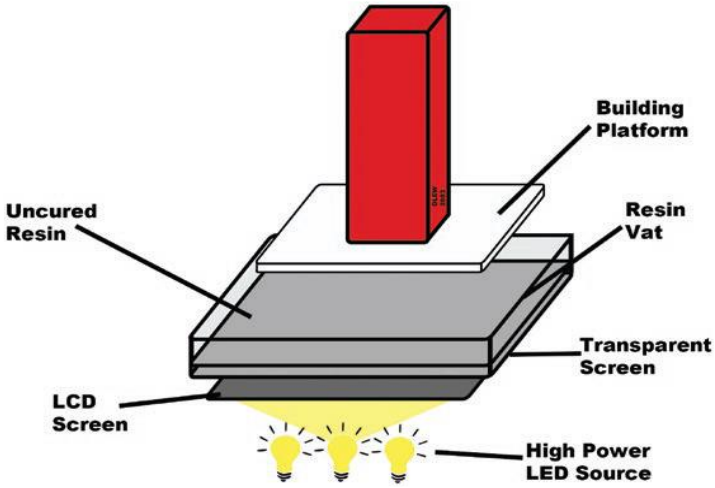

Figure 28. Scheme of LCD 3D printer device

An overview about the principal features of these 3 types of VP devices is given in the Table 1 [105]–[107] with three important characteristics, the type of lamp source with the wavelengths and the resolutions in the axis x, y, z.

Table 1. Comparison of Vat Polymerization techniques

Technique	Lamp source	Minimum z resolution (µm)	Minimum x-y resolution (µm)
SLA	355 nm laser beam	15-20	10
DLP	385-405 LED lamp	15-20	25
LCD	405 nm LED lamp	15-20	32

For what has been said so far, the printing accuracy of any VP 3D printer depends on several factors, considering firstly the resolution along the z-axis, it depends on the smallest displacement the plate can make. Hence regardless of what type of printer it is between SLA, DLP or LED, but depending on mechanics, so precision and type of movement are mainly given by the motor, the motor driver, the various controls and the actuation system which can be lead screw, belt or any other, there is a certain value of resolution along the z-axis, axis of construction of the object, perpendicular to the layer [95]. Resolution in this direction is precisely the minimum thickness of the layer.

Resolution in x and y directions, on the other hand, must be evaluated based on the optical arrangement and source, in SLA printers the xy resolution depends on the

diameter of the laser spot, in DLP on the dimension of the pixel, represented by the size of the micromirror and in LCD printers on the dimension of the pixel of the liquid crystal light masking display [108], [109].
Considering the properties that distinguish this technique from the others, it can be highlighted which are the most convenient uses like the ability to realise complex and intricate designs, so pieces not feasible using standard moulding methods, makes VAT polymerization very competitive for small production lots or highly specialized customization and a very fitting example is the dental field like the printing of individual dental moulds, dentures, or temporary implants, VAT polymerization machinery are used also to produce models for silicon moulding, to print parts for aerodynamic or assembly tests and for flow analysis, for the biomedical field or when it is required that a part to be produced and with a very complex shape be highly detailed, for the style design, and it is often used in the artistic field such as to achieve accurate reproduction of details for small works of art by lost-wax casting or even for jewellery [89].
Materials for this technique are thermosetting and since supports are built in the same material as the piece it is necessary to remove them mechanically, in some cases this process can lead to part damage or resulting inaccuracies in addition to the time and material required, furtherly, the limited dimensional stability of the components due to residual stresses generated is intrinsic of this printing process.
Another point to highlight is that most of the materials applied in VP are thermosetting polymers and it is complex their recycle, however the number of alternatives in biopolymers is increasing [82], [99], [110].
Using this technology for research purposes means exploiting one of its main advantages over the other due to the possibility of testing or varying a combination of chemical compounds and reagents (both liquid and powdered) and thus customising liquid photopolymers by trying to produce parts and designing them by modifying material properties or thinking up new materials [110].

1.5. Principle of photopolymerization

The polymerization is the chemical reaction that is exploited in VP, the polymers are obtained by a process called chain polymerization that occurs thanks to a photo initiator.

Photo initiators are compounds that when irradiated, absorb part of the light and through a chemical transformation generate reactive species which can be radicals or ions. Being immersed in a resin composed from monomers and eventually additives, these radical, anionic, or cationic reactive species initiate the reaction to form a polymer bonding to the monomers of the resin and starting a growth chain polymerization [14], [111].

Radical, cationic, and anionic initiators cannot be used indiscriminately, because the type of reactive centre causing polymerisation varies between different monomers.

Based on the type of species formed by the transformation of the photo initiator and used to start the process, two classes of photopolymerization systems can be distinguished: Ionic polymerization and Free-radical polymerization [14], [111].

Just considering the before mentioned species, it becomes clear that the distinct forms of chain polymerization necessitate dissimilar methodologies. In ionic polymerization, a positive or negative electrovalence must exist at the terminus of the expanding macromolecule, while radical polymerization requires an unpaired electron at the end of the polymer chain [13].

Cationic and anionic polymerization are less used than the free-radical polymerization because ionic initiation is more selective in terms of adaptability with respect to the various monomers thus applications of cationic and anionic polymerizations are limited respect to radical polymerization [13].

Free radical polymerization is widely used especially in additive manufacturing, it consists in three different parts [13], [14], [111].

The first is called initiation, in this phase the photo initiator is hit from the light and its decomposition occurs, this means that the photo initiator molecule is cleaved in two elements called radicals equipped with an active site:

$$\mathrm{I} \xrightarrow{k_d} 2\mathrm{R}^{\bullet} \quad (1)$$

Where I is the photo initiator, $\mathrm{R}^{\bullet}$ is the radical with the active site and k_d is the constant for initiator dissociation, this reaction is driven by heat or light to break the chemical bonds and to produce the radical species [14].

Thus, the radical is transferred to the monomer:

$$\mathrm{R}^{\bullet} + \mathrm{M} \rightarrow \mathrm{RM}^{\bullet} \quad (2)$$

Where M is a monomer in the liquid photo polymerization system and after the joint with the radical group R it became $\mathrm{RM}^{\bullet}$ a polymer chain that can be defined $\mathrm{M_1}^{\bullet}$ that is still able to continue to react and for this reason is called active polymeric chain [14].

The kinetic of the initiation reaction is governed by the constant for initiator dissociation because this reaction is slow respect to the kinetics of the transfer of the radicals to the monomer, so the limiting factor is k_d and r_i [14], the rate of initiation is:

$$r_i = \frac{d[M_1^\bullet]}{dt} = \frac{d[R^\bullet]}{dt} = 2k_d f[I] \quad (3)$$

Where $[M_1^\bullet]$, $[R^\bullet]$ and $[I]$ are the molar concentration respectively of the growing polymer chain, of the radical and of the initiator and f is the efficiency factor, the fraction of the produced radicals which successfully initiate the polymerization, to be taken into account in the kinetics because the radical could be inactivated or transferred back to other species in the chemical system before combining with the monomer [14].

In the second step, called propagation, the active chain formed by one monomer and the active radical centre, joins itself with another monomer, indicated by M, and the active site is transferred to the new end of the chain, obtaining $M_2^\bullet$, a new polymer active chain two monomers long [14].

$$M_1^\bullet + M \xrightarrow{k_p} M_2^\bullet \quad (4)$$

Where k_p is the constant for the chain propagation.

At this point the polymer $M_2^\bullet$ joins another monomer and transfers to it its active site, with the consequent result of a new active chain polymer $M_3^\bullet$ longer by one monomer in degree of polymerization than the previous. This process happens for other monomers which will be joined through the active site transferred each time at the new end of the chain [14]. In general, this reaction take place between an active polymer chain of arbitrary length "i", called $M_i^\bullet$, and another monomer unit M, forming a polymeric active chain with length "i+1" called $M_{i+1}^\bullet$, so, it can be written:

$$M_2^\bullet + M \xrightarrow{k_p} M_3^\bullet \quad (5)$$

$$M_i^\bullet + M \xrightarrow{k_p} M_{i+1}^\bullet \quad (6)$$

As noticed by the previous written reactions, for each single new monomer, the k_p, propagation rate constant is assumed equal, therefore, the overall rate law for the kinetic of the propagation process can be expressed in form of the sum of each rate of the reactions occurred and can be related to the rate of consumption of monomer M [14]. Indicating as $[M]$ the monomer concentration, the rate of propagation is:

$$r_p = -\frac{d[M]}{dt} = k_p[M_1^\bullet][M] + k_p[M_1^\bullet][M] + \cdots k_p[M_i^\bullet][M] \quad (7)$$

Being k_p the same value, as said before, r_p became:

$$r_p = k_p[M]\{[M_1^\bullet] + [M_2^\bullet] + [M_3^\bullet] + \cdots + [M_i^\bullet]\} \quad (8)$$

The sum of the concentrations of all the active chains that take part in the process can be represented by $[M^\bullet]$, the total concentration of the active chains in the process, in this way the r_p can be expressed as follows:

$$r_p = k_p[M][M^\bullet] \quad (9)$$

The last part of the reaction is called termination and in this part the radical is transferred away from the active chain, consequentially there is the formation of inactive polymers, they are no longer able to continue to react and elongate the polymer chain because they have not a radical active site. This final step can occur by means of two mechanisms and both can take place, but the occurrence of one of them may prevail depending on the polymer in question and its conditions [14].
The first mechanism of the termination is called disproportion, when it arises, each of the individual molecules possibly involved transfers away its radical and it forms a inactive chain, so if for example there would be two involved active chain in the liquid polymeric system, after the termination two resultant inactive polymeric chains will be in the system [14].
Instead, in the other mechanism, the combination, a pair of active polymer chains combines and forms a single inactive polymeric chain with length equal to the sum of the lengths of its individual active constituent polymers losing their radical.
By indicating as $M_i^\bullet$ and $M_j^\bullet$ two generic active polymers chain respectively with length or polymerization grade "i" and "j", it is possible to write the reaction mechanism, disproportionation, and combination:

$$M_i^\bullet + M_j^\bullet \xrightarrow{k_{td}} D_i + D_j \quad (10)$$

$$M_i^\bullet + M_j^\bullet \xrightarrow{k_{tc}} D_{i+j} \quad (11)$$

Where D_i and D_j are the polymeric dead chains or inactive chains with length respectively of "i" and "j" and respectively formed from $M_i^\bullet$ and $M_j^\bullet$, instead D_{i+j} the polymeric dead chain or inactive chain obtained from the combination of the same two active chains with length "i+j".
Each of the two mechanisms has its own kinetic constant for the termination rate, in the reactions above they are indicated with k_{td}, constant of termination for disproportionation and k_{tc} constant of termination for combination. To characterize the kinetic of the termination process it can be used the overall termination rate r_t, this last is defined in term of the rate of consumption of the reactants, the active chains and so it is necessary to take in account both the mechanisms and to indicate the concentration of one of them in general, it is used same as in the previous part $[M^\bullet]$:

$$r_t = -\frac{d[M^\bullet]}{dt} = 2k_{td}[M^\bullet][M^\bullet] + 2k_{tc}[M^\bullet][M^\bullet] \quad (12)$$

$$r_t = 2(k_{td} + k_{tc})[M^\bullet]^2 \quad (13)$$

$$r_t = 2k_t[M^\bullet]^2 \quad (14)$$

So as noticed in the relations above, the overall constant of the termination can be indicated as k_t and it is equal to the sum of the constants for combination and for disproportionation [14].

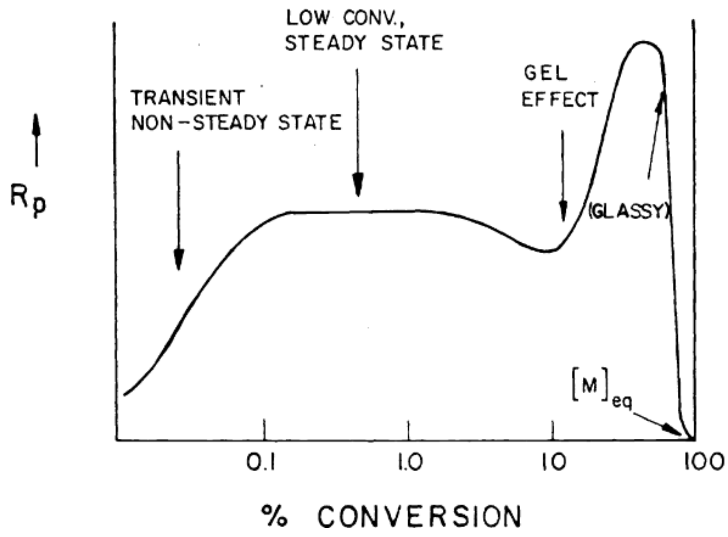

Figure 29. Rate of polymerization as a function of conversion

In Figure 29 [112] it is reported the reaction of polymerization observing the rate of polymerization respect to the rate of conversion of the reactants. Initially, there is a liquid resin, which is a low melting thermoplastic material, up to about 10%, at which point the degree of polymerization experiences a minimum after a plateau phase. Subsequently, gelation occurs, which is the transition from a liquid state to a solid gel state at macroscopic level due to the formation of a 3D network at molecular level. This process is irreversible, and flow is hindered due to the formation of a cross-linked molecular structure. The increasing viscosity of the polymerization system causes an acceleration accompanied by an increase in the molecular weight of the polymer. Finally, there is the vitrification phenomenon, which is the transition from a solid gel state to a solid, glassy, and rigid state [112].

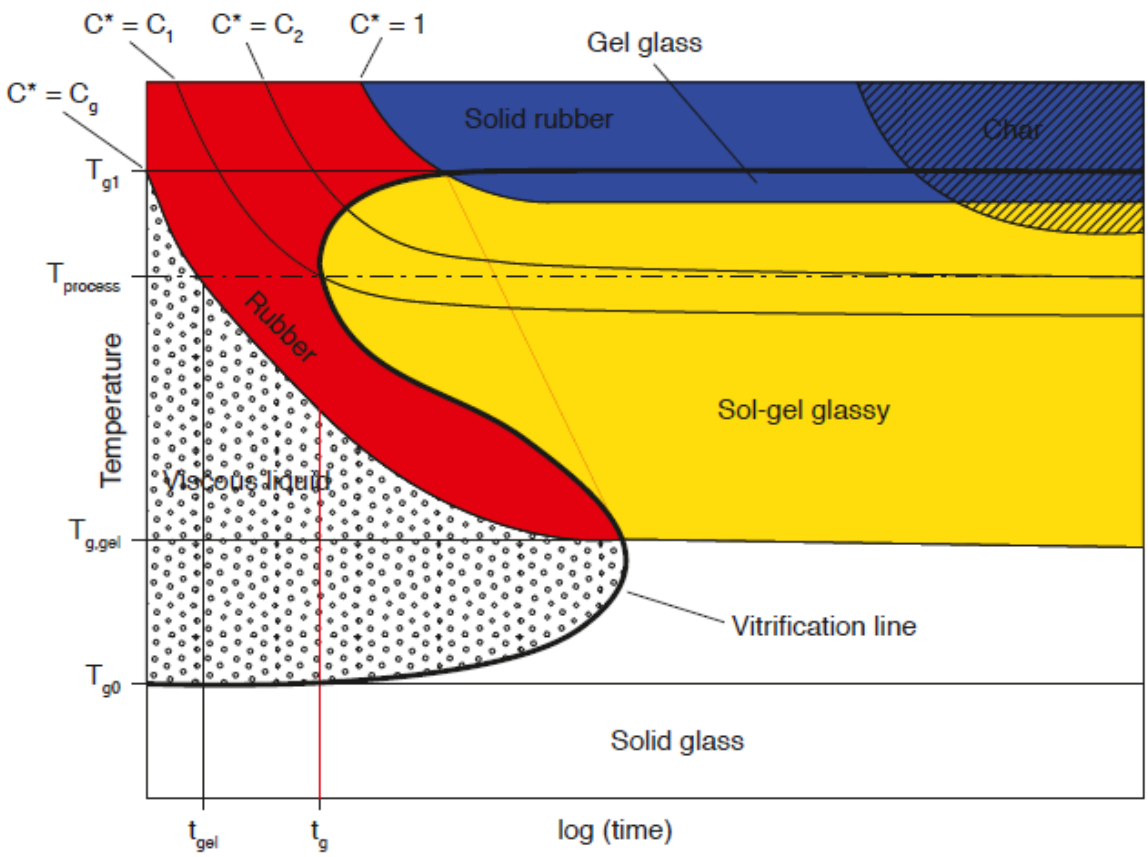

Figure 30. Time-temperature-transformation (TTT) diagram for a thermoset

The curing behaviour of thermosetting resins can be characterized using the time-temperature-transformation (TTT) diagram in Figure 30 [13]. This diagram displays various lines representing constant degrees of cure, including the gel point $C^* = C_g$ and the fully cured resin $C^* = 1$, each with their corresponding glass transition temperatures T_{g1} and $T_{g,gel}$, respectively and it also shows T_{g0} for the uncured resin and the S-shaped vitrification line are also shown. In the diagram are also represented the viscous liquid region where the resin has not yet reached the gel point and the "char" region instead should be avoided during processing to prevent thermal degradation of the polymer[13].

During polymerization or curing process the conversion of the reactants, the molecular weight and cross-linking density of the polymer increase, for this reason T_g of the curing polymer increases and depending on process temperature, vitrification may occur. Vitrification is the transition from solid gel state to solid glassy rigid state, it occurs when T_g reaches the processing temperature of the polymer causing inhibition of diffusion processes and consequentially of chemical reactions too. After vitrification, the resin results not fully cured a post-curing process is needed. If after gelation T_g does not reach processing temperature there is not vitrification, diffusion processes can proceed and the chemical reactions can go to completion, with C reaching the value 1, meaning resin fully cured. The vitrification line represents the

temperature boundary at which the glass transition temperature becomes the processing temperature and below this line, the curing process is slow due to limited diffusion [13], [14].

The diagram displays a hypothetical process temperature and shows the material reaching the gel point at $t = t_{gel}$ and the vitrification line at $t = t_g$, achieving a degree of cure C_1 with a glass transition temperature equal to the processing temperature. The material continues to cure slowly until it reaches a degree of cure just below C_2 [13].

1.6. 3D printable formulations

Photopolymers before irradiation are liquid resins sensitive to specific wavelength radiations. In the field of 3D printing, it is required they present main characteristics as high reactivity to the radiation, low activation energy, limited volatility and toxicity, stable viscosity, low shrinkage, reduced sensitivity to humidity and good mechanical properties after polymerization [113].

A typical formulation is composed of a base resin, which may make up almost the entirety of the formulation or as little as 25% by weight of it, additives, among the most important of which there are reactive diluents usually present in percentages between 15 and 60% by weight and finally there are surfactants, pigments, fillers, and stabilisers making up a maximum of 50% of the photopolymer. The use of photo initiator is necessary in a range between 1 to 8 wt.% of the formulation.

The free-radical polymerizable resins, rich in unsaturated C=C double bonds and acrylate or methacrylate terminations, are widely used and commercially available because these are functionalities with high reactivity to light irradiation and their reaction mechanisms are known and reliable [113]. The first resins patents, registered in 1989 and 1990 and SLA dedicated, concern compositions prepared from acrylates, they had a good reactivity, but the parts produced where weak and inaccurate due to shrinkage and curling [59], [114].

The choice of type of resins narrows the field as to the type of photo initiator to be used, acrylates and unsaturated polyesters cross-link by the radical route, epoxy- and vinyl ether-terminated oligomers are polymerised by the cationic route. These processes therefore require the respective chemical species to initiate the processes [115]–[117].

In general, resin functionality is the first characteristic to consider, which consists in the number of available functionalities leading to polymerization. Other important characteristics to consider are the viscosity and the kinetic reaction also concerning the time and the complexity of the process, the hydrophobicity, the shelf life, volatility, odour, and toxicity. All these properties can help to determine how the resin should be used and how it should be handled during the preparation and 3D printing. Finally, the shrinkage, the cost, and obviously, the final mechanical and functional characteristic of the polymerized product are also dependent from the reactive functionalities of the resins [118], [119]. There are further functionalities like unsaturated polyester, vinyl, vinyl ether systems and each group have its own characteristics for example vinyl is used in application where chemical resistance is needed [120]. All of them are useful in the monomers or in the oligomers which constitute the resin, in fact, as pointed out before, the photopolymers for VP are based on a monomer or oligomer resin that gives the principal features to the final polymer [113].

The widespread methacrylate or acrylate-based resins for VP polymerisation have their criticality in the shrinkage that the polymer undergoes during radical polymerisation. Otherwise, to reduce the effects of this drawback, a solution is to create a polymer from methacrylate/acrylate and epoxide resins. These hybrid systems combine the main advantages of both types of resins, they are formed by free-radical polymerization of the acrylic resin and using appropriate photo initiators by cationic polymerization of epoxy resins, then bonding the two networks, copolymerizing, it can be obtained systems with the low shrinkage of epoxy resins and the high curing speed, low sensitivity to humidity, and the good mechanical properties of acrylic resins [121], [122].

Another phenomenon that has an impact on the light-curing of acrylate-based resins is the oxygen inhibition, double carbon bonds join with the free radicals, it can occur that these radicals on the primary chains react with the oxygen, creating carbonyl groups and peroxide radicals and they are no longer able to react with other C=C double bonds of the other acrylates, interrupting the polymeric chains growth and leading to an incomplete curing of the polymer [123]. Limiting or eliminating the contact between the oxygen and the resin can be used to avoid oxygen inhibition, for example through inert nitrogen atmosphere, other solutions are to increase the photo-initiator' s concentration or the duration and intensity of the light irradiation, to increase the curing rate, another way is to introduce reducing agent hydrogen donors. However the oxygen inhibition in some cases may be a deliberate process in vat polymerization 3D printing, in fact, since unreacted C=C remain on the polymerised layer, they can react with the next layer double bonds, obtaining a stronger adhesion between layers, in addition, considering the passage of the remotion of the piece from the printing plate that in some cases can result difficult and may lead to damage to the part, a first layer suffering from oxygen inhibition can result easier to be detached so the oxygen-inhibition in the initial phases of the printing could be a positive effect to avoid too much adhesion between polymerized material and the vat's bottom [124].

In general, additives are used to adapt both the properties of the resin and of the material after polymerisation to various needs. Reactive diluents, specifically adjust viscosity and so the processability and the solubility of particles like fillers, dyes, or powder photo initiators. The concentration and the structure of the reagent characterise, as already mentioned, the viscosity and solubility of the resin, which is the primary purpose of using reactive diluents, they also affect the volatility of the formulation and the affinity with the photopolymer components, instead by the point of view of the cured polymer, its mechanical and thermomechanical properties [125]. The importance of reactive diluent is linked to its properties of miscibility with the other components, be in a liquid and non-viscous state at room temperature, have low volatility and toxicity, have good thermal stability at process temperatures, be

highly reactive to irradiation and help impart good thermo-mechanical properties to the polymer [126].

When choosing reactive diluents, it is important to consider the high volatility of many of them, since a low viscosity component has a low molecular weight and could therefore be very volatile, and that when using such reactants, a high concentration will reduce the cross-linking density if they are not very reactive, resulting in a more homogeneous structure and a lower transition temperature[127]. In free-radical polymerisation systems, monofunctional elements give a lower cross-linking density and are used to obtain more flexible polymers, but among them, non-acrylates or methacrylates, like styrene, are very volatile and toxic, and their use is being abandoned, whereas acrylates like are more used because they do not present this problem [127].

On the contrary, multifunctional elements, like hexanediol diacrylate (HDDA), are more involved in the polymerisation process and are very reactive, leading to higher cross-linked networks. However, if the functionality is excessively elevated the risk could be a drastic increase in crosslinking density, resulting in very hard and brittle polymers[128].

Photo initiators are essential components of the chemical composition of the resins for VP polymerization, they determine the efficiency of the reticulation reaction and consequentially the accuracy and resolution of the printed part and they affect the process times too.

Each photo initiator has its own absorbance spectrum that depends on its chemical structure, this means that each photo initiator absorbs effectively specific wavelengths and intensity. In Figure 31, some photo initiators are reported with their absorption wavelength peaks. Therefore, it is important to fit the wavelength range of the photo initiator and the radiation source [129].

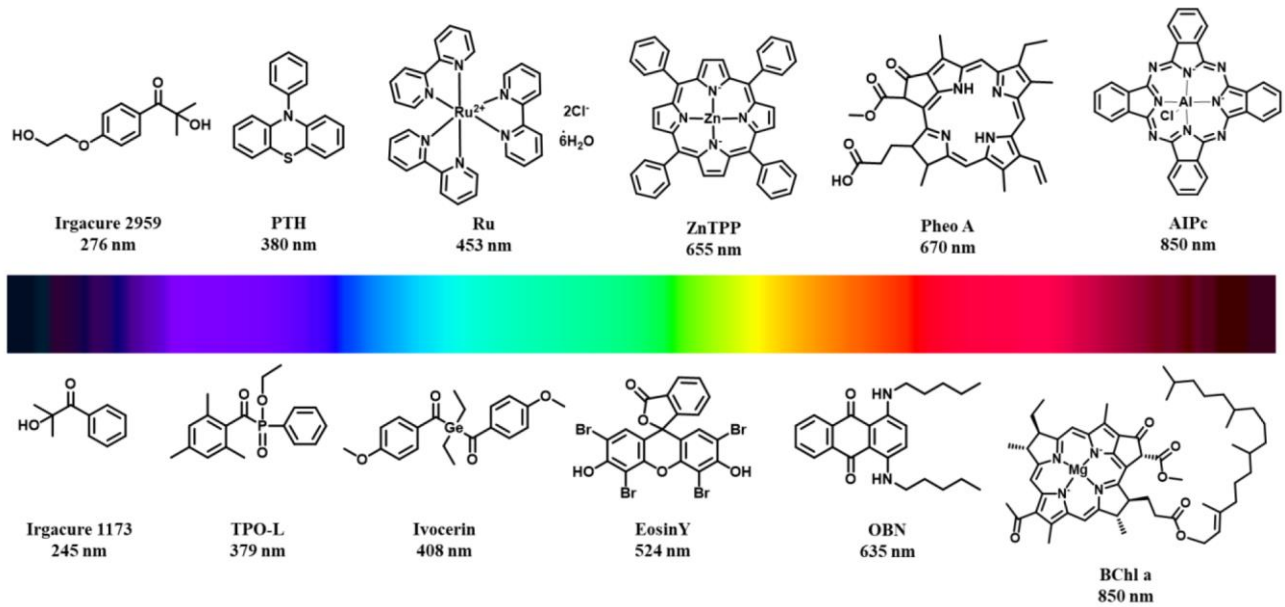

Figure 31. Examples of photo initiators and their absorption peaks

As said before, the two different ways to initiate the polymerization involve the use of free-radical photo initiators[116] or cationic photo initiators. The second particles, for example sulphonium salt[130], in the appropriate systems generate Bronsted or Lewis acids that can polymerize epoxides or vinyl ethers. However, the most used reaction is the free-radical photopolymerization where radicals that are formed link to the double unsaturated bonds of the monomers or oligomers.
Free radical system photo initiators are classified in two types depending on the mechanism to generate reactive species, the type first Norris reaction and the type second Norris reaction. The first type mechanism happens when photo initiators absorb light, generate through the homolytic cleavage of the sigma bond between carbonyl carbon and alpha carbon two radicals, in fact in most of them there are aromatic carbonyl groups which undergo rapid bond cleavage. Each radical can link to a monomer starting to initiate the chain growth or can eliminate a C=O forming an alkane. Instead in the Norris second type mechanism the photo initiators are uncleavable organic molecules able to absorb a photon and to pass in the long living excited triplet state, in this state they acquire an electron from a co-initiator or extract a gamma hydrogen from a co-initiator to transfer it to a carbonyl oxygen creating a diradical [131].
In the initiating system different photo initiators could be used, by combining for example, type I and type II compounds or thermal and light-absorbing initiators. These different ways can generate systems that have a broader wavelength absorption spectrum [131].
Many other additives can then be added depending on the properties that we want to impart to the material for some specific application, such as surfactants, anti-foaming agents, levelling agents, plasticisers, flow regulators, stabilisers, fillers also in the form of nanoparticles and dyes [132]. These last additives are very used in many applications, they are principally represented by organic or organometallic molecules used in low concentrations balanced in dependence of the resin composition and chose according to the type of the irradiating light. Obviously dyes give a colour to the resin but the fundamental structural effect of them is the printing accuracy and printed part definition increase that takes place confining the penetration of light in the z- axis of the printer taking advantage of better control of the cure depth, especially for resins that would be basically transparent, this effect rise with the increase of dyes concentration, bearing in mind, however, that a high concentration could lead to a decrease in the reactivity of the photopolymer and the efficiency of the photo initiator[133].
Instead, fillers or nanofillers, if nanometric in size, are dispersed in the continuous matrix of the resin as reinforcements or to modify the performance of the material, that is defined polymer composite. As with all composite materials, the mechanical properties of composite polymers are determined by those of both the reinforcing material and the matrix. Nanofillers are organic, inorganic, or metallic compounds

that, when used with 3D printing techniques, can tailor mechanical strength, thermal resistance, and electrical conductivity. Some examples of nanofillers are carbon nanotubes, graphene, and nano clay[132].

An interesting variant of additives is represented by bio-fillers derived from agricultural or food waste materials, which are used to lower costs and as colorants, and can also affect thermomechanical properties. In the context of 3D printing, they can improve resolution, being used as dyes confining light when used in transparent resins[134], [135].

2. Aim of the work

Bio-based materials are a rapidly growing topic in research and industry, driven by the desire to promote eco-friendly technological development.

The aim of this thesis is to investigate the 3D printability of a bio-based photocurable resin with two different reactants, already available on the market, by using vat polymerization with an LCD-based radiation arrangement, to define the best parameters optimization for the additive manufacturing process.

The monomer used as polymeric starting material was an acrylate epoxidized soybean oil (AESO), identified as a promising bio-based matrix for the purpose, together with two different reactive biodegradable diluents, tetrahydrofurfuryl acrylate (THFA) and iso bornyl methacrylate (IBOMA), which were chosen to improve the 3D printability of the soybean oil resin addressing issues associated with AESO in 3D printing applications, such as its high viscosity. The photopolymerization reactions were performed in the LCD 3D printer machine in air by adding a photo initiator opportunely selected with sufficient reactivity and suitable to be used in combination with the resin, at the specific wavelengths of the machine used for the 3D printing process. The photo initiator phenyl bis(2,4,6-trimethylbenzoyl) phosphine oxide, known as BAPO, was evaluated as an ideal candidate for such requirements.

In the first part of the study, different photocured polymers were prepared by LCD 3D printing with different diluent percentages, and fully characterized by thermal and mechanical point of view.

Subsequently, the 3D printability of four different bio-based polymeric composites was investigated and tested, by selecting one of the best photocurable resin formulations for each diluent, based on their processability and properties. The bio-based composites were prepared by adding 5 wt.% of two different bio-fillers, coming from renewable sources, like wine and corn processing wastes, to the chosen ideal soybean oil-based formulation. The composites realized were then characterized to assess the effect of the bio-filler on the final polymeric properties. Loading a thermosetting polymer with such fillers is more advantageous as it has the potentiality to reduce costs while maintaining or increasing the material's bio-based nature and sustainability. Furthermore, the use of innovative technologies such as additive manufacturing fits well within this sustainability framework, as these processes can be designed to use raw materials more efficiently and could also be used to create complex, customizable objects in line with a pull production approach that reduces waste. Moreover, there are not many bio-based materials available and suitable for vat polymerization additive manufacturing that on the other hand is an ideal technology for research into new polymers since allows to modify the liquid resin poured into the printer tank before photopolymerization. This thesis seeks to contribute to the development of new sustainable materials that can be utilized in

emerging technologies, by using innovative bio-based soybean oil thermosetting resin and sustainable additives.

The use of such materials can lead to innovative and green solutions that address the ever-growing environmental challenges faced by society today. By exploring the properties and characteristics of these materials, this research aims to provide valuable insights into their potential applications and how they can be optimized to meet sustainability goals. Through this work, new avenues for sustainable manufacturing and production can be opened, leading to a brighter and more sustainable future for all.

3. Characterisation techniques

In this work, the characteristics of the bio-based thermoset polymers and composites containing bio-fillers were evaluated by means of thermal and mechanical tests, and by the ASTM standard test for the determination of the gel content performed on the specimens obtained after the 3D printing vat polymerization process. Viscosity measurements were performed on the liquid resin formulations.

3.1. Thermal measurements

Thermal analysis techniques were employed to characterize thermal properties of the studied materials. This evaluation is very important to determine for example the thermal stability or the behaviour of the polymeric materials and composites.
The tests performed were Thermogravimetric Analysis (TGA) and Differential Scanning Calorimetry (DSC).

3.1.1. Thermogravimetric Analysis

Thermogravimetric analysis (TGA) is a thermal analysis technique used to measure the mass degradation of a material as the temperature increases. The specimen used in the test is put in the analysis chamber, that in most of the instruments can arrive at around 1200 °C [136], where it is subjected to controlled temperature changes over a specific time interval. The variables to consider during the measurement are time, temperature, and mass, which can be performed in vacuum, air, or inert gas.
The polymeric mass can be directly measured while temperature and time are parameters controlled by the machine, allowing accurate and precise monitoring of the sample under analysis.
TGA can be static, also called isothermal, when the weight change is analysed over a specific time at a constant temperature, or dynamic, with linear increasing of the temperature, the minimum rates are typically less than 100 K/min [136]–[138]. Temperature can be also increased through discrete isothermal steps, in a quasi-static approach. The data from these tests are usually presented like in the example shown in Figure 32, indicating the percentage of mass remained respect to the initial sample weight, as the temperature increase, often together with the alteration in weight (called derivative weight in the figure and coloured in grey) [136].

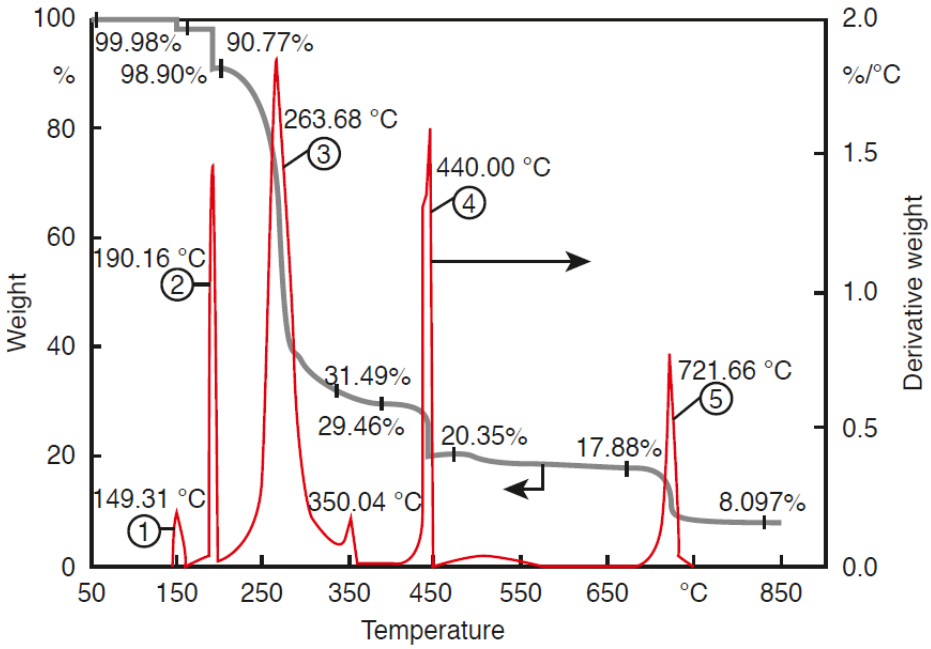

Figure 32. Example of TGA thermogram

Thermogravimetric analysis (TGA) can reveal significant temperature values at which physical transformations or chemical reactions. It is commonly employed to determine specific properties of materials that exhibit weight loss or gain due to decomposition, oxidation, or volatilization of substances, as for example moisture. The technique can verify the complete degradation cycle of a sample and assess the thermal stability of a material at its operational temperature. TGA can also characterize materials through analysing distinctive decomposition patterns, investigate degradation mechanisms and reaction kinetics, and establish the organic and inorganic content of a sample [139].

In this thesis the TGA/SDTA 851e instrument by Mettler-Toledo, like those in Figure 33, was employed to carry out the TGA analysis under an air atmosphere, in a temperature range from 25 to 900 degrees with a heating rate of 10 degrees/min.

Figure 33. TGA/SDTA 851e by Mettler-Toledo

3.1.2. Differential Scanning Calorimetry

Differential scanning calorimetry (DSC) is a type of thermal analysis technique in which a test sample is analysed in parallel with a reference sample of known thermal properties. The two samples are kept at the same temperature while this last gradually increases, and the difference in heat flow between the two materials is measured. So, the term differential refers to the comparison between the tested and the reference sample. DSC requires small samples with mass smaller than 10 mg and the used reference materials have known properties, like mercury or zinc, are used for standardization [136].

The result of a DSC test is a heat flow curve as function of temperature, or time, as shown in Figure 34 [140].

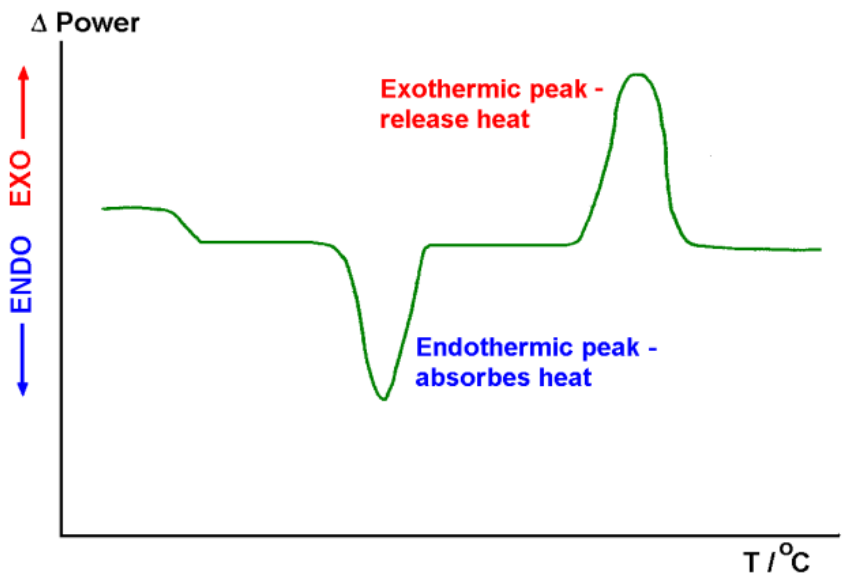

Figure 34. Typical DSC graph

DSC allows determining the material's heat capacity, additionally during heating, various thermal transitions can be observed, such as the glass transition, crystallization, and melting, which are detectable as peaks or dips in heat quantity versus temperature graphs.

The material's purity can be evaluated from DSC observing an eventual melting point lowering respect to the pure. Finally, anomalous peaks may indicate the presence of impurities in the sample [140].
In Figure 35 there is the DSC 214 Polyma Equipment, manufactured by the Netzsch Group, the device used for the tests conducted in this thesis. The temperature range for the experiments with this instrument is from -50 to 250 °C, both in cooling and heating phase, the rates of heating and cooling are of 10 °C/min and the tests were performed by conducting two heating cycles and one cooling cycle for each sample. The instrument is equipped with a gas flow controller for the heating chamber, a nitrogen flow with rate of 50 mL/min.

Figure 35. DSC 214 Polyma Equipment by Netzsch Group

3.2. Test for Determination of Gel Content

The gel content, or insoluble fraction, is a measure of the crosslinking in the thermoset polymers. The crosslinked material, in fact, is insoluble, and crystallinity fraction in the polymer can be determined through solvent extraction following the standard by ASTM designation D2765-16 [141], "Test method for Determination of Gel Content and Swell Ratio of Crosslinked polymer".

The gel content indicates the weight percentage of crosslinked polymer that remains insoluble in a solvent, following specific extraction conditions. In the case of this work, the gel content was evaluated by using extraction in chloroform. In contrast, the swell ratio measures the ratio between the volume of a swollen gel and its volume in the unswollen state. Gel content of polymers has a significant impact on their properties [142], so its determination is crucial for effective control of the crosslinking process and quality assessment of the final products.

These tests can also be applied to polymer composites containing fillers, provided if the filler is insoluble in the solvent and if there is sufficient crosslinking to prevent the migration of the filler during the extraction as emphasized by the standard.

In this thesis, the tests were performed on the thermoset polymer in the specific formulations identified for the composite preparation, as well as on the resulting biobased composites.

There are three test methods according to D2765-16: Method A, that is the reference method, Method B, and Method C. The last is the one used in this thesis, and it involves extracting a single piece of material from solvent. This method provides extraction values from 3% to 9% lower than the reference method but allows for the determination of the swell ratio and the degree of crosslinking of a polymer is defined by percent extract, using solvent that attacks the non-crosslinked portion of the polymer. The percent extract is a measure of the amount of soluble polymer in the gel phase at the end of the immersion period, in absence of chemical degradation, a higher degree of crosslinking results in lower amount of percent extract.

The test was carried out following the standard indication. The bio-based photocured samples of crosslinked polymer were weighed and immersed in chloroform for 24 hours, ensuring that they were fully submerged in the solvent. Once verified that the solvent completely covered the specimens at the end of the immersion period, that is a necessary condition for the success of the test, they were removed from chloroform and then dried overnight in oven at 80 °C. Finally, the weight was evaluated and the percentage of extraction were calculated after these weight measurements and thus, the insoluble gel fraction in the material can be determined as the complementary value of the extract fraction, obtained by subtracting the extract fraction from 100%.

3.3. Mechanical tests

To evaluate the mechanical and viscoelastic properties of bio-based thermosets and composites obtained through 3D printing, tensile tests and Dynamic Mechanical Analysis (DMA) were performed. These tests provide essential parameters for characterizing a material and can yield important information regarding the material's reliability, strength, and response to various stresses. Through this evaluation, it is possible to determine whether the bio-based material is a suitable alternative to traditional synthetic materials and for which kind of applications.

3.3.1. Tensile test

The mechanical properties of polymer materials are often characterized using stress-strain testing, which measures parameters such as modulus of elasticity, yield strength, and tensile strength. However, these properties are highly sensitive to factors such as deformation rate and temperature, as well as the specific chemical environment [143].

Polymer materials can display three distinct types of stress-strain behaviour, ranging from brittle fracture to plastic deformation to completely elastic behaviour [143]. Thermoset polymers typically exhibit behaviour like that of brittle materials [144], although the specific shape of stress-strain curves can vary depending on the material formulation [145].

In Figure 36, there is the stress strain graph with some characteristic points, according to ASTM Designation: D638 – 14. The standard explains that tensile strength is the maximum tensile stress sustained by the specimen during the test. If it occurs at the yield point, it is designated tensile strength at yield, if it occurs at break, it is designated tensile strength at break. Yield strength, if present is defined as the stress at the yield point, the first point on the curve at which an increase in strain occurs without an increase in Stress.

Young modulus is defined as the ratio of stress (nominal) to corresponding strain below the proportional limit of a material.

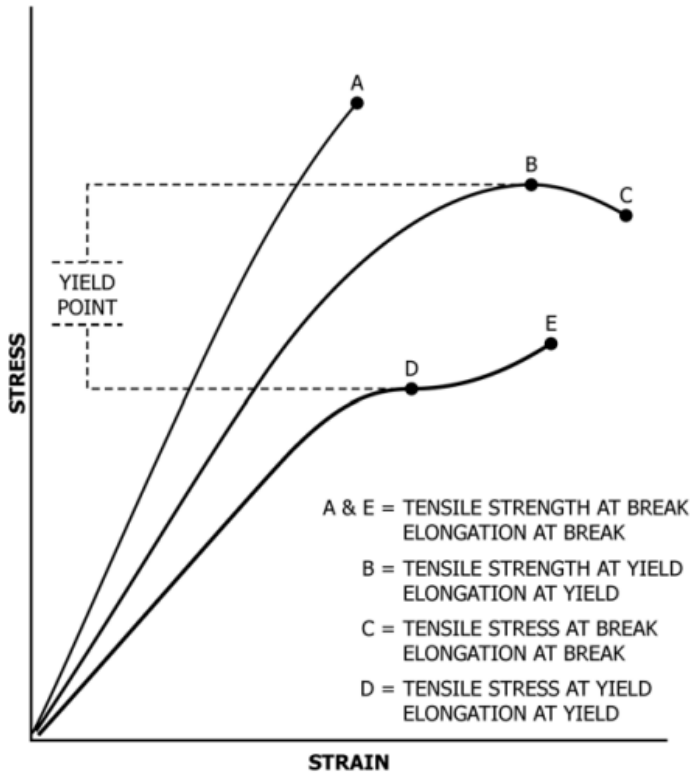

Figure 36. Stress strain graph with characteristic points according to ASTM Designation: D638 − 14

Yield strength, if present is defined as the stress at the yield point, the first point on the curve at which an increase in strain occurs without an increase in Stress. Tensile strength corresponds to the stress at which fracture occurs [143].
ASTM Designation: D638 − 14 provides standardized testing procedures for polymer materials, including five different types of test specimens, with the specific choice depending on the material and application at hand, in this thesis have been used specimen of the type 5 with gauge length of 26 mm, width of 4 mm and thickness of 2 mm.
The instrument used to perform tensile tests is shown in Figure 37. It is an Instron 5966, equipped with 2 kN pneumatic grips using a 2 kN load cell (<0.25% error), with a deformation rate of 5 mm/min and a grip separation of 50 mm. Deformation is calculated using a displacement transducer.

Figure 37. Instron 5966, instrument for the tensile test

3.3.2. Dynamic Mechanical Thermal Analysis

Dynamic Mechanical Thermal Analysis (DMTA) is a technique used to study the viscoelastic behaviour of the polymeric material and allows to determine storage modulus E' and loss modulus E'', and their ratio $\tan\delta$.

E' characterizes a material's ability to store elastic energy when exposed to a cyclic stress and is therefore a measure of its stiffness. Conversely, E'' measures the material's capacity to dissipate energy when exposed to a cyclic stress, for instance, by reducing vibrations. Instead $\tan\delta = E''/E'$ is a metric that reveals the amount of energy dissipated relative to the amount stored when the material is subjected to a cyclic stress [146]. The ability to store or dissipate energy in polymers depends on the Temperature, for this reason the minimum value of the tangent delta is typically observed at the T_g of the material. This occurs because the material becomes more viscous at temperatures below T_g, which reduces its ability to dissipate energy resulting in lower $\tan\delta$. In contrast, at temperature above T_g, the material becomes less rigid and more elastic, resulting in higher $\tan\delta$. Consequently, the minimum value of $\tan\delta$ represents the material's transition from an elastic to a viscous behaviour, T_g [146].

Therefore, DMTA peak in the $\tan\delta$ trend provides a more accurate determination of T_g respect to DSC, that gives the possibility to estimate this value like explained in 3.1.2. section.

There are various testing apparatus types to conduct DMTA, like torsion pendulum and torsional braid based on the free-vibration approach in which is recorded as a function of time at a constant temperature the damping of an oscillating bar or cylinder polymer sample. More recent instruments apply sinusoidal strain in form of tensile, flexure, compression, shear, or torsional stress can be in the form of tensile, flexure, compression, shear, or torsional stress to the sample and the stress response is recorded as a function of temperature at different frequencies [146].

In this thesis the examination was conducted using a Triton Technology DMTA device. The experiment was conducted under uniaxial oscillating stress with an amplitude of 1 N and a frequency of 1 Hz. The experiment was terminated once the material reached the rubbery plateau, a temperature range below its melting point where the modulus behaviour is nearly constant.

3.4. Measurement of viscosity

Viscosity is a very important parameter for a photocurable resin in a vat polymerization process, due to its influence on the printing parameters and consequentially on the printing time.

The viscosity of a fluid is measured using a viscometer, which comes in different types. Various types of viscometers are available to measure the viscosity of a fluid, all based on the common principle of measuring the fluid's resistance to motion. However, the method of achieving this measurement differs among different types of viscometers. Specifically, rotational viscometers measure the resistance of the fluid to the rotation of a body immersed in it, orifice viscometers measure the pressure required to flow the fluid through an orifice, and ball drop viscometers measure the time taken for a known amount of fluid to flow through a capillary.

The viscosity of the photocurable soybean oil resin formulations containing the two different diluents at different concentrations were measured using the instrument reported in Figure 38, a Brookfield DVE LV v 1.0.0 by AMETEK Brookfield. It is a rotational viscometer, equipped with an electric motor that spins a spindle inside the fluid being measured for viscosity. The spindle can have various shapes depending on the application, in the tests for this characterization the spindle s61 cylinder was used, the same reported in Figure 38.

Figure 38. Brookfield DVE LV v 1.0.0 viscometer by AMETEK Brookfield and its spindle s61

As the motor rotates the spindle, the viscometer measures the fluid's resistance to the movement through a torque sensor. The viscometer can operate at various speeds, but the measure is most accurate within a specific speed range, the ideal range of rotational speed for a specific fluid depends on its viscosity, with less viscous polymers generally requiring lower speeds. From the value of rotational speed and the respective shear stress value, result of the fluid opposition to motion, the viscosity value is revealed. It is important that shear stress never falls below 10%, or else the measurement becomes unreliable.

The samples were prepared using 500 mL beakers filled with 350 mL of resin. The beakers were positioned in front of the spindle of the viscometer, and the spindle was then immersed in the resin almost completely, leaving only one centimetre of the highest part of the cylinder outside the liquid. This was done to prevent interference with the measurement from the bottom of the beaker.

Once the spindle was properly positioned, the test began. First, the range of rotation speed suitable for the liquid being measured for the viscosity parameter was identified. The device used for testing assisted in this step by excluding speeds that were too low or too high, as indicated by a shear stress below 10 percent or a warning of measurement impossibility, respectively.

After identifying the appropriate range of speeds, data for speed, stress, and viscosity were revealed.

4. Materials and methods

4.1. AESO

The monomer of the bio-based photocurable resins prepared and tested in this thesis is Acrylated Epoxidized Soybean Oil (AESO). The synthesis of this monomer starts from the soybean oil, which is firstly epoxidized. The reaction can be carried out for example using the peracetic method, resulting in epoxidized soybean oil (ESO). The second step is the acrylation of ESO to obtain AESO that is performed by introducing acrylic acid, an unsaturated monomer, into the oxirane groups of ESO [147]–[149].
In Figure 39 [150] it is reported the chemical structure of acrylate epoxidized soybean oil.

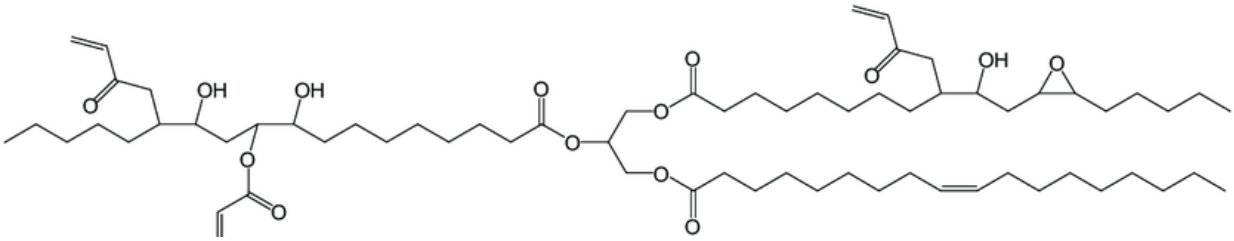

Figure 39. AESO chemical structure

Acrylate epoxidized soybean oil was purchased from Merck, it appears as a viscous liquid of yellow to amber colour, according to the supplier its density is 1.04 g/mL at 25 °C.

4.2. IBOMA

Iso bornyl methacrylate (IBOMA) is a monofunctional bio-based reactive diluent, originated from pine sap, its structure is in Figure 40. It was purchased from Merck, the density is 0.983 g/mL at 25 °C, is a transparent liquid with viscosity of 10-15 mPa·s and glass transition temperature of 170 ℃.
IBOMA is a monomer of methacrylic acid and can efficiently decrease the viscosity of the polymer solution. It is used in many patents to produce coatings and pressure sensitive adhesives and it can be potentially a substitute of methyl methacrylate or styrene as diluent. IBOMA is characterized by low viscosity and low shrinkage potential, this makes it also promising alternative to TEGDMA, a conventional diluent monomer used in dental resin formulations [151]–[153].

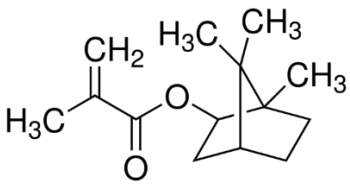

Figure 40. IBOMA chemical structure

4.3. THFA

Tetrahydrofurfuryl acrylate (THFA) is a bio-based acrylic monomer that contains a tetrahydrofuran ring in its chemical structure. Starting from biomass, cellulose, hemicellulose, and lignin can be obtained, then hemicellulose can be converted into THFA [154]. It is used as a monomer in the synthesis of acrylic resins, particularly to enhance the water resistance and toughness of acrylic resins. Additionally, THFA can be used as a diluent to reduce the viscosity of polymer solutions during the preparation of coatings, adhesives, and other resin-based products [155]–[157].
THFA was purchased for this thesis from Merck, it has a molecular weight of 156.18 and density of 1.064 g/mL at 25 °C, it is a transparent liquid, and its chemical structure is shown in Figure 41.

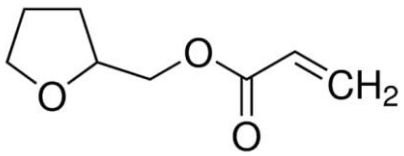

Figure 41. THFA chemical structure

4.4. Photo initiator: BAPO

Phenyl bis(2,4,6-trimethylbenzoyl) phosphine oxide, also known as bis acylphosphine oxides (BAPO), with the chemical structure reported in Figure 42 is a type of radical photo initiator commonly used in the photopolymerization of acrylate-based resins and coatings. BAPO offers high reactivity, low odour, and low toxicity. Its use has been reported in various applications including dental materials, printing inks, and electronics [158], [159].

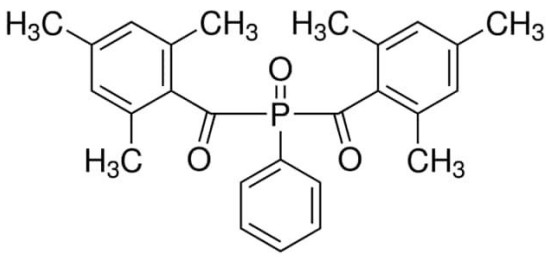

Figure 42. BAPO chemical structure

In Figure 43 [50] there is a comparison of some of the most used photo initiators, BAPO has certainly the bigger absorbance respect to all the others for each wavelength. In the same work by Lebedevaite and Ostrauskaite it is resulted the most efficient photo initiator due to the highly cross-linked network of AESO resin photopolymerized with BAPO [50].

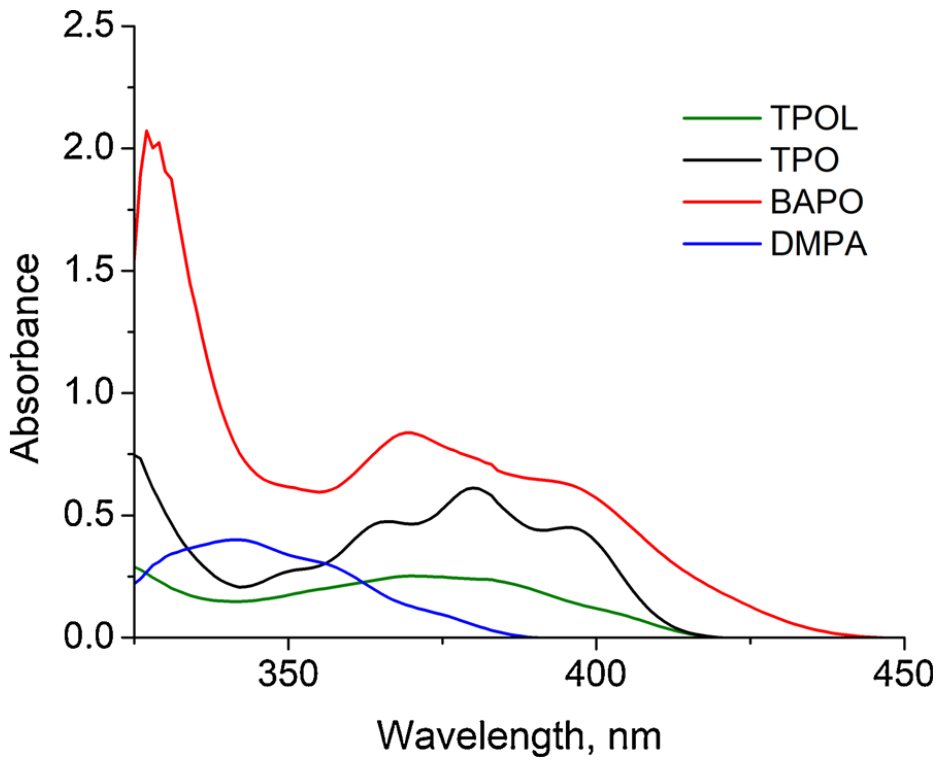

Figure 43. UV/VISIBLE spectra of photo initiators: TPOL, TPO, BAPO, and DMPA

4.5. Bio-fillers

GTF by AgroMateriae srl is a natural bio-filler derived from corn by-products, a yellow powder that can be used to enhance the sustainability and economic viability of traditional polymers and biopolymers and reinforcing their properties.

WPL-CF by AgroMateriae srl is a natural bio-filler Wine Plastics Filler (WPL-CF) by AgroMateriae srl is a red powder produced from grape pomace, the solid residue of grape pressing, a waste from the wine production, through environmentally friendly processes. It can be added in high concentrations (up to 60%) to several types of plastics and bioplastics.

These bio-fillers can be used to reinforce conventional polymers and bio-based polymers and to improve their sustainability and cost-effectiveness. Tables 2 and 3 report the supplier data sheets of these two bio-based fillers.

GTF and WPL-CF are typically used in concentrations from 5 to 40% (w/w), depending on the desired final properties. Notably, GTF and WTL-CF can serve as a natural colorant and simultaneously can reduce the costs and the carbon footprint through the replacement of equivalent amounts of polymer, at the same time the rate of biodegradation in biodegradable polymers increases.

In this research, each of the two bio-fillers was dried separately in an 80°C oven for 4 hours according to the manufacturer's recommendation. The bio-fillers were then added to their respective batches of photocurable soybean oil-based formulations in

a quantity of 5 wt.% relative to the total amount of the formulation, as per the experimental design.

Table 2. Typical properties of GTF filler by AgroMateriae srl

Typical properties	Typical Value	Unit	Test method
Agro-waste type	Corn by-products	-	-
Agro-waste origin	Emilia-Romagna (IT)	-	-
Physical Appearance	Yellow powder	-	-
Moisture content	< 3%	w/w	ISO 665-2000
Real particle density (23 °C)	1.436	g/ cm³	ISO 12154:2014
pH	5.0 ± 0.5	-	Internal procedure
Mean Particle size (d50)	18 ± 2	µm	Dry laser granulometry
Top cut size (d99)	72 ± 2	µm	Dry laser granulometry
Thermal Stability (T15)	266 ± 3	°C	TGA (in N2)
Renewable C content	44 ± 2	% w/w	Internal procedure
Renewable CHNO content	94 ± 2	% w/w	Internal procedure
Industrial Compostable	yes	-	EN 13423

Table 3. Typical properties of WPL-CF filler by AgroMateriae srl

Typical properties	Typical Value	Unit	Test Method
Agro-waste type	Wine by-products	-	-
Agro-waste origin	Emilia-Romagna (IT)	-	-
Physical Appearance	Purple/brown powder	-	-
Moisture content	< 3%	w/w	ISO 665-2000
Real particle density (23°C)	1.621	g/cm³	ISO 12154:2014
pH	3.5 ± 0.5	-	Internal procedure
Mean Particle size (d50)	14 ± 3	µm	Dry laser granulometry
Top cut size (d99)	49 ± 3	µm	Dry laser granulometry
Thermal Stability (T15)	271 ± 3	°C	TGA (in N2)
Renewable C content	38 ± 4	% w/w	Internal procedure
Renewable CHNO content	nd	% w/w	Internal procedure
Industrial Compostable	yes	-	EN 13423

4.6. 3D Printing Formulations

The scientific research for this thesis, once individuated the bio-based monomer was focused on bio-based reactive diluents that could be used to facilitate the 3D printing process of the AESO-based resin. Two reactive liquid diluents, iso bornyl methacrylate (IBOMA) and tetrahydrofurfuryl acrylate (THFA), were identified. After analysing the most suitable photoinitiators for AESO-IBOMA or AESO-THFA-based resins, BAPO was used as photoinitiator. Several formulations were prepared and examined to evaluate the properties of the materials changing the ratio between AESO and each one of the two diluents. The two bio-fillers derived from agro-food wastes (GTF and WPL-CF) were used for the preparation of the polymeric composite formulations.
In total eight different formulations of resin were prepared, which are summarized in Table 4.

Table 4. Resin formulations

	AESO in wt.%	Diluent in wt.%	BAPO in wt.%
AESO + IBOMA	90	10	2
AESO + IBOMA	80	20	2
AESO + IBOMA	70	30	2
AESO + IBOMA	60	40	2
AESO + IBOMA	50	50	2
AESO + THFA	90	10	2
AESO + THFA	80	20	2
AESO + THFA	70	30	2
AESO + THFA	60	40	2
AESO + THFA	50	50	2

The 90:10 formulations for both the diluents were prepared but they resulted too much viscous, and not able to be printed.
Additionally, four different formulations of composites were prepared, by adding 5wt.% of the two bio-fillers, as reported in Table 5.

Table 5. Composite formulations

	AESO wt.%	Diluent wt.%	BAPO wt.% + diluent	Bio-filler wt.%
AESO + IBOMA + GTF	60	40	2	5
AESO + IBOMA + WPL-CF	60	40	2	5
AESO + THFA + GTF	60	40	2	5
AESO + THFA + WPL-CF	60	40	2	5

4.7. 3D Printing and post curing

The photocurable formulations were printed using two different 3D printers. Initially, tests to print the resins were performed using a Formlabs Form2 printer by Formlabs, but the printer parameters could not be changed. For research scope, it was more suitable a so-called open parameter 3D printer and subsequently a Phrozen Sonic Mini 8K printer was used. In addition, an Anycubic Wash & Cure Plus by Anycubic was used for post-curing. process

In Figure 44 the Phrozen Sonic Mini 8K by Phrozen is depicted, a vat polymerization 3D printer LCD Type, or MSLA. The size of this printer was small, with a volume of 29 (L) x 29(W) x 43H cm and a weight of 13 kg.

Figure 44. Phrozen Sonic Mini 8K by Phrozen

This made it both space-saving and useful for research purposes, as the small size of the resin vat allows for using a small quantity of resin. Therefore, it is possible to perform printing tests without the concern of preparing excessive amounts of resin or wasting feedstock material. The Light Source is a Linear Projection LED Module, which has xy resolution of 22 µm, while z resolution or Layer Thickness is in the range 0.01-0.30 mm, the printing volume is 16.5 (L) x 7.2(W) x 18(H) cm.

This manufacturer provides as slicer software CHITUBOX V1.9.0 or above versions. By means of this software it is possible to load the STL file of the part into the printing volume, choose the orientation of the piece, and apply supports that connect the piece to the printing platform.

There are several options available for adjusting the printing parameters, among them, it is possible to choose and size the supports for the parts to be printed. These support structures can be very specific and offer a wide range of possibilities in terms of shape, thickness, and density.
The printer from Phrozen has free parameters, and the Chitubox program allows for the modification of all printing parameters as shown in Figure 45, between them there are layer thickness, or thickness of the slicing, called “Layer Height”, the exposure time and the velocity of the platform during the process.

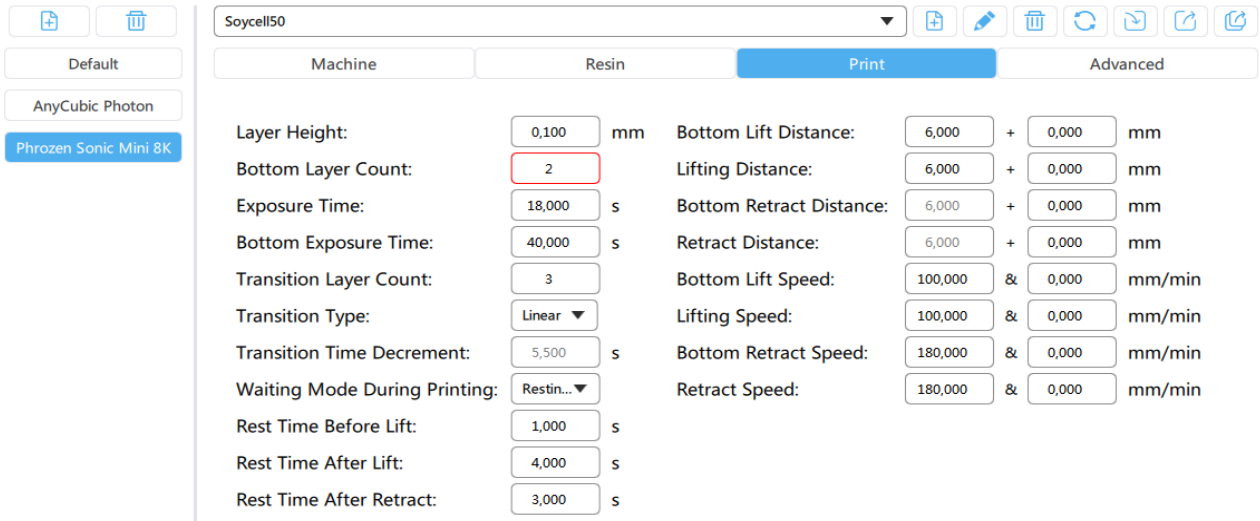

Figure 45. Chitubox window for adjusting printing parameters.

After setting the appropriate parameters, slicing can be performed to generate the file ready for printing. The generated print file can be transferred to the printer using a USB flash drive, and process can be initiated via the 3.5" Touch Panel display present on the printer.
The Anycubic Wash & Cure Plus, in Figure 46, is the tool used for washing and curing the printed parts. It uses a 405nm UV lamp for post-curing, and it is possible to choose between the two washing and curing modes using the dedicated button. By using the knob, it is possible to adjust the curing and washing time, which is displayed on an LED indicator. The process duration can be selected between 1 minute to 60 minutes.

Figure 46. Anycubic Wash & Cure Plus by Anycubic

The Wash and Cure plus machine is a desktop unit, which has dimensions of 290 mm (L) x 270 mm (W) x 479 mm (H) and a weight of 6.5 kg. The washing basket dimensions are 192mm (L) x 120 mm (W) x 290 mm (H), while the dimensions for the suspension cleaning are 92 mm (L) x 120 mm (W) x 235 mm (H).

5. Preparation and 3D printing of the resins

Through a comprehensive review of the relevant literature, the components of the resin required for 3D printing using the Vat polymerization technique were identified. Initially, the Form2 printer from Formlabs, which is an SLA printer that does not allow for changes in printing parameters, was used. However, considering the specific objectives of this thesis study, it was deemed more advantageous to have the ability to modify the printing parameters. Consequently, the Sonic Mini 8k from Phrozen was subsequently employed.

Various photocurable resin formulations were prepared for both composite materials and thermosets. In Table 6 the resins are listed with their respective resin formulation acronym formed by the initial of the monomer, AESO slash separated from two initials for the specific diluents used, IBOMA or THFA separated by a slash and with the respective percentages by weight, separated by colons. For the bio-based composites, the numbers of the initial letter of the bio-fillers are added together with their percentage. In both thermosets and composites, the percentage of BAPO is not indicated, as it is always 2% by weight of the sum of diluent and monomer. These acronyms will be used to refer to the resins and composites.

Table 6. Resin and composite acronyms

AESO 80% + IBOMA 20% + BAPO	A/IB 80:20
AESO 70% + IBOMA 30% + BAPO	A/IB 70:30
AESO 60% + IBOMA 40% + BAPO	A/IB 60:40
AESO 50% + IBOMA 50% + BAPO	A/IB 50:50
AESO 80% + THFA 20% + BAPO	A/TH 80:20
AESO 70% + THFA 30% + BAPO	A/TH 70:30
AESO 60% + THFA 40% + BAPO	A/TH 60:40
AESO 50% + THFA 50% + BAPO	A/TH 50:50
AESO 60% + IBOMA 40% + BAPO + GTF (5%)	A/IB 60:40 g5
AESO 60% + IBOMA 40% + BAPO + WPL (5%)	A/IB 60:40 w5
AESO 60% + THFA 40% + BAPO + GTF (5%)	A/TH 60:40 g5
AESO 60% + THFA 40% + BAPO + WPL (5%)	A/TH 60:40 w5

Multiple attempts were made to refine both the resin preparation technique and identify the most suitable printing parameters.
The printability of each resin was first verified, and the corresponding printing parameters were established. Subsequently, minimizing the presence of air bubbles was identified as a crucial element, as their presence had the potential to jeopardize the success of the mechanical testing phase of the printed samples.

5.1. Preparation of the resins

The resins were prepared according to the formulations described in Table 6, where it can be noticed that the percentage of the photo initiator is 2 wt.% of the total weight for each formulation.

The easiest way to incorporate the right quantity of photo initiator was by dissolving it in the two diluents, which are the least viscous liquids involved in the formulations. Consequently, the first step of the preparation was the dispersion of the photo initiator in the reactive diluent. It was observed for both the diluents that when the photo initiator was uniformly dispersed, the result is a yellow-coloured liquid without suspended particles like shown in Figure 47.

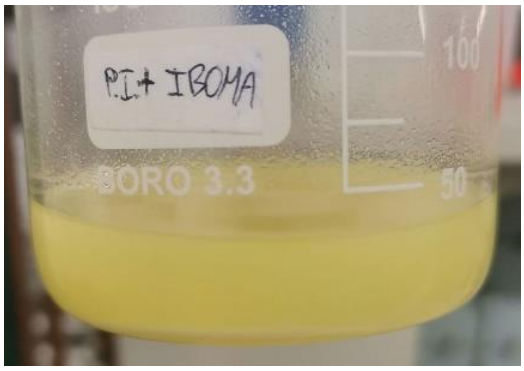

Figure 47. BAPO dissolved in IBOMA

The addition of the third reactant, AESO, is much simpler and faster if the diluent and photo initiator mixture is properly prepared. Magnetic stirrers were used to facilitate the dispersion process of the photo initiator, which takes less time in THFA (approximately from one to two hours) respect to IBOMA (four or five hours). However, the process can be accelerated by alternating stirring with immersing the beaker with the materials in water in ultrasound instrument for about 15 minutes every 30 minutes. The mechanical effects of ultrasound vibrations and the heating of the liquid facilitate a faster dispersion process.

Upon completion of the dispersion, AESO was added, and the mixing was performed manually with the assistance of ultrasound. The application of heat and vibrations facilitated the fluid becoming homogeneous Serving to make the process less time-consuming. After an initial manual mixing, the beaker was left in ultrasound for approximately half an hour, then manually mixed again, and finally left in ultrasound for another half an hour. This process was repeated until the fluid turned in a yellow colour, without any suspended particles, signs of turbidity, or air bubbles for both IBOMA and THFA formulations, like reported in Figure 48, which shows the resin A/TH 70:30 immediately after the preparation and ready for the 3D printing process.

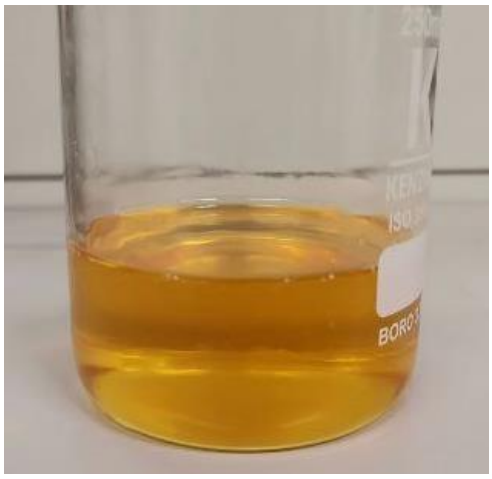

Figure 48. Resin A/TH 70:30

Formulations with THFA more easily achieve the desired homogeneity and clarity condition. The mixing process, alternated with the use of ultrasound for 30-minute intervals, was repeated two or three times for THFA formulations, while for IBOMA formulations the process was generally repeated 4 or 5 times.
Both formulations are prone to the formation of air bubbles, and ultrasound was found to be the most effective method to remove them. However, any agitation or stirring of the resins could result in the formation of air bubbles, particularly in the case of the IBOMA resin formulations.
Initially, mixtures containing 90% by weight of AESO and 10% of IBOMA, as well as mixtures of 90% by weight of AESO and 10% of THFA, were attempted. However, the resulting resins were too viscous, they showed little difference compared to pure AESO in term of viscosity. As a result, the 80:20 mixtures were identified as the ones with the least amount of diluent and suitable for LCD 3D printing.
Starting form Ai8020 and At8020, prepared and then printed with the definitions of the printing parameters, the others resin formulations were prepared by gradually increasing the diluent percentage. Each resin was obtained, and its parameters were printed and defined before moving on to the production of the next one, starting from IBOMA resins, in the following order:
Ai8020, Ai7030, Ai6040, Ai5050, At8020, At7030, At6040 and At5050.
From the perspective of resin preparation, it was observed that THFA is a diluent that dissolves the AESO more rapidly than IBOMA. THFA promotes easier dispersion of the photoinitiator too and the formation of air bubbles is significantly reduced compared to IBOMA. As the percentage of diluent increases, there is a lower tendency for the formation of air bubbles in THFA and the same applies to the IBOMA-based resin.

5.2. 3D printing of the resins

Various printing tests were carried out to optimize the printing parameters and to assess how well the resins adapted to this 3D printing process by LCD. For all resins, the first printing attempt when a new resin was poured into the tank for the first time, was a sample to check the printing resolution of a dental resin. This sample is very thin and rich in details, and based on its definition, modifications can be made to the parameters related to the resin resolution.

The specimen for the resolution test is shown in Figure 49, it is the result of irradiation parameters refining for A/IB 70:30.

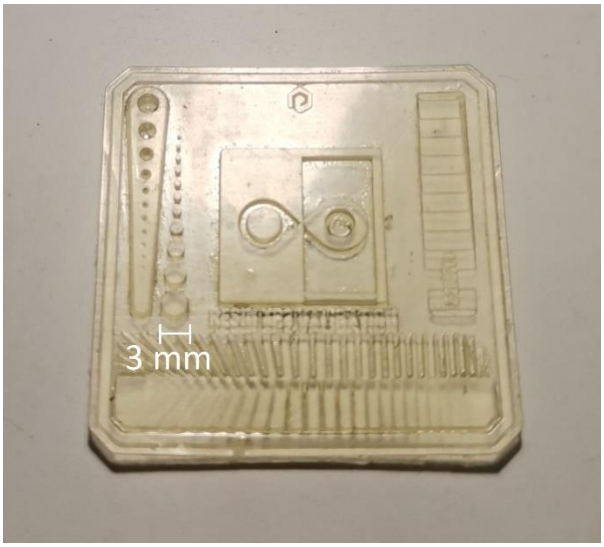

Figure 49. Test for resin resolution of A/IB 70:30

Through this type of preliminary printing test, the irradiation time values were refined for each polymer.

Subsequently, dog bone-shaped samples type 5 of tensile stress tests designation a rectangular specimen were printed. These samples were initially printed using supports, allowing the optimal printing parameters to be refined. These parameters, in addition to ensuring good resolution of the final object resulting from the previous test, also enabled the construction of supports that could bear the weight of samples built with overlapping layers, even with larger surface areas or heavier pieces and under different inclination conditions.

However, for DMA and tensile, it was necessary to print samples without any defects that could interfere. The presence of supports inevitably generates some marks on the surface that is connected to the base attached to the printing plate. Therefore, samples attached to the plate and without supports were printed using the parameters established from previous tests, considered definitive.

Figure 50 shows dog bone-shaped sample of A/TH 70:30 as printed with supports, while Figure 51 shows the same samples of A/TH 70:30 but printed attached to the

plate. It is evident that there are visible marks due to the detachment of the piece from the supports in the former. These marks were minimized as much as possible, but it was still preferred to print samples attached to the plate and then remove them delicately to obtain smooth and almost perfect surfaces.

Figure 50. Sample of A/TH 70:30 printed with supports

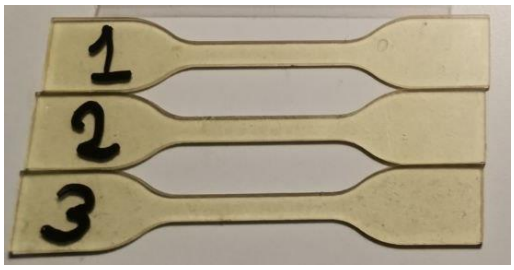

Figure 51. Sample of A/TH 70:30 printed attached to the printing plate

The printing parameters obtained through the described process are reported in Table 7 for A/IB resins and in Table 8 for A/TH resins.

Table 7. A/IB resins printing parameters

	A/IB 80:20	A/IB 70:30	A/IB 60:40	A/IB 50:50
Layer height (mm)	0,1	0,1	0,1	0,1
Exposure time (s)	10	8	12	14
Bottom exposure time (s)	40	30	30	35
Rest time before lift (s)	3	3	0	0
Rest time after lift (s)	25	18	4	3
Rest time after retract (s)	15	10	3	3
Bottom lift distance (mm)	20	15	7	5
Lifting distance (mm)	20	15	6	5
Bottom retract distance (mm)	20	15	7	5
Retract distance (mm)	20	15	6	5
Bottom lift speed (mm/min)	60	80	60	80
Lifting speed (mm/min)	60	80	60	80
Bottom retract speed (mm/min)	160	180	150	160
Retract speed (mm/min)	160	180	150	160

Table 8. A/TH resins printing parameters

	A/TH 80:20	A/TH 70:30	A/TH 60:40	A/TH 50:50
Layer height (mm)	0,1	0,1	0,1	0,1
Exposure time (s)	15	15	18	18
Bottom exposure time (s)	40	40	40	40
Rest time before lift (s)	3	0	0	1
Rest time after lift (s)	40	7	5	4
Rest time after retract (s)	10	4	3	3
Bottom lift distance (mm)	15	8	6	6
Lifting distance (mm)	15	8	6	6
Bottom retract distance (mm)	15	8	6	6
Retract distance (mm)	15	8	6	6
Bottom lift speed (mm/min)	50	80	90	100
Lifting speed (mm/min)	50	80	90	100
Bottom retract speed (mm/min)	140	160	170	180
Retract speed (mm/min)	140	160	170	180

Upon observing Tables 7 and 8, it is noticeable that higher diluent weight decreases printing times, despite larger amounts of AESO making the resin slightly more reactive, as evidenced by the small difference in irradiation times.
To overcome the high viscosity of resins with higher AESO content, it was necessary to increase the intervals between the irradiation of one layer and the next to allow the resin to flow into the areas of the vat left empty and to drip off from the polymerized resin attached to the platform, especially when the STL model presents dense structures like supports or when there are regions inside the part that need to remain empty, otherwise the definition and resolution of these areas would be poor. This increase in times is evidenced by all the lower values of the platform movement velocity and the by larger rest position waiting intervals in higher AESO content in A/TH and A/IB resins. These times had greater impact on the final time compared to the small differences in irradiation times.
The A/TH resin printing times are lower than A/IB resins because THFA has a higher diluent effect.
With these parameters, it is possible to print objects with complex shapes and excellent definitions, as shown in Figure 52.

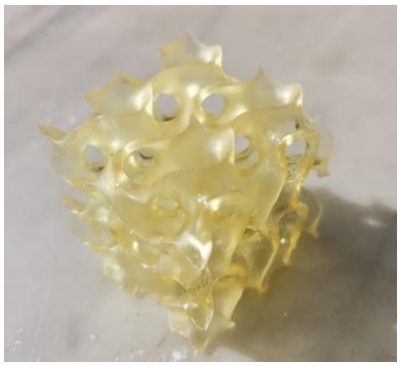

Figure 52. Gyroid cube printed with A/IB 50:50

The strength of the supports that hold objects of the order of magnitude of the printing volume of the used device has been verified.
After the printing process, all the obtained parts were subjected to post-curing for 10 minutes per side after being washed in water using an ultrasonic bath for a period of 5 minutes.
However, to further characterize the thermosetting polymer materials, certain samples were deliberately left uncured for testing purposes.

5.3. Preparation of the bio-based composites

After establishing the printing parameters and characterizing the materials with respect to their properties, the focus shifted towards the preparation and printing of composite materials.

A/IB 60:40 and A/TH 60:40 was selected based on printability test results.

Compatibility tests between the two fillers were then carried out.

The test involved dispersing 5% by weight of each filler in 5 ml resin samples, followed by manual mixing and sonication for about an hour. Through the vibrations and heating, the resins appeared homogeneous, with a yellow colour for GTF and a purple colour for WPL-CF. The appearance of the resin was monitored every hour to evaluate the sedimentation of the powder. After 4 hours, the liquid composites remained homogeneous as shown in Figure 53 and Figure 54.

Figure 53. Resin sample of A/IB 60:40 charged with 5% in weight of WPL-CF after 4 hours

Figure 54. Resin sample of A/TH 60:40 charged with 5% in weight of WPL-CF after 4 hours

After 8 hours, the liquid samples were still coloured, but the surface had a colour lighter than the bottom. Finally, after 24 hours, the difference in colour of the resin sample became slightly more pronounced, and the presence of sedimented powder became evident for the first time.

Considering a reasonable processability interval of 6-8 hours without remixing the resin, a weight percentage of 5% was deemed appropriate. Increasing the percentage would have further decreased this time window and risked obtaining a piece with a variable filler density along the length of the part in case of printing of larger parts.

5.4. 3D printing of the composites

To verify the printability of the composites formulations the same process to define the printing parameters was used, however in this case the first try was close to the result due to the possibility to use the parameters of resins not loaded.
The printing parameters obtained through the described process are reported in Table 9 for all the composites.

Table 9. Composites printing parameters

	A/IB 60:40 g5	A/IB 60:40 w5	A/TH 60:40 g5	A/IB 60:40 w5
Layer height (mm)	0,1	0,1	0,1	0,1
Exposure time (s)	18	18	25	25
Bottom exposure time (s)	40	40	45	45
Rest time before lift (s)	3	3	5	5
Rest time after lift (s)	8	8	8	8
Rest time after retract (s)	6	6	6	6
Bottom lift distance (mm)	8	8	8	8
Lifting distance (mm)	8	8	8	8
Bottom retract distance (mm)	8	8	8	8
Retract distance (mm)	8	8	8	8
Bottom lift speed (mm/min)	50	50	70	70
Lifting speed (mm/min)	50	50	70	70
Bottom retract speed (mm/min)	130	130	150	150
Retract speed (mm/min)	130	130	150	150

The irradiation times are lightly higher respect to A/IB 60:40 and A/TH 60:40 due to the dye effect of the filler, less light penetrates.
Additionally larger time intervals for rest position and lower velocities for the platform have been used because of filler effect on resin density.
There is no difference between the parameters used for a composite based on the same diluent but with different fillers.
After the printing process is complete, all composite material parts undergo a post-curing treatment of 10 minutes on each side. Following this, the test specimens were washed for 5 minutes in an ultrasonic bath filled with water.

6. Results

6.1. Viscosity tests result

The viscosity of photopolymer resins has a critical role in the success of 3D printing processes, affecting flow characteristics and uniform layer thickness. The addition of reactive diluents to photopolymer resins can significantly influence viscosity and ultimately impact printability. By measuring the viscosity of various photopolymer formulations with differing reactive diluent contents, it is possible to identify which are more easily usable and printable prior to 3D printing.

The results of viscosity measurements are represented in Table 10 for resins with IBOMA and in Table 11 for resins with THFA.

Table 10. A/IB formulations viscosity

	A/IB 80:20		A/IB 70:30		A/IB 60:40		A/IB 50:50	
Spindle speed rotation (RPM)	Shear (%)	Viscosity [cP]	Shear (%)	Viscosity [cP]	Shear (%)	Viscosity [cP]	Shear (%)	Viscosity [cP]
20	/	/	/	/	/	/	69,80	209,4
12	/	/	/	/	38,40	463	41,50	207,5
10	/	/	/	/	38,40	463,2	34,60	207,6
6	/	/	/	/	38,40	459	20,50	205
5	/	/	92,6	1154,00	38,40	460,8	17,10	205,2
4	/	/	76,90	1154,00	30,60	459,00	13,40	201,00
3	/	/	57,50	1150,00	23,00	460,00	10,10	202,00
2,5	/	/	48,00	1152,00	19,10	458,40	/	/
2	92,90	2787	38,40	1152,00	15,30	459,00	/	/
1,5	70	2788	28,70	1148,00	11,50	460,00	/	/
1	46,40	2784	19,30	1158,00	/	/	/	/
0,6	27,80	2780	11,60	1160,00	/	/	/	/
0,5	23,10	2772	/	/	/	/	/	/
0,3	13,90	2780	/	/	/	/	/	/

Table 11. A/TH formulations viscosity

	A/TH 80:20		A/TH 70:30		A/TH 60:40		A/TH 50:50	
Spindle speed rotation (RPM)	Shear (%)	Viscosity [cP]	Shear (%)	Viscosity [cP]	Shear (%)	Viscosity [cP]	Shear (%)	Viscosity [cP]
100	/	/	/	/	/	/	98,6	59,16
60	/	/	/	/	/	/	58,4	58,4
50	/	/	/	/	/	/	48,5	58,2
30	/	/	/	/	65,90	131,6	28,70	57,4
20	/	/	/	/	43,40	130,2	18,50	55,8
12	/	/	67,50	337	25,30	126,5	10,80	54
10	/	/	56,20	337,2	21,10	126,6	/	/
6	/	/	33,50	335	12,50	125	/	/
5	/	/	27,90	334,8	10,30	123,6	/	/
4	85,20	1278	22,20	333	/	/	/	/
3	64,00	1280	16,70	334	/	/	/	/
2,5	53,30	1279	13,80	331,2	/	/	/	/
2	42,60	1278	11,10	333	/	/	/	/
1,5	32,00	1280	/	/	/	/	/	/
1	21,30	1278	/	/	/	/	/	/
0,6	12,80	1280	/	/	/	/	/	/
0,5	10,60	1272	/	/	/	/	/	/

THFA has a higher dilution capacity than IBOMA, from this tables it is evident the higher viscosity of the polymers with IBOMA in their composition, consequentially also the conditions of the measurements are different respect to A/TH resins.
In vat polymerization 3D printing, the optimal viscosity range of a resin is typically set between 800 and 900 cP. However, some resins such as A/IB 80:20, A/IB 70:30, and A/TH 80:20 that exceed this range can still be successfully printed using the 3D LCD technique, albeit with longer printing times.

6.2. 3D printing results

Having found the appropriate printing parameters for each of the formulations with varying weight percentages of monomer and each of the diluents, numerous specimens were printed, some rectangular in shape, while others were dog bone shaped as indicated by ASTM standard.

The identified printing parameters allowed for the printing of all test specimens, even with the use of support structures. Figure 55 shows images of all these specimens with their supports and the base attached to the plate.

Figure 55. Specimens of A/IB 70:30 with their supports and the bases attached to the printing platform

Given that these parameters have also been refined based on the definition of printing details, these resins can be used to produce parts with complex and detail-rich shapes, even on a very small scale, on the order of millimetres. Figure 56 shows a gyroidal cube that has been 3D printed using the A/TH 60:40 polymer and Figure 57 illustrates the same printed object with its supports attached to the base. Its complex geometry and characteristic dimension of 10 cm make it unlikely to be produced using non-additive manufacturing techniques.

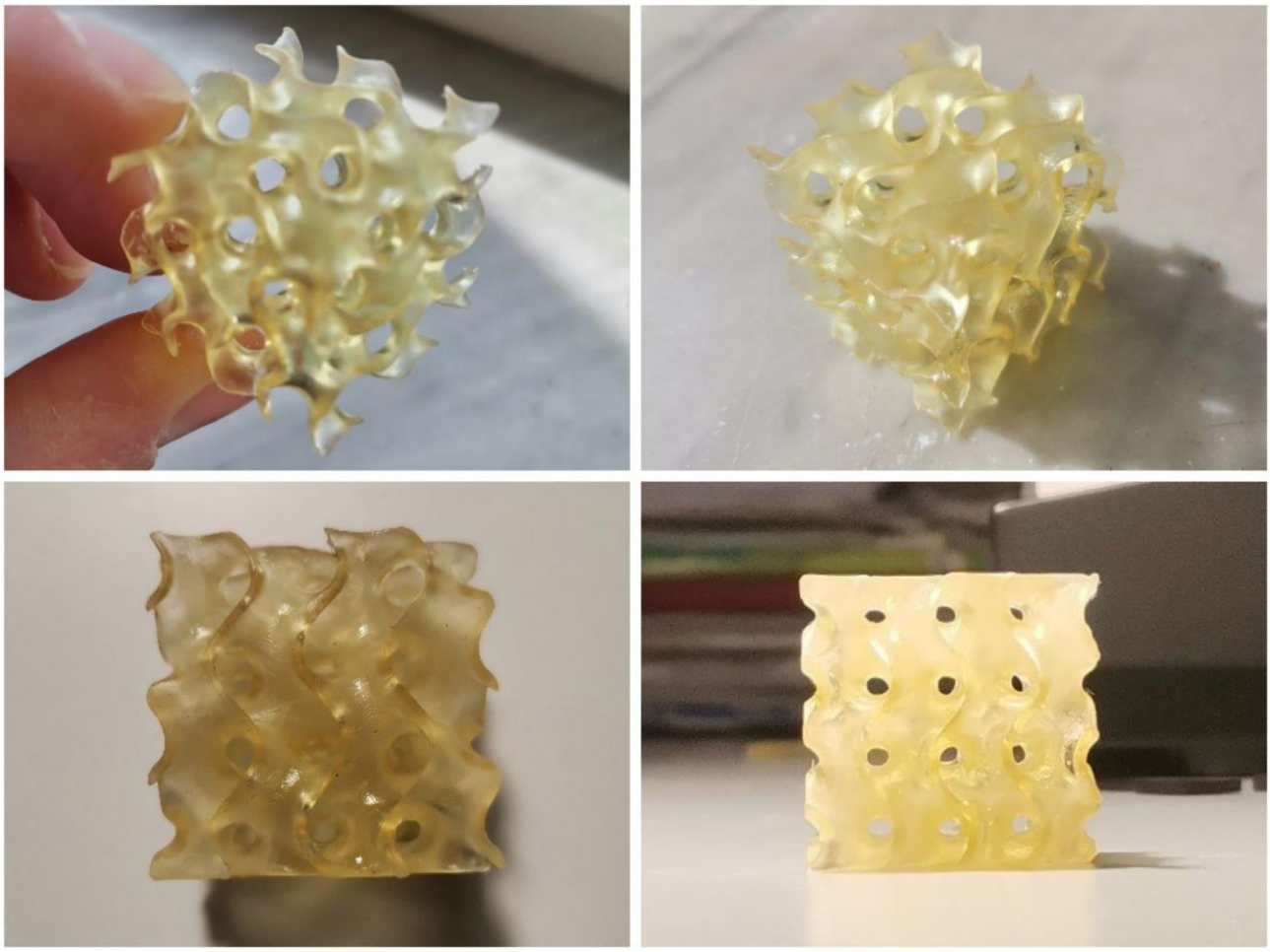

Figure 56. Gyroidal cube, a complex shape 3D printed with A/IB 50:50

Figure 57. Gyroidal cube in A/IB 50:50 with its supports attached to the base

In Figure 58 it is reported a model of a bevel gear 3D printed in A/IB 50:50. In this case the dimensions involved are very limited, the central hole diameter is 3 mm and the height of the part is 5 cm. The result is precise, confirming the good resolution obtained with this 3D printing parameters and using this LCD 3D printer.

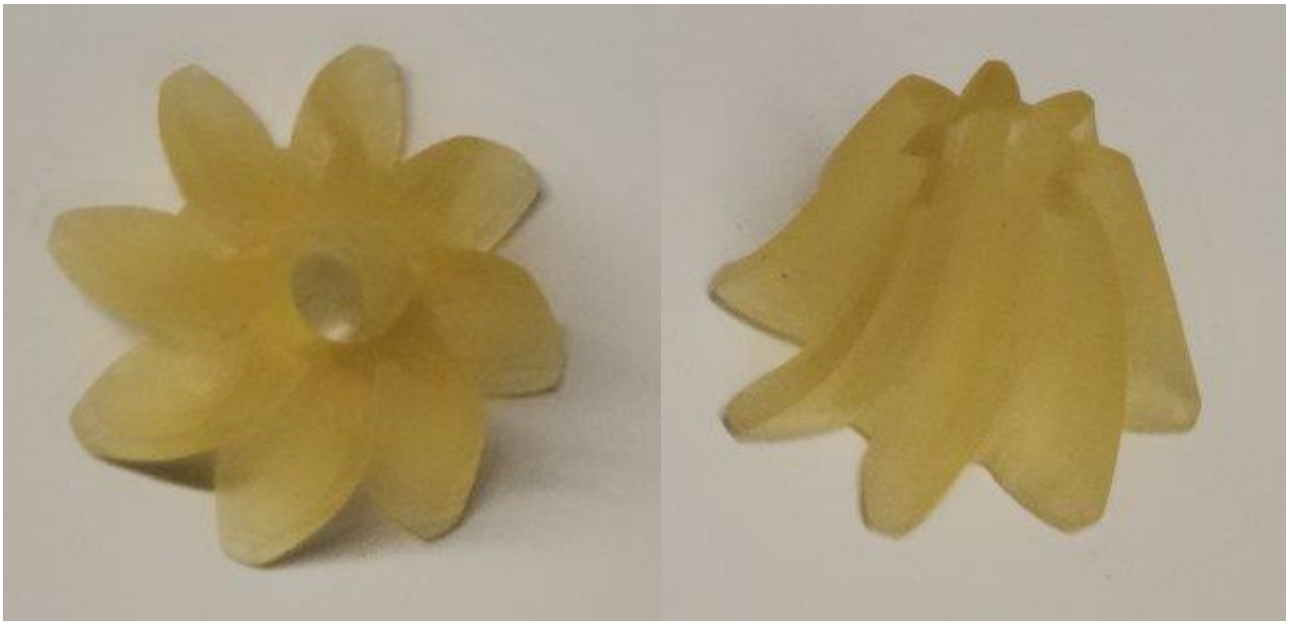

Figure 58. Bevel gear 3D printed in A/IB 50:50

The printing parameters for bio-based composites were also refined to meet the requirements for both resolution and detail, as well as strength and support definition. In this case, both bone-shaped and rectangular test samples attached to the print bed were printed, resulting in very smooth and precise surfaces. Furthermore, using support structures, test samples for the resolution validation were printed to refine resolution, the results are reported in Figure 59 and Figure 60.

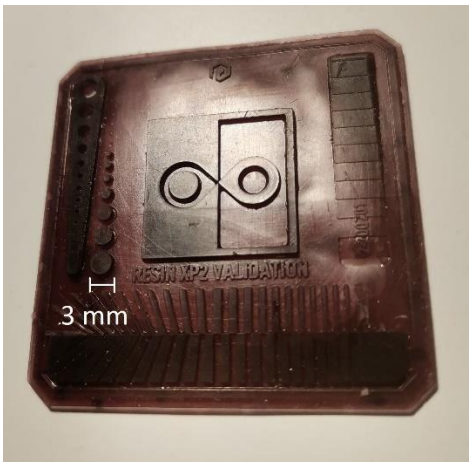

Figure 59. Test for resin resolution of A/IB 60:40 w5

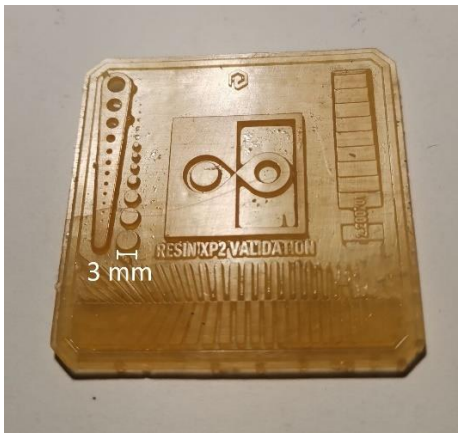

Figure 60. Test for resin resolution of A/TH 60:40 g5

In Figure 61 and Figure 62, the specimens for the tensile tests with gauge length of 26 mm and the rectangular specimens with dimensions 25 mm (L) x 10 mm (W) x 2 mm (T) printed with composite materials can be seen.

Figure 61. Tensile test specimen in A/IB 60:40 g5 and rectangular specimen in A/IB 60:40 w5

Figure 62. Rectangular specimen in A/TH 60:40 g5 an tensile test specimen in A/TH 60:40 w5

With A/IB 60:40 g5, A/TH 60:40 g5, A/IB 60:40 w5 and A/IB 60:40 w5 composites, it is possible to print complex-shaped objects made of bio-based polymer material, the first two are yellow coloured and the second two are purple coloured. The rotor printed in Figure 63 with the maximum external diameter of 3 cm has been printed with A/IB 60:40 g5.

Figure 63. Rotor printed in A/IB 60:40 g5

The printing times are another interesting result to understand how the various printing parameters affect the duration of the process. Times of the process are presented in form of time to print one layer with thickness of 0,1 mm in the table 12 and they were computed by factoring in the platform's submersion time, pause duration, and irradiation of a normal internal layer of the piece, as well as the lift time with waiting periods after irradiation and rest times following retraction, all starting from the retracted position.

Table 12. Printing time for each layer

	Printing time for a layer of 0,1 mm [min]
A/IB 80:20	1,80
A/IB 70:30	1,19
A/IB 60:40	0,62
A/IB 50:50	0,52
A/IB 60:40 w5	1,03
A/IB 60:40 g5	1,03
A/TH 80:20	1,95
A/TH 70:30	0,73
A/TH 60:40	0,64
A/TH 50:50	0,62
A/TH 60:40 w5	1,07
A/TH 60:40 g5	1,07

6.3. Gel content test results

The test to determine the percentage of gel has been performed on two groups of material sample formed by the four composites and the resins A/IB 60:40 and A/TH 60:40 obviously after post-curing to notice the percentage of crosslinked material. The results are given in Table 13.

Table 13. Gel content test results

		Gel percentage
First group	A/IB 60:40 g5	97,99%
	A/TH 60:40 g5	99,05%
	A/TH 60:40 w5	99,25%
	A/IB 60:40 w5	96,87%
	A/IB 60:40	99,11%
	A/TH 60:40	99,60%
Second group	A/IB 60:40 g5	98,03%
	A/TH 60:40 g5	98,61%
	A/TH 60:40 w5	98,87%
	A/IB 60:40 w5	97,26%
	A/IB 60:40	99,33%
	A/TH 60:40	99,16%

The gel percent value calculated as: $\left(1-\frac{W_i-W_f}{W_i}\right)\times 100$, where W_i is the initial weight of the sample, before the test and W_f is the final weight of the sample, after the test and drying in oven. The gel percentages obtained as the average of the results of the two tests performed for each thermoset and for each composite are reported in the Table 14:

Table 14. Gel percentage of composites and thermosets

	Gel percentage
A/IB 60:40 g5	98,01%
A/TH 60:40 g5	98,83%
A/TH 60:40 w5	99,06%
A/IB 60:40 w5	97,07%
A/IB 60:40	99,22%
A/TH 60:40	99,38%

6.4. DSC results

The results of the DSC tests carried out on samples of post-cured and non-post-cured thermosets and post-cured composites are shown in the graphs in this section.
In Figure 64 are reported the DSC curves of A/IB 50:50 of both post-cured and not post-cured.

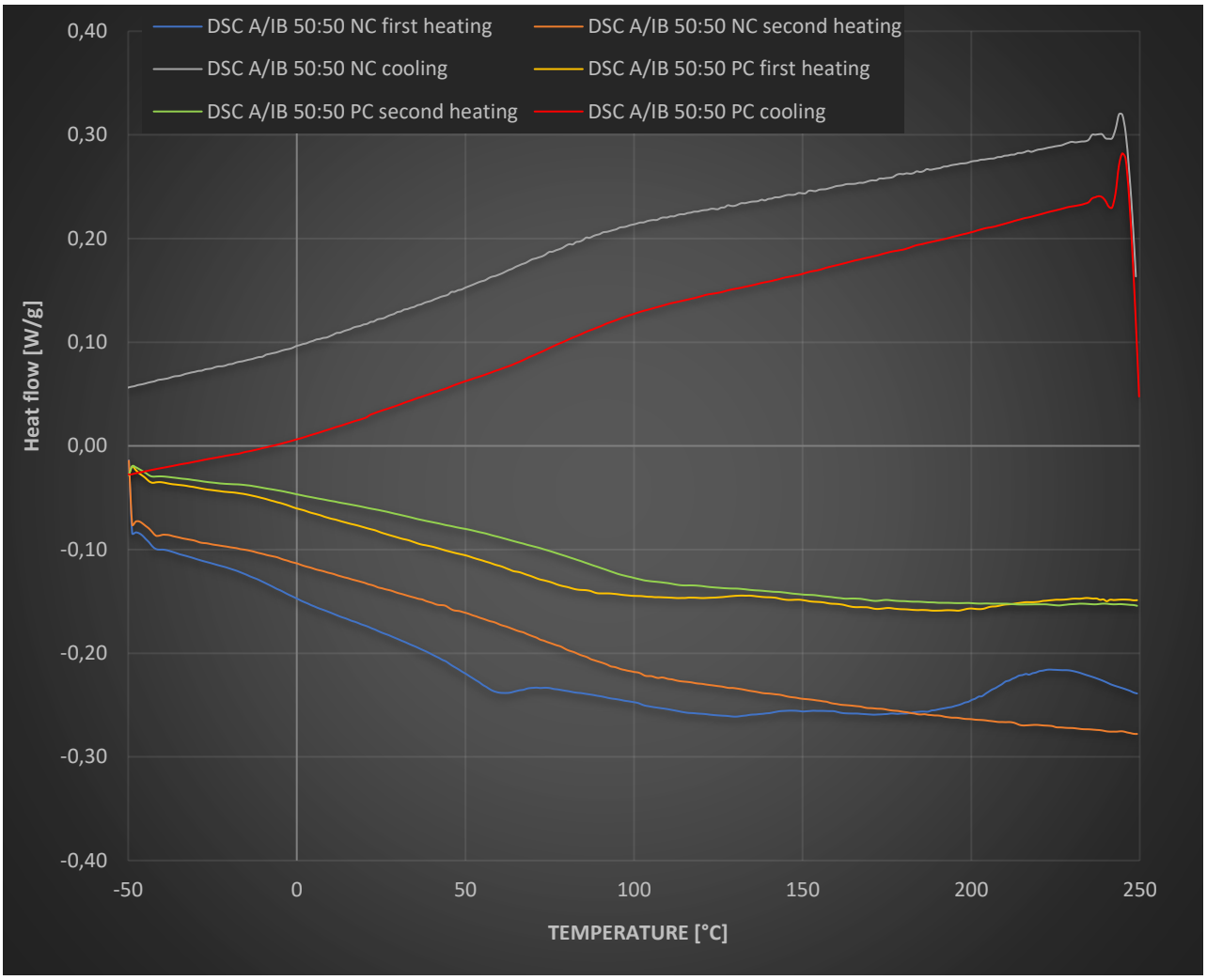

Figure 64. DSC curves for A/IB 50:50 post-cured and not post-cured

It can be immediately noticed that the A/IB 50:50 not post-cured sample undergoes an exothermic peak around 220 °C during the first heating and this peak is absent in all other curves.
The peak indicates that a curing reaction leading to the formation of cross-linking between the polymer molecules has occurred. During the curing reaction, chemical energy is released in the form of heat, which is detected as a peak in the DSC curve. This happens only for this sample because it is non-post-cured, and therefore, a portion of the material has not undergone cross-linking. In contrast, in post-cured samples, the fraction of cross-linked polymer is almost 100%, and this curing reaction

triggered by the temperature does not occur. The same applies to the second heating, where there is no curing reaction and hence no peak since the sample has become cross-linked after the first heating. The absence of an exothermic peak demonstrates that the post-cured polymer has a percentage of cross-linked material very close to 100%, thus confirming the data obtained from the insoluble fraction percentage or gel content test.

Another characteristic, in this case common to all the curves in the graph, is their first change in slope that can be observed at a temperature higher than 50°C but lower than 75-80°C. A change in slope of the DSC curve is evidence of a variation in the specific heat of the material, and the variation of this quantity is a signal of the transition from the glassy state to the rubbery state, the glass transition, therefore at this temperature range, there should be the T_g.

In figure 65 the comparison between not post-cured and post-cured samples has been evaluated in the case of the other diluent, in particular, with A/TH 80:20 resin.

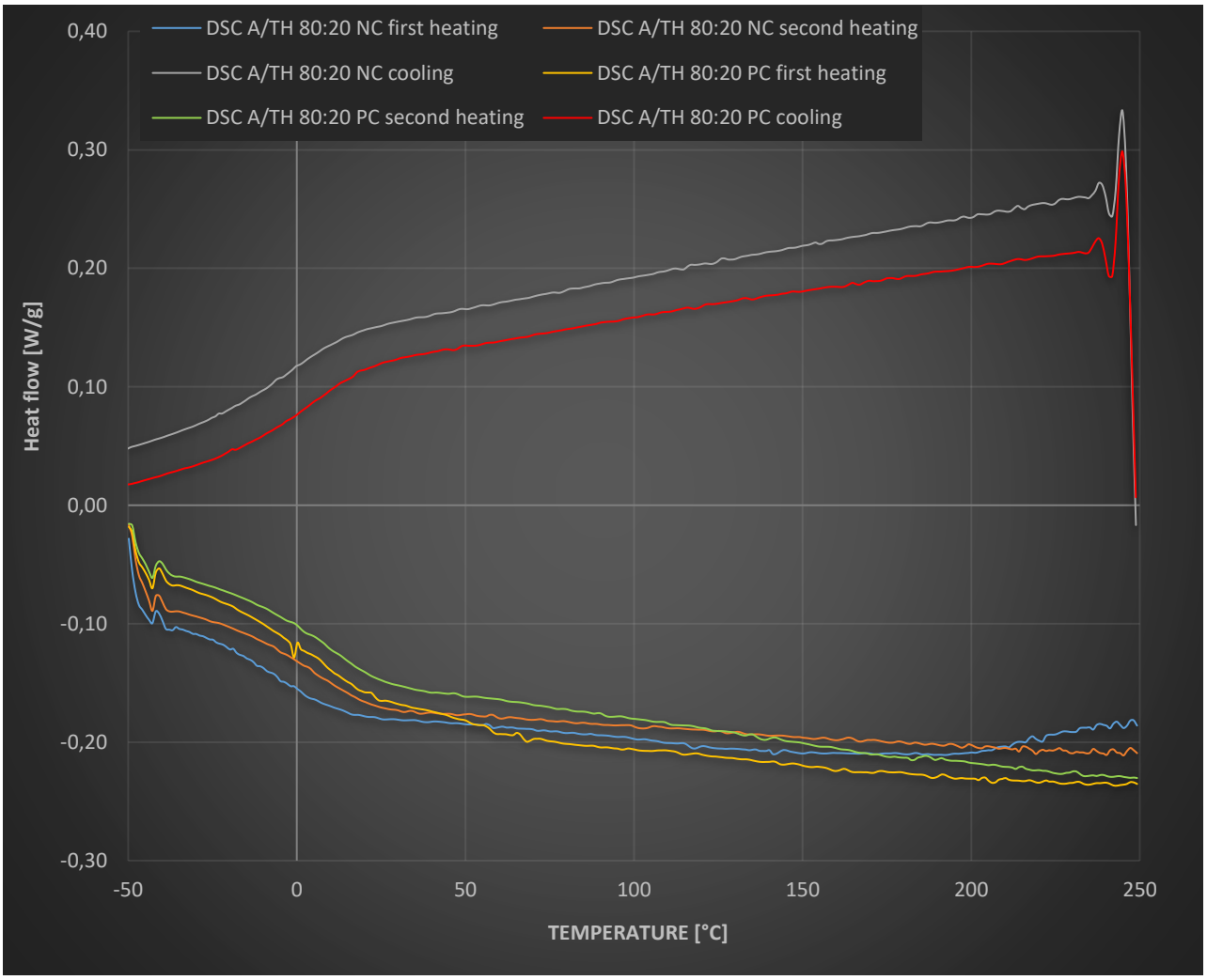

Figure 65. DSC curves for A/TH 80:20 post-cured and not post-cured

With A/TH 80:20 as well, it is clear the presence of the exothermic peak due to curing reaction activation around 210 °C in the first heating and its absence in the other curves in which the curing reaction has been completed or by the first heating or by the post-curing. In this case too, there is consistency with the results of the gel content test.
Additionally, T_g in the polymer with THFA as diluent has a lower value, the change in slope of the curves is exhibited a range between 10 °C and 25-30 °C.
A more direct comparison to evaluate the differences in the curves of two different polymer types, A/IB and A/TH, is shown in the Figure 66, where both the first heating and cooling of post-cured and non-post-cured A/IB 70:30 and A/TH 70:30 are visible.

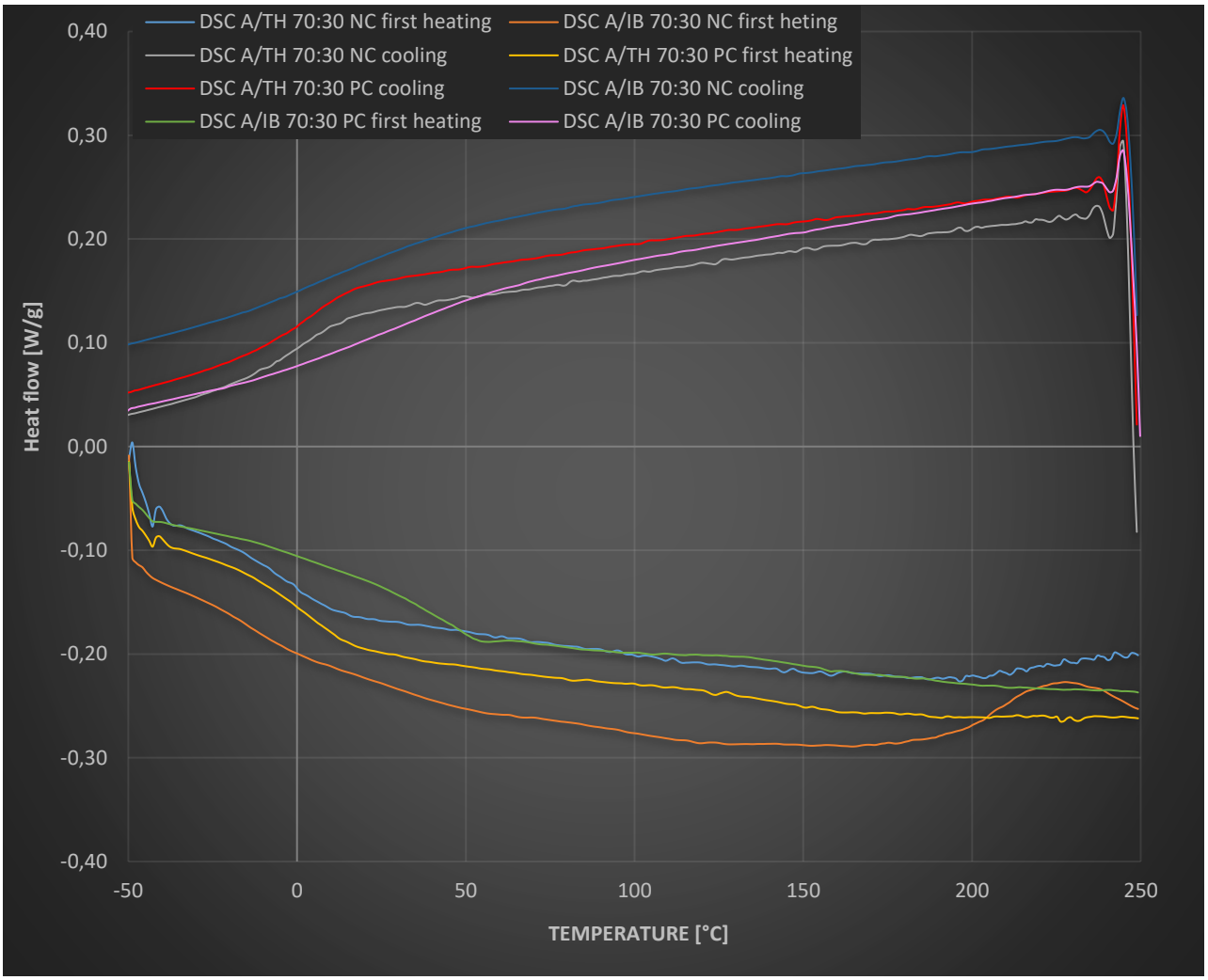

Figure 66. Comparison between DSC curves of A/IB 70:30 and A/TH 70:30

The findings obtained from examining Figures 64 and 65 are consistent with the trend depicted in Figure 66, in fact the change in slope and therefore the T_g for the polymers with IBOMA occurs at higher temperatures respect to THFA diluent-based thermosets. For the former, it is between 60 and 80 °C, while for the latter, it is between 5 °C and 25 °C. Again, the exothermic peak is visible only in the curves related to the first heating of non-post-cured samples.
Finally, the DSC results for the composites are in Figures 67 and 68, they are reported together with the reference thermoset used for the composite formulations, respectively A/IB 60:40 and A/TH 60:40.
All composites were characterized only after post-curing, therefore in the DSC graphs only the trends of the first and second heating and cooling for post-cured composites and post-cured thermoset polymers without bio-fillers are shown.

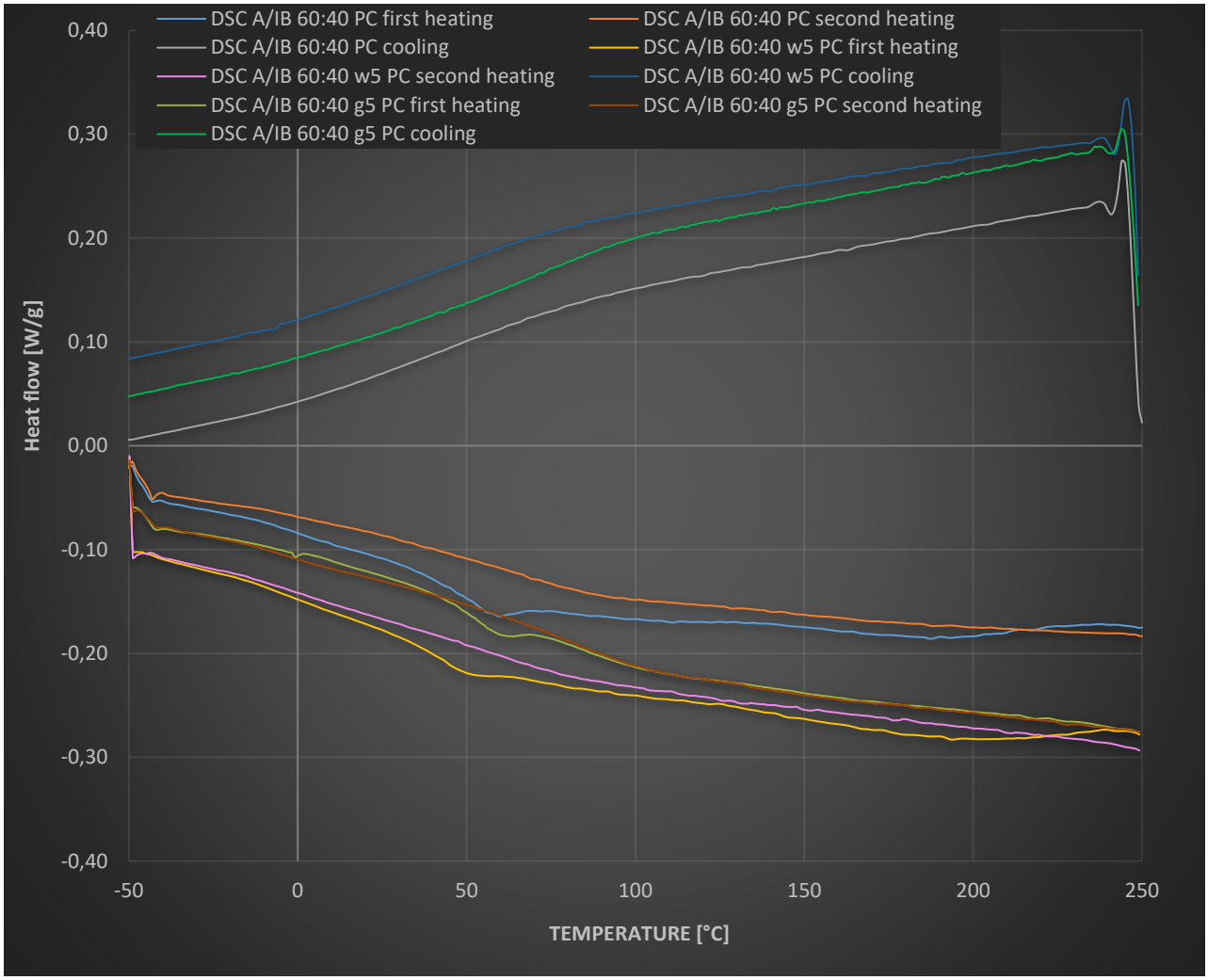

Figure 67. DSC curves for composites A/IB 60:40 w5 and A/IB 60:40 g5 compared with A/IB 60:40

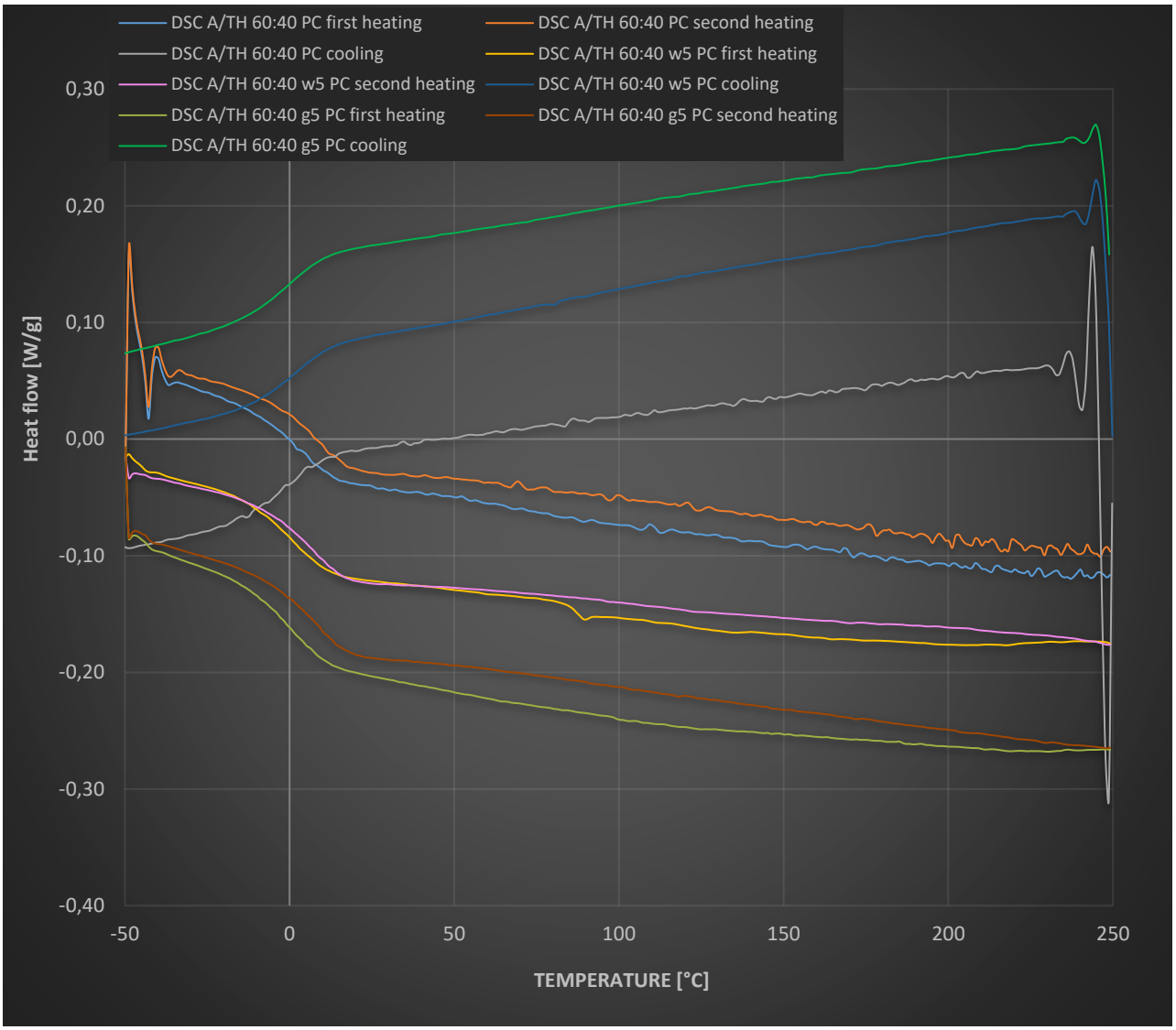

Figure 68. DSC curves for composites A/TH 60:40 w5 and A/TH 60:40 g5 compared with A/TH 60:40

Compared to the unloaded polymer, the composites formed with both base resins do not appear to have a different transition value.

From the observation of the DSC test results, it can be asserted that the glass transition temperature of the AESO and THFA-based polymer is around 10°C, while the AESO and IBOMA-based polymer shows a change of slope in the heat flow trend correspondent to T_g at around 75°C and it was not evident any significant change in these values with varying weight percentages of the diluents.

6.5. TGA results

This section presents the findings of the TGA analysis carried out by using the Mettler-Toledo instrument, with results exported via the included software.

Firstly, from the thermograms and the DTGA curves reported in Figure 69 and Figure 70, which show the curves obtained for A/IB 50:50 post-cured and non-post-cured, respectively, and the curves of A/TH 80:20 post-cured and non-post-cured, it can be observed that there are no significant differences in the thermal behaviours of samples with the same chemical composition, whether subjected to post-curing or not. Post-curing does not have any effects on the thermal properties. Therefore, the subsequent considerations were based on the results obtained on post-cured specimens.

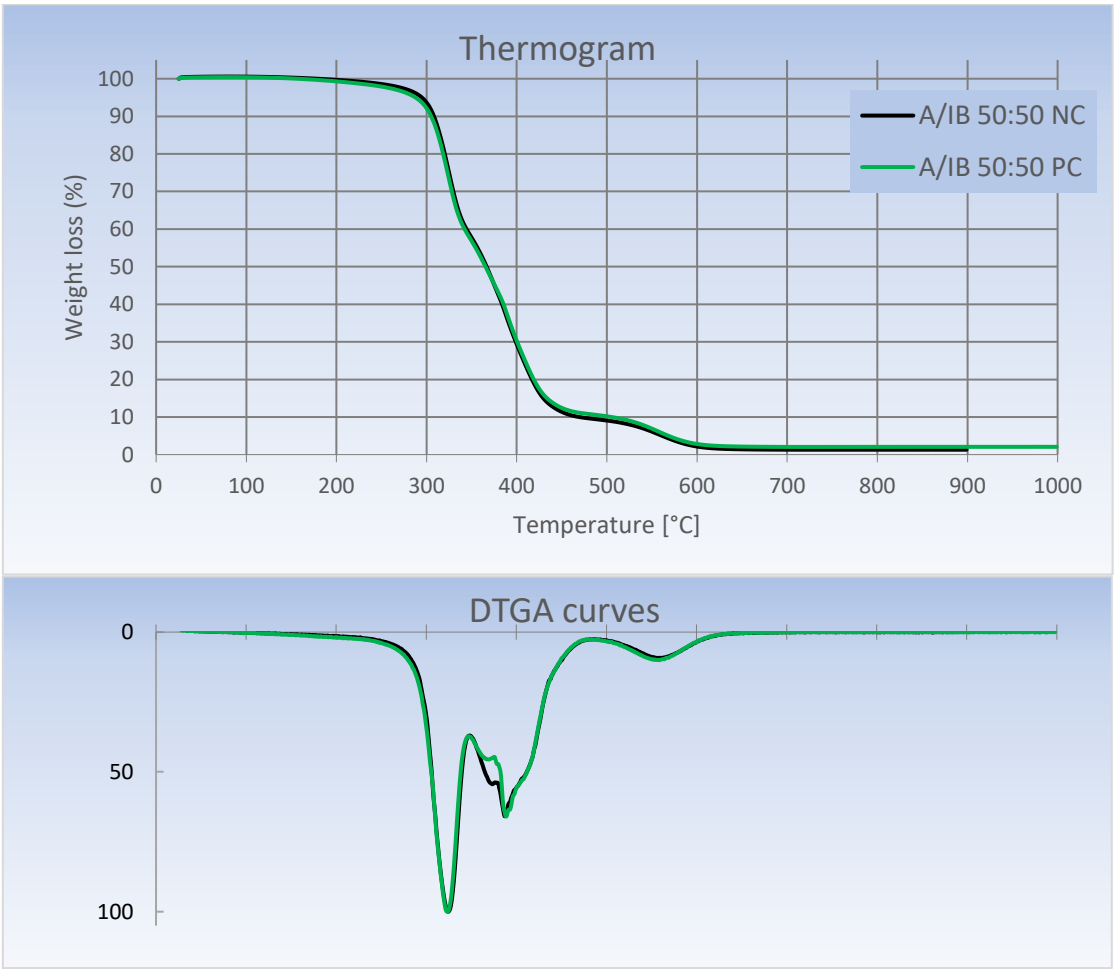

Figure 69. Thermogram and DTGA curves for A/IB 50:50 non-post-cured and post-cured

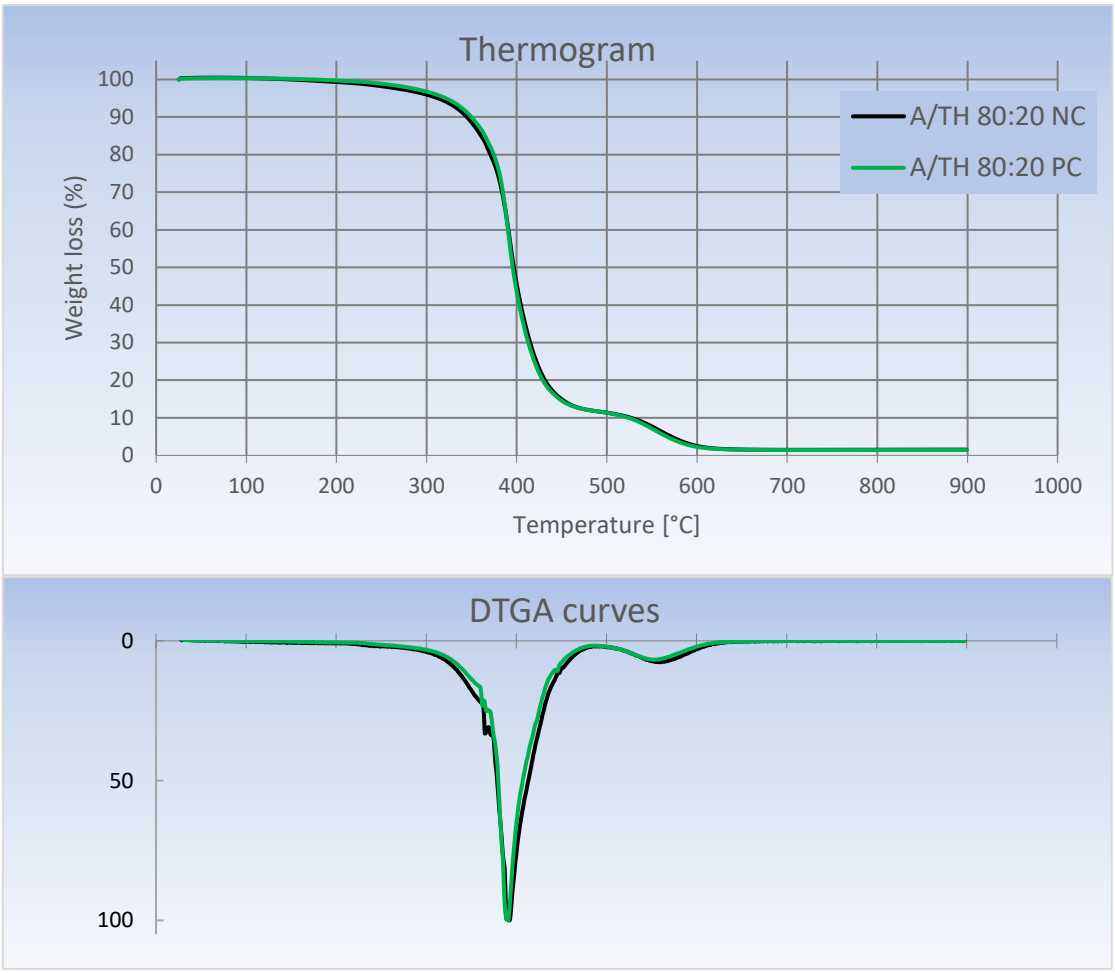

Figure 70. Thermogram and DTGA curves for A/TH 80:20 non-post-cured and post-cured

Differences in the degradation behaviours of the two polymers can already be observed. The A/IB 50:50 polymer shows the maximum degradation rate at a temperature of 325 °C. In fact, the percentage weight loss immediately after 300 °C for the A/IB polymer shows a more significant slope compared to the THFA polymer, whose weight loss derivative instead shows a maximum at 389°C.

For each resin containing IBOMA or THFA as diluent, this section presents two thermograms and the DTGA graphs, as shown in Figure 71 and Figure 72 that allow for a comparison of the curve trends as the percentage of AESO and reactive diluent varies.

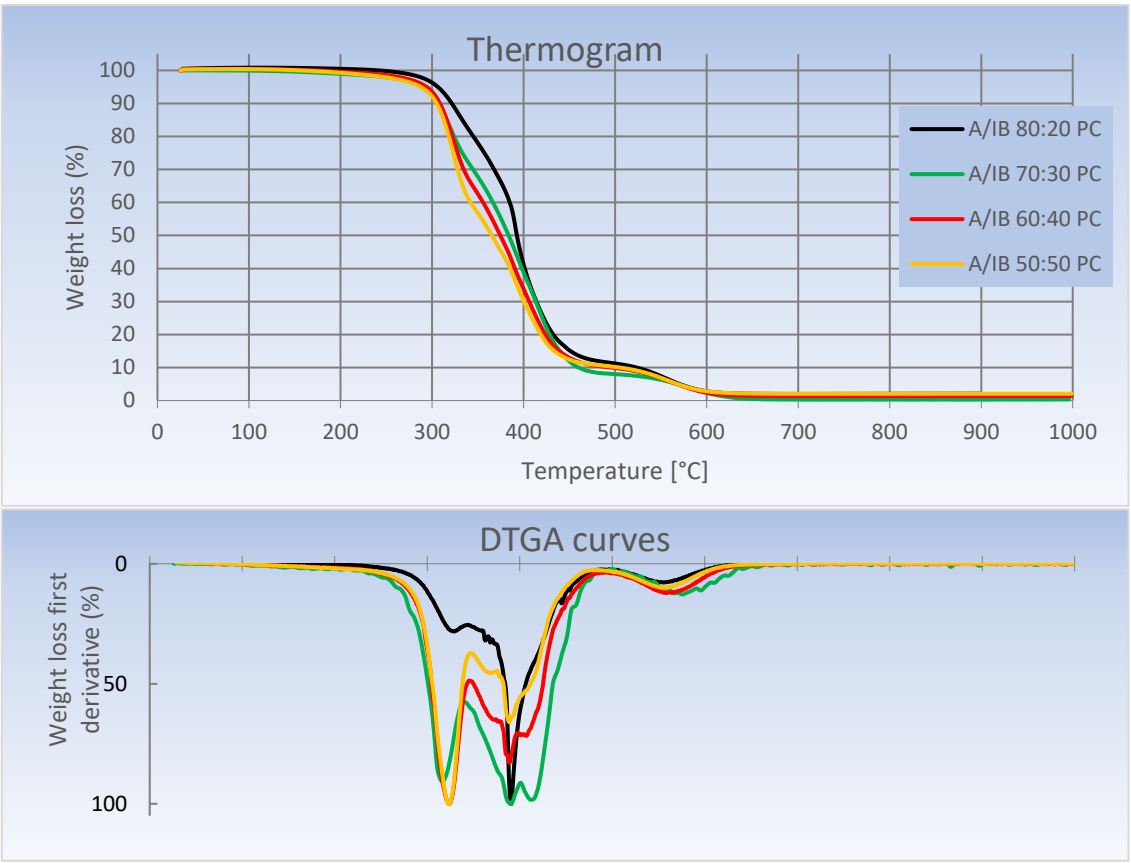

Figure 71. Thermogram and DTGA graph comparing the curve trends of resins A/IB resins as the percentage of AESO and reactive diluent varies.

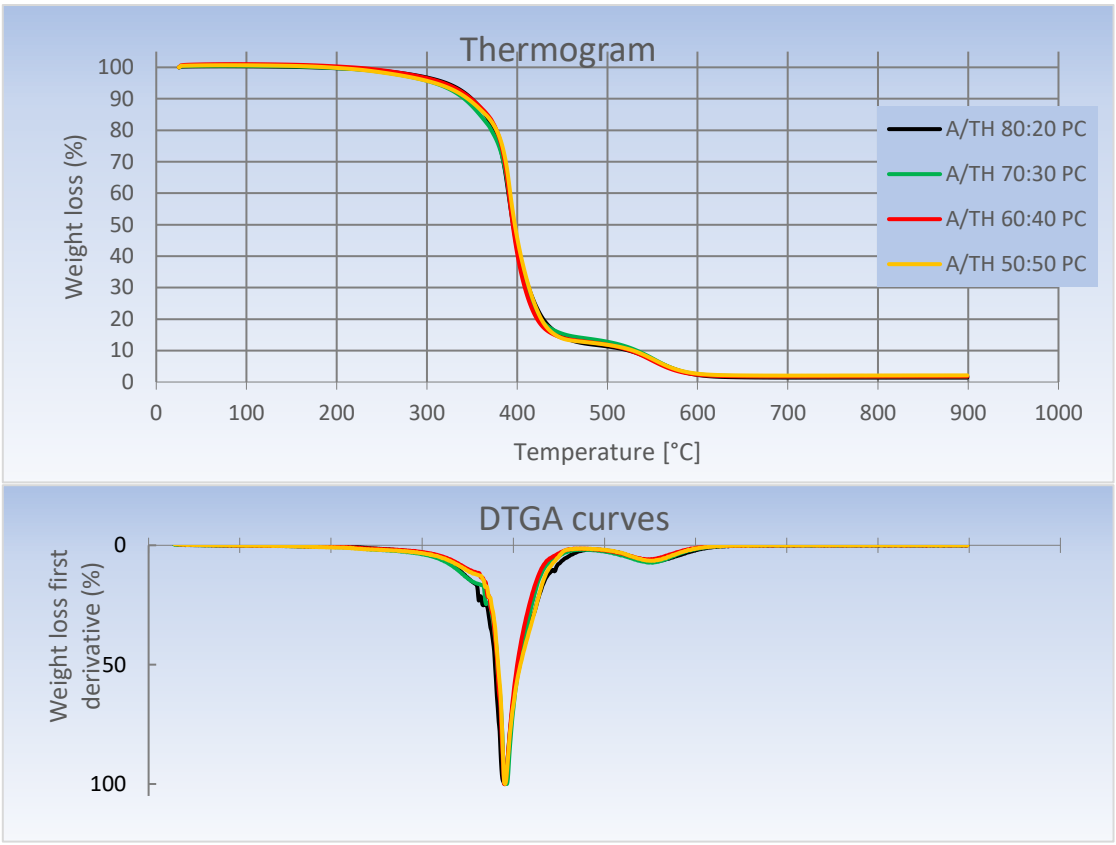

Figure 72. Thermogram and DTGA graph comparing the curve trends of resins A/TH resins as the percentage of AESO and reactive diluent varies.

These trends confirm the presence of a maximum in the weight loss derivative around 325°C in polymers with IBOMA, which is not present in the DTGA curve of polymers with THFA. Furthermore, decreasing the IBOMA percentage the peak became smaller, this can confirm that it is linked to the presence of IBOMA.

It can be observed for A/TH thermosets that the different weight ratios of AESO and THFA affect the degradation behaviour and its derivative significantly less.

To better notice the differences in curve behaviours for resins based on different diluents, Figure 73 can be examined, which shows the TGA results for two resins with 60% AESO but different diluents.

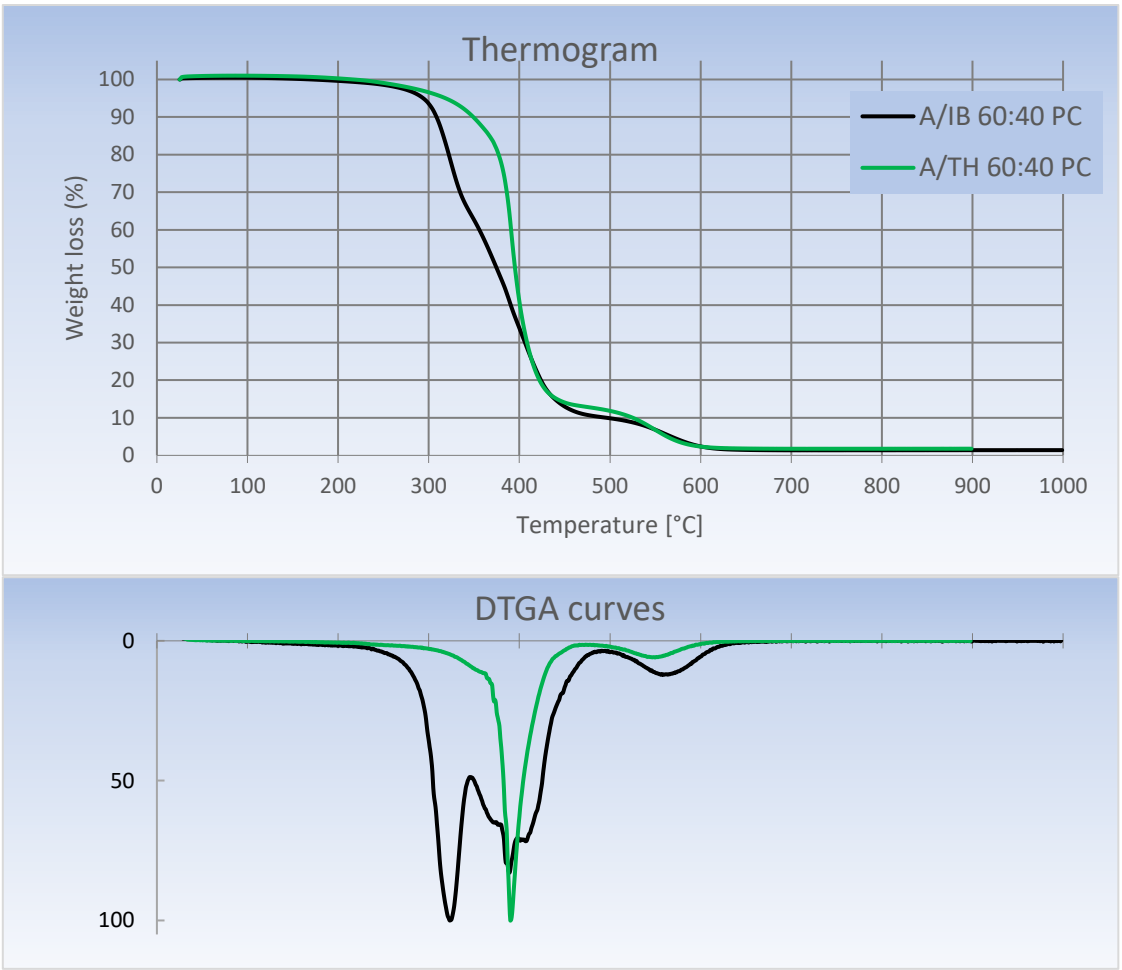

Figure 73. Comparison of TGA and DTGA curve trends for A/IB 60:40 and A/TH 60:40

The two degradation paths exhibit the bigger difference in their trend between 300 and 400 degrees. Notably, at around 370 degrees, there is a significant variance in the proportion of degraded polymer, with A/IB 60:40 experiencing approximately 40% degradation, compared to the THFA-based thermoset which experiences only 10% degradation. Furthermore, when considering both DTGA curves on a single graph, it becomes apparent that A/TH 60:40 does not exhibit a degradation peak at temperatures below 350 degrees.

The last graphs show the thermal behaviours of the bio-based composites containing IBOMA as diluent and the two different bio-fillers at 5 wt.%, in Figure 74, and those containing THFA as diluent and their respective bio-fillers, in Figure 75. In both cases, the TGA curves of the composites were plotted together with those of their respective unloaded resins, A/IB 60:40 and A/TH 60:40, enabling a direct comparison of the effects of bio-filler addition.

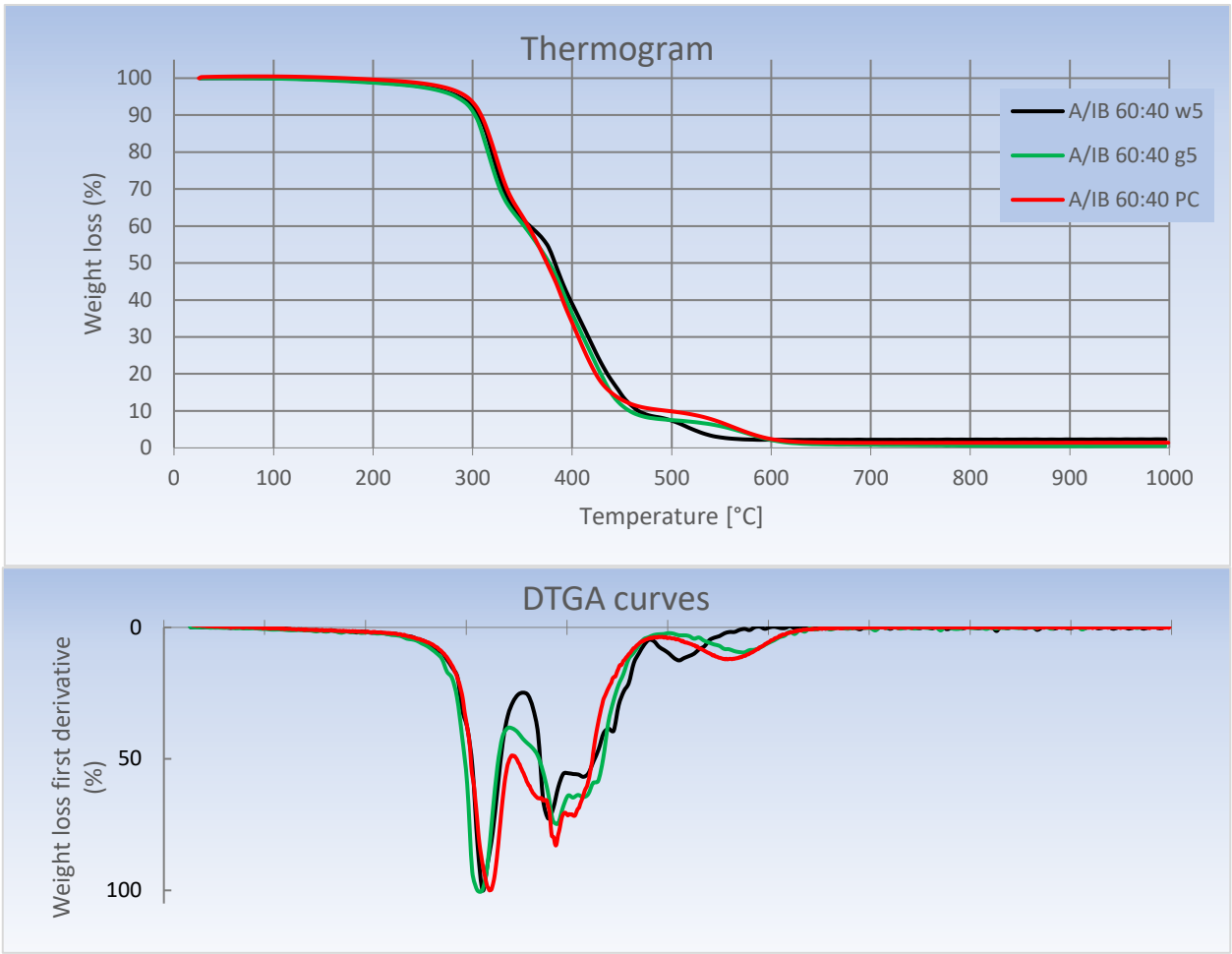

Figure 74. TGA and DTGA curves of composites A/IB 60:40 w5 and A/IB 60:40 g5 compared with the unloaded thermoset A/IB 60:40.

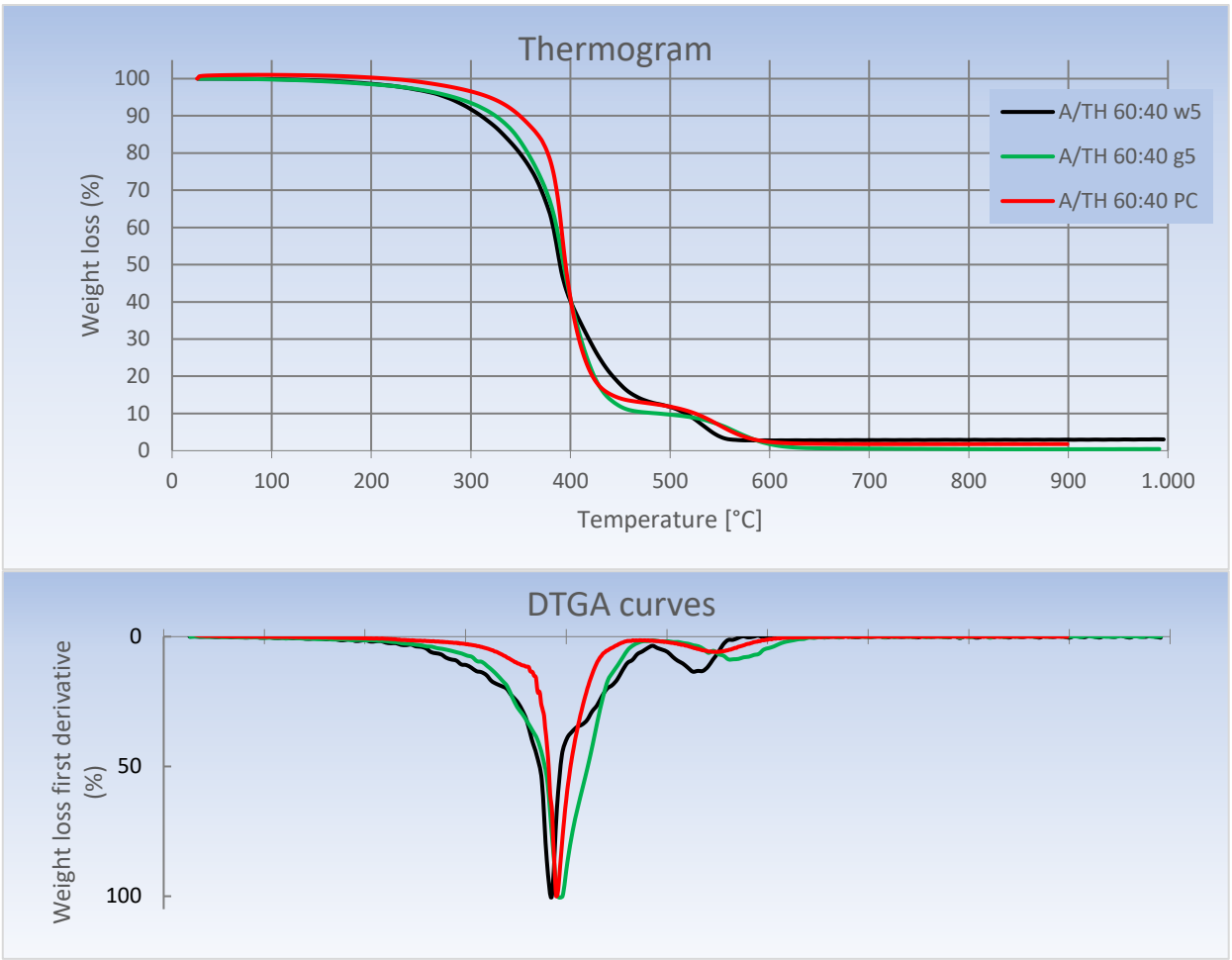

Figure 75. TGA and DTGA curves of composites A/TH 60:40 w5 and A/TH 60:40 g5 compared with the unloaded thermoset A/TH 60:40.

From the graphs concerning the bio-based composites, it appears evident that the presence of the bio-fillers does not increase the resistance to degradation that occurs with an increase in temperature but there is only a slightly slower degradation exhibited by the THFA-based polymer between 300 and 400 degrees.

6.6. Tensile test results

Tensile tests were conducted on three specimens that were not subjected to post-curing and on three specimens that were subjected to post-curing for each formulation.

During the test, not all specimens fractured within the gauge length, some fractured within the clamping zones, in particular, all specimens A/TH not post-cured and all the specimens A/TH post-cured are failed to the clamping zones.

The values of elastic modulus, ultimate strain, and ultimate tensile strength were statistically determined for each formulation by taking the mean of the results obtained from testing each material, both for specimens that underwent post-curing and those that did not. The mechanical properties for each thermoset are available in Table 15 determined from the tensile tests, these materials did not exhibit a behaviour that could allow the evaluation of yield strain and yield stress.

Table 15. Mechanical properties of the thermosets of the various compositions

	Elastic modulus [MPa]	Ultimate Strain [%]	Ultimate Tensile Strength [MPa]
A/IB 80:20 NC	32,7	19,3	3,7
A/IB 70:30 NC	20,9	19,3	2,2
A/IB 60:40 NC	291,5	24,2	12,2
A/IB 50:50 NC	327,8	34,0	12,0
A/IB 80:20 PC	203,2	15,6	10,0
A/IB 70:30 PC	708,7	12,8	22,3
A/IB 60:40 PC	522,4	13,6	16,9
A/IB 50:50 PC	1013,6	9,6	33,9
A/TH 80:20 NC	9,4	6,2	0,5
A/TH 70:30 NC	9,2	5,4	0,4
A/TH 60:40 NC	5,2	3,2	0,2
A/TH 50:50 NC	8,9	5,5	0,4
A/TH 80:20 PC	9,4	6,2	0,5
A/TH 70:30 PC	9,2	5,4	0,4
A/TH 60:40 PC	5,2	3,2	0,2
A/TH 50:50 PC	8,9	5,5	0,4

The large difference in the results obtained from the tensile tests is evident, and certainly A/IB with percentages of diluent ranging from 50% to 30 %, which has elastic modulus between 600 MPa and 1000 MPa and ultimate strength between 20 and 40

MPa after post-curing, could be used as an alternative to many petroleum-based epoxy resins or polyurethanes.
Conversely THFA based thermosets are materials with low strength and low elastic modulus that exhibits low deformation prior to failure, they could be utilized only in applications that prioritize lightweight and flexibility rather than high mechanical strength.
Tensile testing was also performed on composite materials, testing samples of each of the four composites. The values of elastic modulus, strain at break, and tensile strength for each composite were calculated as the means of the results obtained from the tests conducted on each composite. These values are presented in Table 16.

Table 16. Mechanical properties of the composites

	Elastic modulus [MPa]	Ultimate strain (%)	Ultimate tensile strength [MPa]
A/IB 60:40 g5	879,5	7,5	26,5
A/IB 60:40 w5	750,6	10,4	21,6
A/TH 60:40 g4	13,4	9,8	1,1
A/TH 60:40 w5	12,7	10,2	1,0

It is noteworthy that, in this case, all the composite specimens that were printed using THFA as a diluent experienced failure in the clamping zones, while those printed using IBOMA as a diluent experienced failure in the gauge length.

By comparing the values of elastic modulus and ultimate tensile strength in Table 16 with those from the tensile tests of A/IB 60:40 and A/TH 60:40 thermoset polymers post-cured, the composite values result higher. Table 17 provides a simpler comparison as it includes the values of the composites alongside those of their respective non-reinforced base resins.

Table 17. Tensile tests results of composites and their respective unloaded post-cured polymers.

	Elastic modulus [MPa]	Strain at break (%)	Ultimate tensile strength [MPa]
A/IB 60:40 g5	879,5	7,5	26,5
A/IB 60:40 w5	750,6	10,4	21,6
A/IB 60:40 PC	522,4	13,6	16,9
A/TH 60:40 g4	13,4	9,8	1,1
A/TH 60:40 w5	12,7	10,2	1,0
A/TH 60:40 PC	5,2	3,2	0,2

It is evident from Table 17 that the addition of bio-fillers has significantly increased the elastic modulus of the AESO and IBOMA composite material by about 44% for WPL-CF and about 68% for GTF. Tensile strength has also seen a considerable increase of about 30% for WPL-CF and about 60% for GTF. On the other hand, the strain at break is lower than that of the polymer without bio-fillers, contrary to what happens for the composite based on THFA as a diluent, which sees an increase in strain at break compared to its respective non-loaded polymer. The values of elastic modulus and ultimate tensile strength also increase, which is equivalent to more than doubling these properties with the addition of bio-fillers in the THFA and AESO-based polymer, however, the values remain low.

6.7. DMTA results

In this paragraph, the results of dynamic mechanical thermal analysis (DMTA) performed on thermosetting polymer specimens A/IB 60:40 and A/TH 60:40 after post-curing and specimens of the composites materials A/IB 60:40 w5, A/IB 60:40 g5, A/TH 60:40 w5, A/TH 60:40 g5.

The DMTA results provide insights into the viscoelastic behaviour of the materials, which is critical for understanding their mechanical properties and performance under different loading conditions.

The graph in Figure 76 shows the results for A/IB 60:40 after post-curing. The tan δ trend indicates a peak at a temperature of 90°C, which corresponds to the T_g of the material. This result is more reliable than the one obtained from DSC analysis and is higher by approximately 10°C.

The storage modulus E', reaches high values for temperatures between 0 and 50°C, confirming the results obtained with the tensile tests, being storage modulus the viscoelastic property that describes the ability of a material to store elastic energy when subjected to periodic deformations. Instead, the loss modulus, E'', has a maximum around 80°C but its value is not higher than 25-30 MPa.

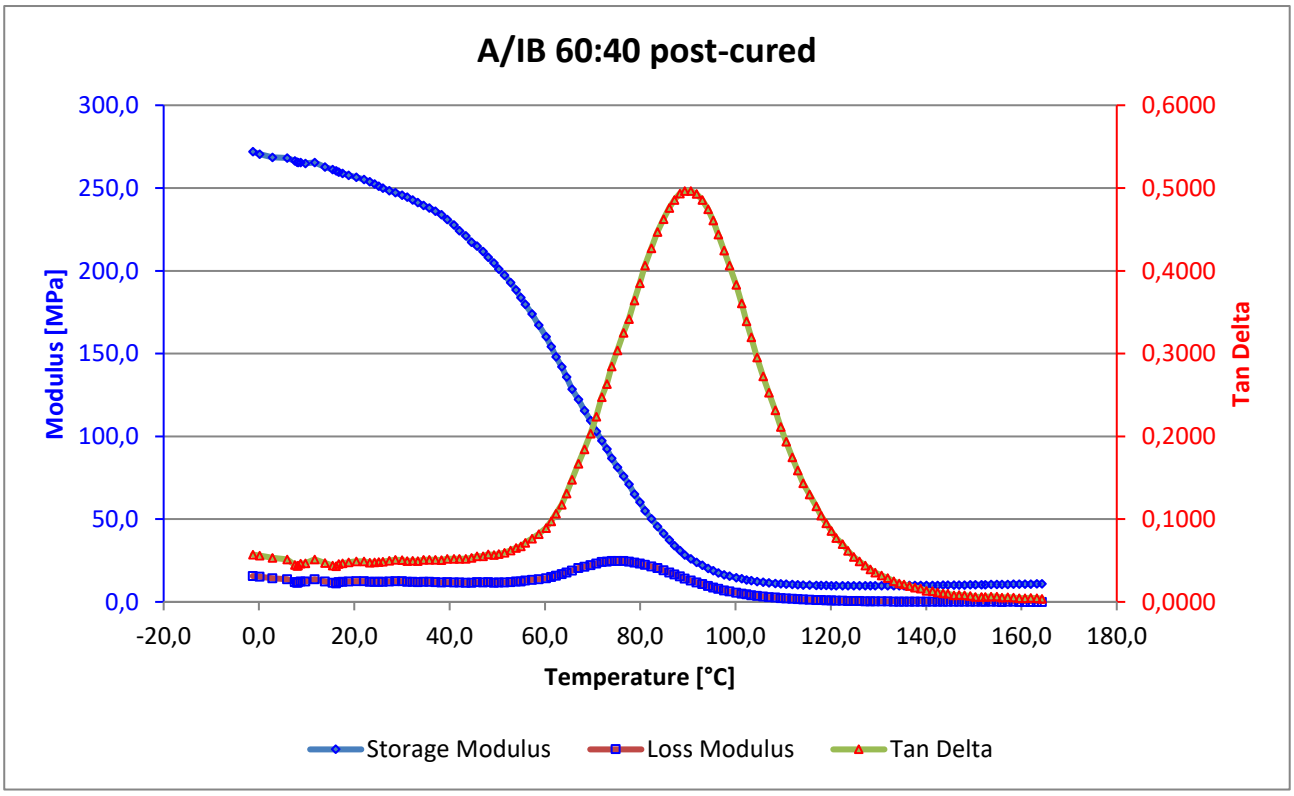

Figure 76. DMTA results for A/IB 60:40 post-cured

In Figure 77 and in Figure 78 there are the curves obtained by the DMTA for composites with IBOMA as diluent.

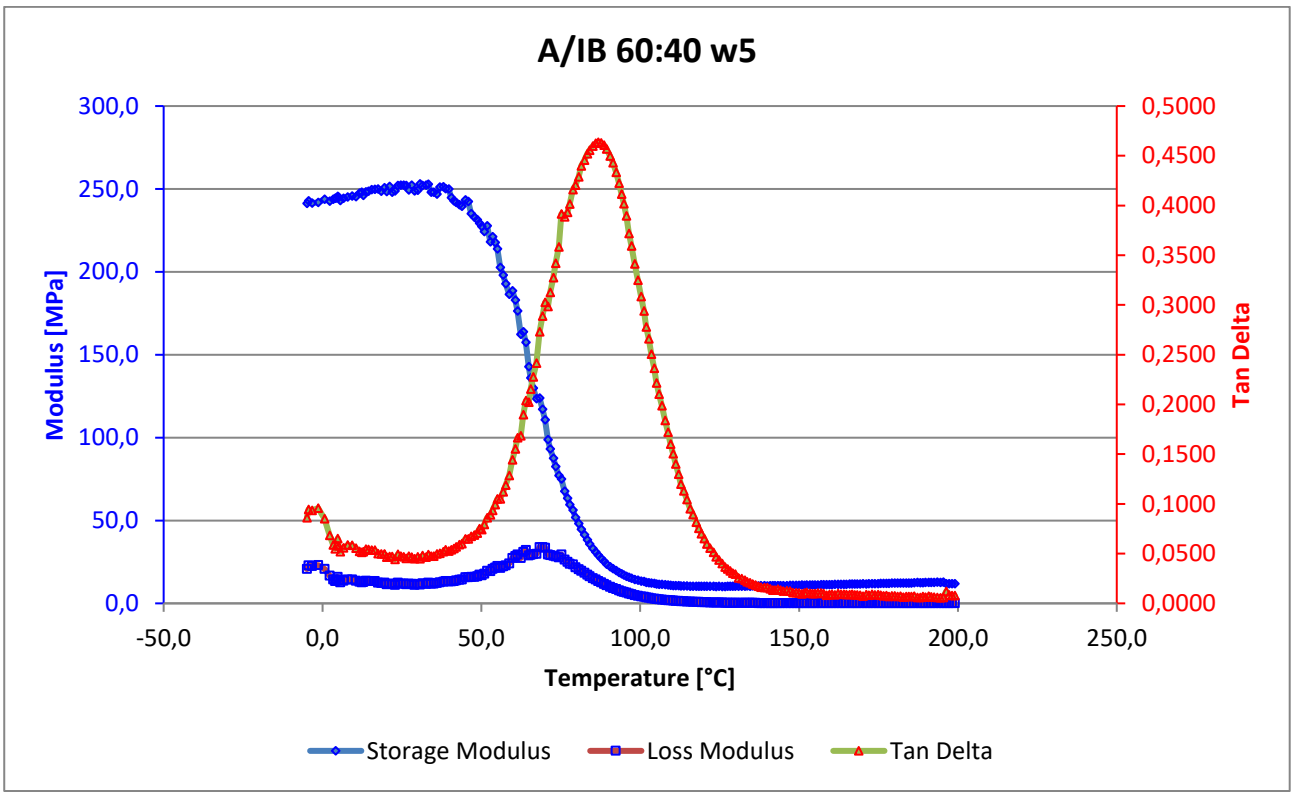

Figure 77. DMTA results for A/IB 60:40 w5

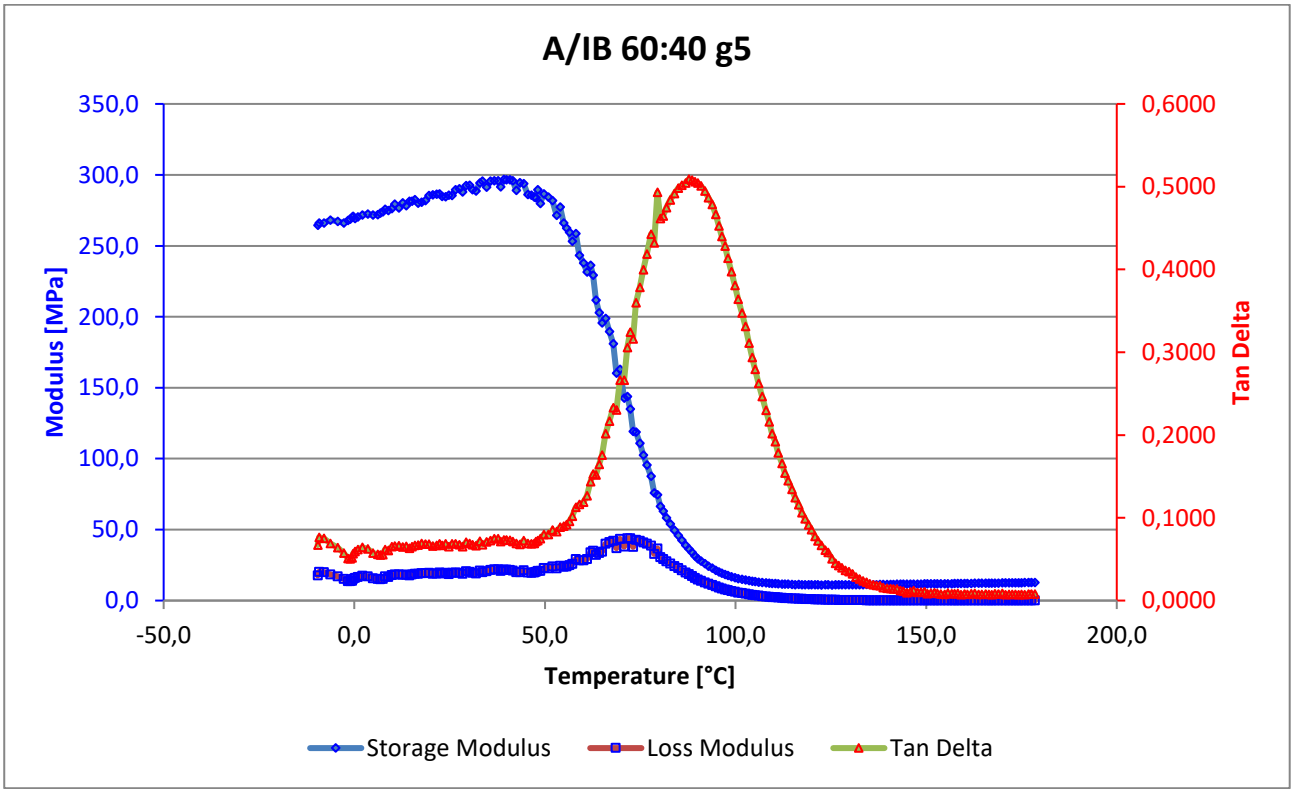

Figure 78. DMTA results for A/IB 60:40 g5

From the graphs in Figures 77 and 78 no significant deviation in the viscoelastic behaviorare noticeable between the two composites and the base thermoset polymer. The T_g is always around 90 °C, and there is not a large difference in the peak values of the storage modulus and loss modulus compared to the curves in Figure 76, which refers to A/IB 60:40 post-cured. The greatest difference is observed for the A/IB 60:40 g5 composite, with storage modulus that reaches 300 MPa and loss modulus that almost reaches 50 MPa.
In Figure 79, E', E'' and $\tan\delta$ trends for the A/TH 60:40 thermoset polymer post-cured are shown. The peak in the tangent behavior can be observed at around 30 °C. Therefore, the evaluation of Tg based on DSC results was not too far off, as the difference results still around 10 °C.
E' has lower values respect to E' of A/IB resin for temperatures between 0 and 50°, additionally in this range of themperature the curve decreases rapidly. E'', for this polymer too, reaches values around 40 MPa, but before 20°C.

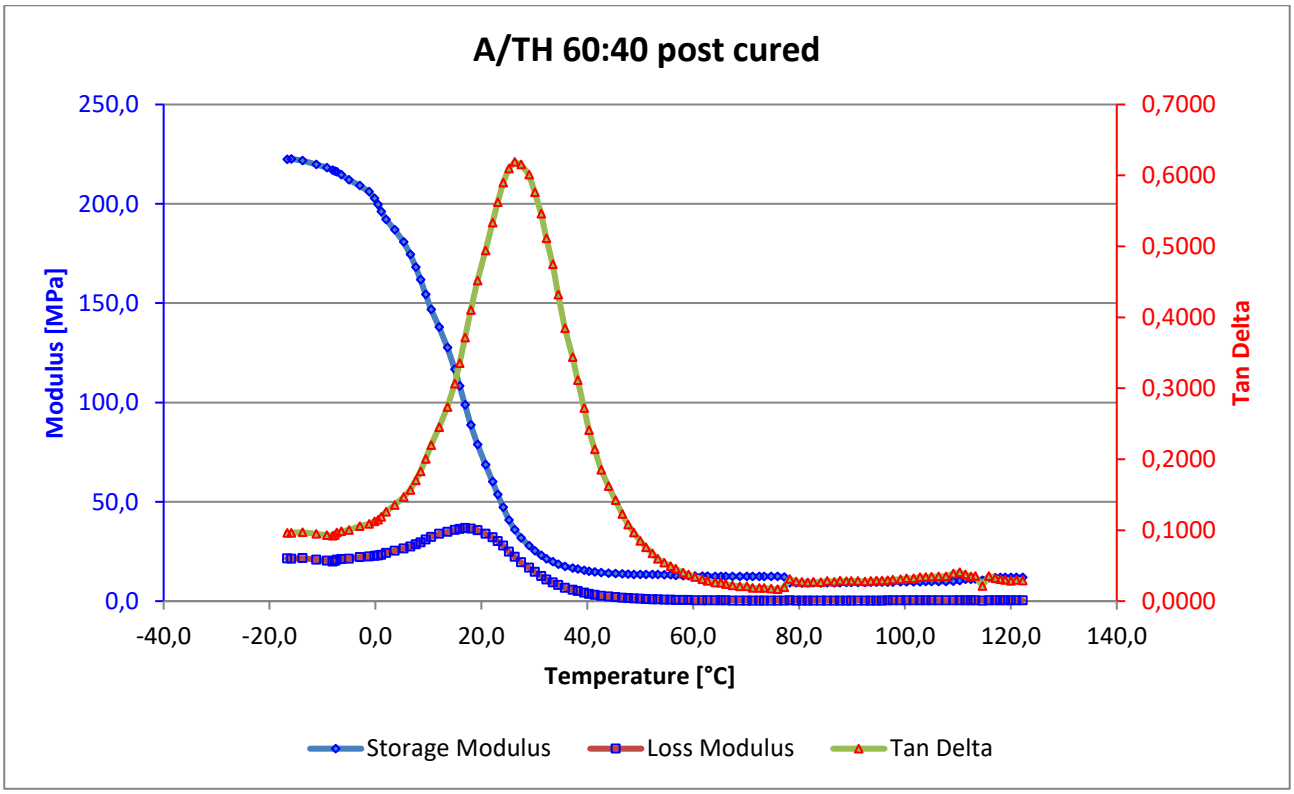

Figure 79. DMTA results for A/TH 60:40 post-cured

The last two graphs in Figure 80 and 81 show the resulting behaviours from DMTA for composites based on the reactive diluent THFA. In this case too, there are no particular differences compared to the reference polymer, A/TH 60:40.

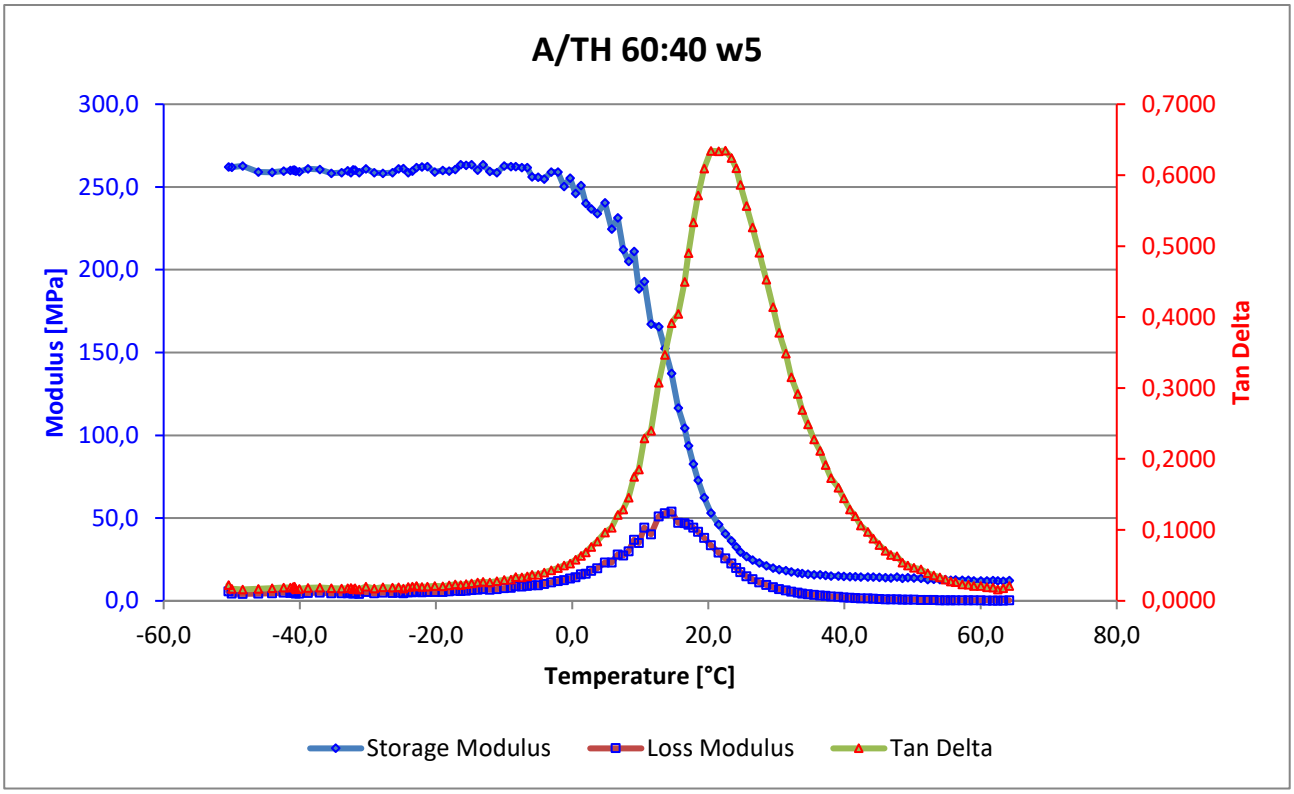

Figure 80. DMTA results for A/TH 60:40 w5

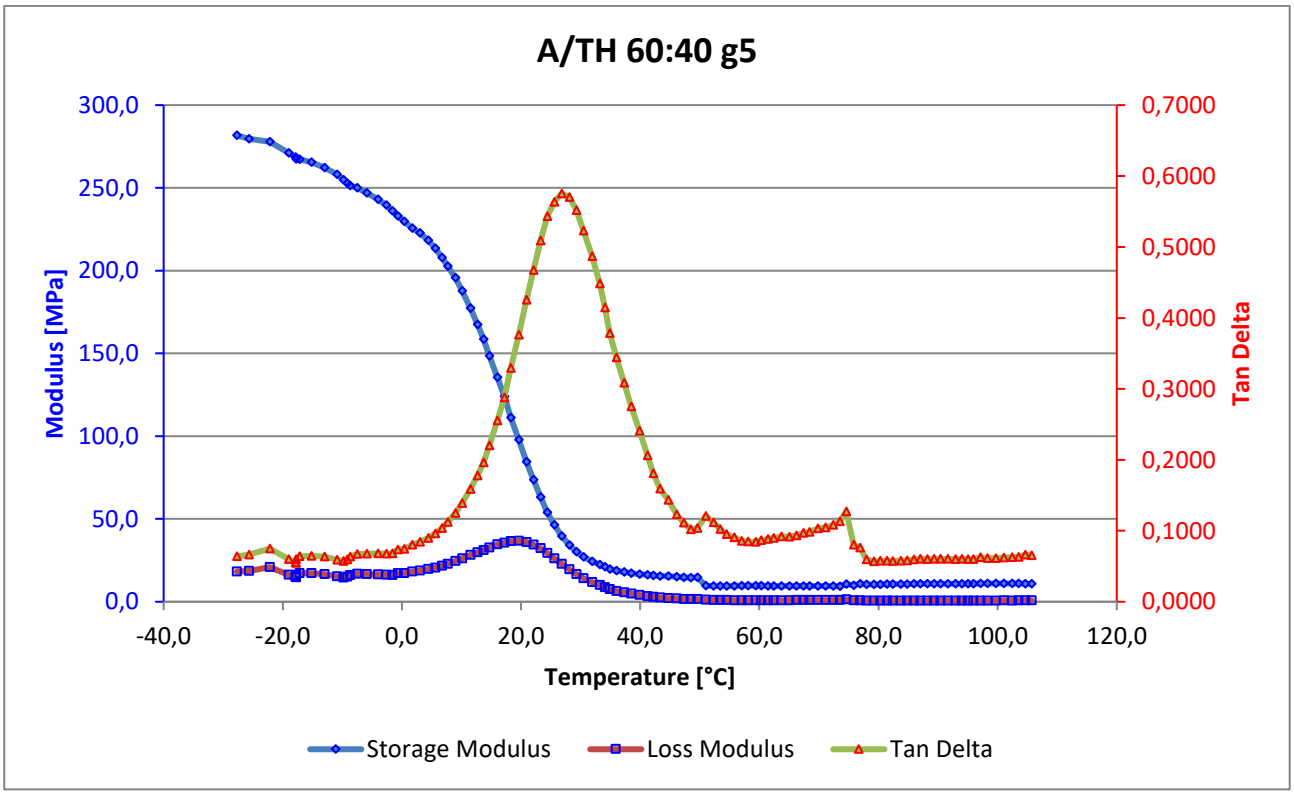

Figure 81. DMTA results for A/TH 60:40 g5

7. Conclusions

The objective of this work was to investigate the printability of a new bio-based polymer using LCD 3D printing and to characterize the material realized by additive manufacturing. This objective was achieved by identifying AESO, a derivative of soybean oil, as the starting bio-based monomer, and IBOMA and THFA as diluents, which are derived from pine resin and hemicellulose, respectively.

This work was highly experimental and innovative since AESO is not commonly used as the main monomer in a photopolymerizable resin for 3D printing. In the few cases where it is used, it is often combined with non-bio-based reactive diluents, whereas in this work, the final material is highly bio-based due to the bio-based origin of all the reactants involved.

The approach used allowed for exploration of various formulations by attempting to print the polymeric materials, varying the weight percentage of the reagents. In this way, printing parameters that ensured excellent resolution and precision in the details of the printed object, without requiring too much time for the printing process, were identified.

The definition of printing parameters required numerous tests. The results became increasingly satisfactory for each individual formulation as the parameters were modified. All the issues that the formulations presented were addressed, for example, low-diluent resins were found to be very difficult to print. Looking at the viscosity test results for each resin, they were found to be outside the range suitable for vat polymerization processes. However, these resins were still successfully printed, and with each attempt, a smoother and more efficient printing process was achieved, albeit taking longer than prints with more diluent. Obtaining parameters for each individual formulation provided the opportunity to compare the various formulations and characterize them individually. In this way has been highlighted the impact and influence of the individual diluent on the final material.

This approach reveals the choice of two diluents to be very interesting as each confers certain characteristics to the material. IBOMA, when used in combination with AESO, generates a material with good mechanical properties after printing and post-curing, especially when used in a percentage higher than 60%. On the other hand, THFA is much less resistant, as can be seen from the tensile test results. It is a soft rubbery polymer, a low-strength and low-Young's modulus material that could be suitable for lightweight, flexible applications like medical masks, equipment components, toys, and sports gear. The qualities of this type of resins are relative to the simplicity of preparation, the process requires less time compared to IBOMA and, above all, is less subjected to air bubble formation. The use of THFA in lower percentages results in a less viscous resin, and already at around 30% in weight, its effect as a diluent is noticeable.

The insoluble fraction percentage obtained from the test reveals that the polymers and composites after post-curing are almost entirely made up of cross-linked and insoluble material. TGA analysis shows that none of the materials considered, both unfilled and filled thermosets, show a degradation of 10% before 300 degrees, which is an excellent result in terms of thermal stability. While the DSC reveals the temperature ranges of the glass transition, which are lower for the A/TH thermosets, below 20°C, while for A/IB are around 75°C. This difference is also reflected in the behaviour of these two different materials in tensile tests.
The screening study of all possible combinations of diluents and monomers for both IBOMA and THFA, leading to the printing and characterization of each of these resins, is highly useful as an initial study for a research line that may concern this type of material. In this thesis work, a step forward has already been taken by using bio-fillers derived from the processing waste of wine WPL-CF and corn processing waste GTF.
Once the two resins that exhibited both good processability and interesting mechanical properties of deformation for A/TH 60:40 and of resistance for A/IB 60:40 were identified, these two fillers were separately mixed with the two resins to obtain four bio-based polymer composite materials. The fillers first acted as colorants and, in addition, do not have effects on the thermal properties of the material. Furthermore, these bio-fillers can reduce the cost of the final material.
Moreover, the results of the tensile tests are very interesting. The bio-fillers used to reinforce the bio-based polymers, significantly increase the elastic modulus and tensile strength. This effect is particularly visible in the AESO and IBOMA-based composites, where the elastic modulus reaches almost 900 MPa and the tensile strength reaches almost 30 MPa. This result could be a starting point for further research in this direction confirming that, by dispersing 5 wt.% of these bio-fillers in the soybean oil resin and photocuring the formulation by LCD 3D printing can be realized bio-based composites with improved performances. Additionally, investigating the possibility of increasing the weight percentage of bio-fillers and evaluating the effect of such an increase on the composite properties could also be worthwhile. Bio-based samples with complex shapes and intricate details were obtained by using this 3D printing technology, which are difficult to reproduce with other technologies. AESO is a monomer that is being widely evaluated for its promising biodegradability and biocompatibility. A further investigation of this work based on these aspects regarding these types of materials could open interesting scenarios for their application in many application fields. For example, they could be used to produce prostheses or other personalized medical devices due to the ability to print objects with complex shapes and intricate details. Additionally, they could also be used in the food industry to produce eco-friendly packaging.
Finally, these materials could find application in the fashion and clothing industry, where sustainability and the use of eco-friendly materials are becoming increasingly important for consumers.

Further exploration of the effect of adding these bio-based fillers could be carried out, perhaps by varying their quantity to better assess their impact on the mechanical properties of the composite material. Additionally, other bio-based diluents could be considered for use alongside those used in this work or as an alternative to them, potentially providing an even wider range of properties for AESO-based thermoset polymers suitable for vat polymerization 3D printing. Finally, as mentioned earlier, important steps would be to study the biocompatibility of these materials and their biodegradability.

References

[1] W. Leal Filho *et al.*, “An overview of the problems posed by plastic products and the role of extended producer responsibility in Europe,” *J Clean Prod*, vol. 214, pp. 550–558, Mar. 2019, doi: 10.1016/j.jclepro.2018.12.256.

[2] *Global Plastics Outlook*. OECD, 2022. doi: 10.1787/de747aef-en.

[3] H. O. Paipa-Alvarez, W. Palacios Alvarado, and B. Medina Delgado, “Biodegradable thermosets polymers as an alternative solution to pollution generated by plastics,” in *Journal of Physics: Conference Series*, IOP Publishing Ltd, Nov. 2020. doi: 10.1088/1742-6596/1672/1/012013.

[4] “THE COMMITTEE OF THE REGIONS A lead market initiative for Europe” [Online]. Available: http://ec.europa.eu/invest-in-research/action/2006_ahogroup_en.htm.

[5] P. T. Anastas and J. C. Warner, *Green Chemistry: Theory and Practice*. New York: Oxford University Press, 1998.

[6] S. Spierling *et al.*, “Bio-based plastics - A review of environmental, social and economic impact assessments,” *J Clean Prod*, vol. 185, pp. 476–491, Jun. 2018, doi: 10.1016/j.jclepro.2018.03.014.

[7] T. D. Ngo, A. Kashani, G. Imbalzano, K. T. Q. Nguyen, and D. Hui, “Additive manufacturing (3D printing): A review of materials, methods, applications and challenges,” *Composites Part B: Engineering*, vol. 143. Elsevier Ltd, pp. 172–196, Jun. 15, 2018. doi: 10.1016/j.compositesb.2018.02.012.

[8] L. J. Tan, W. Zhu, and K. Zhou, “Recent Progress on Polymer Materials for Additive Manufacturing,” *Advanced Functional Materials*, vol. 30, no. 43. Wiley-VCH Verlag, Oct. 01, 2020. doi: 10.1002/adfm.202003062.

[9] A. B. Kousaalya, “Sustainable Photo-curable Polymers in Additive Manufacturing Arena: A Review,” in *Sustainability & Green Polymer Chemistry*, American Chemical Society, 2020.

[10] J. Jiang, X. Xu, and J. Stringer, “Optimization of Process Planning for Reducing Material Waste in Extrusion Based Additive Manufacturing,” *Robot Comput Integr Manuf*, vol. 59, pp. 317–325, 2019, doi: https://doi.org/10.1016/j.rcim.2019.05.007.

[11] A. Alfaify, M. Saleh, F. M. Abdullah, and A. M. Al-Ahmari, “Design for additive manufacturing: A systematic review,” *Sustainability (Switzerland)*, vol. 12, no. 19. MDPI, Oct. 01, 2020. doi: 10.3390/SU12197936.

[12] S. Ford and M. Despeisse, “Additive manufacturing and sustainability: an exploratory study of the advantages and challenges,” *J Clean Prod*, vol. 137, pp. 1573–1587, Nov. 2016, doi: 10.1016/j.jclepro.2016.04.150.

[13] T. A. Osswald and G. Menges, “Material Science of Polymers for Engineers,” 3rd ed.Munich: Hanser, 2012, pp. 6–12.

[14] G. Odian, *Principles of Polymerization*, Fourth. Hoboken, New Jersey: Published by John Wiley & Sons, Inc., 2004.
[15] "3. Characteristics, Applications and Properties of Polymers."
[16] R. O. Ebewele, *Polymer Science and Technology*. CRC Press, 2000.
[17] R. J. Young, P. A. Lovell, and M. C. Jones, *Introduction to Polymers*, 3rd ed. CRC Press, 2011.
[18] P. Atkins and J. de Paula, "The Properties of Gases," in *Atkins' Physical Chemistry*, Oxford University Press, 2010, pp. 10–11.
[19] P. C. Painter and M. M. Coleman, *Essentials of Polymer Science and Engineering*. Lancaster: DEStech Publication, Inc., 2009.
[20] W. D. Jr. Callister and D. G. Rethwish, *Materials Science and Engineering, an introduction*, 10th ed. Wiley, 2017.
[21] A. Y. Coran, "Chemistry of the vulcanization and protection of elastomers: A review of the achievements," in *Journal of Applied Polymer Science*, John Wiley and Sons Inc., Jan. 2003, pp. 24–30. doi: 10.1002/app.11659.
[22] S. M. Dwivedi D Mahajan, "COST OPTIMIZATION OF ENGINE ROCKER COVER BY INTRODUCING NYLON 66 IN MANUFACTURING," 2017. [Online]. Available: https://www.researchgate.net/publication/331247113
[23] H. Düzcükoğlu, "Study on development of polyamide gears for improvement of load-carrying capacity," *Tribol Int*, vol. 42, no. 8, pp. 1146–1153, Aug. 2009, doi: 10.1016/j.triboint.2009.03.009.
[24] A. Das and P. Mahanwar, "A brief discussion on advances in polyurethane applications," *Advanced Industrial and Engineering Polymer Research*, vol. 3, no. 3. KeAi Communications Co., pp. 93–101, Jul. 01, 2020. doi: 10.1016/j.aiepr.2020.07.002.
[25] M. A. Curran, "Bio-based Materials," in *Kirk-Othmer Encyclopedia of Chemical Technology*, Inc. John Wiley & Sons, Ed., Hoboken, 2010, pp. 1–19.
[26] R. P. Babu, K. O'Connor, and R. Seeram, "Current progress on bio-based polymers and their future trends," *Prog Biomater*, vol. 2, no. 1, p. 8, 2013, doi: 10.1186/2194-0517-2-8.
[27] I. Vroman and L. Tighzert, "Biodegradable polymers," *Materials*, vol. 2, no. 2. pp. 307–344, 2009. doi: 10.3390/ma2020307.
[28] S. Miao, P. Wang, Z. Su, and S. Zhang, "Vegetable-oil-based polymers as future polymeric biomaterials," *Acta Biomaterialia*, vol. 10, no. 4. Elsevier Ltd, pp. 1692–1704, 2014. doi: 10.1016/j.actbio.2013.08.040.
[29] M. M. Reddy, S. Vivekanandhan, M. Misra, S. K. Bhatia, and A. K. Mohanty, "Biobased plastics and bionanocomposites: Current status and future opportunities," *Progress in Polymer Science*, vol. 38, no. 10–11. Elsevier Ltd, pp. 1653–1689, 2013. doi: 10.1016/j.progpolymsci.2013.05.006.

[30] D. M. Miu, M. C. Eremia, and M. Moscovici, “Polyhydroxyalkanoates (PHAs) as Biomaterials in Tissue Engineering: Production, Isolation, Characterization,” *Materials*, vol. 15, no. 4. MDPI, Feb. 01, 2022. doi: 10.3390/ma15041410.

[31] L. P. Muthe, K. Pickering, and C. Gauss, “A Review of 3D/4D Printing of Poly-Lactic Acid Composites with Bio-Derived Reinforcements,” *Composites Part C: Open Access*, vol. 8. Elsevier B.V., Aug. 01, 2022. doi: 10.1016/j.jcomc.2022.100271.

[32] Z. U. Arif, M. Y. Khalid, R. Noroozi, A. Sadeghianmaryan, M. Jalalvand, and M. Hossain, “Recent advances in 3D-printed polylactide and polycaprolactone-based biomaterials for tissue engineering applications,” *International Journal of Biological Macromolecules*, vol. 218. Elsevier B.V., pp. 930–968, Oct. 01, 2022. doi: 10.1016/j.ijbiomac.2022.07.140.

[33] M. Shahbazi and H. Jäger, “Current Status in the Utilization of Biobased Polymers for 3D Printing Process: A Systematic Review of the Materials, Processes, and Challenges,” *ACS Applied Bio Materials*, vol. 4, no. 1. American Chemical Society, pp. 325–369, Jan. 18, 2021. doi: 10.1021/acsabm.0c01379.

[34] E. Yang, S. Miao, J. Zhong, Z. Zhang, D. K. Mills, and L. G. Zhang, “Bio-Based Polymers for 3D Printing of Bioscaffolds,” *Polymer Reviews*, vol. 58, no. 4. Taylor and Francis Inc., pp. 668–687, Oct. 02, 2018. doi: 10.1080/15583724.2018.1484761.

[35] M. Galià, L. M. de Espinosa, J. C. Ronda, G. Lligadas, and V. Cádiz, “Vegetable oil-based thermosetting polymers,” *European Journal of Lipid Science and Technology*, vol. 112, no. 1. pp. 87–96, Feb. 2010. doi: 10.1002/ejlt.200900096.

[36] C. Zhang, T. F. Garrison, S. A. Madbouly, and M. R. Kessler, “Recent advances in vegetable oil-based polymers and their composites,” *Progress in Polymer Science*, vol. 71. Elsevier Ltd, pp. 91–143, Aug. 01, 2017. doi: 10.1016/j.progpolymsci.2016.12.009.

[37] Z. Liu *et al.*, “Phosphoester cross-linked vegetable oil to construct a biodegradable and biocompatible elastomer,” *Soft Matter*, vol. 8, no. 21, pp. 5888–5895, Jun. 2012, doi: 10.1039/c2sm25115a.

[38] A. Barkane *et al.*, “Uv-light curing of 3d printing inks from vegetable oils for stereolithography,” *Polymers (Basel)*, vol. 13, no. 8, Apr. 2021, doi: 10.3390/polym13081195.

[39] F. Seniha Güner, Y. Yağci, and A. Tuncer Erciyes, “Polymers from triglyceride oils,” *Progress in Polymer Science (Oxford)*, vol. 31, no. 7. pp. 633–670, Jul. 2006. doi: 10.1016/j.progpolymsci.2006.07.001.

[40] A. M. Salih *et al.*, “Synthesis of radiation curable palm oil-based epoxy acrylate: NMR and FTIR spectroscopic investigations,” *Molecules*, vol. 20, no. 8, pp. 14191–14211, Aug. 2015, doi: 10.3390/molecules200814191.

[41] J. La Scala and R. P. Wool, “Property analysis of triglyceride-based thermosets,” *Polymer (Guildf)*, vol. 46, no. 1, pp. 61–69, Jan. 2005, doi: 10.1016/j.polymer.2004.11.002.
[42] S. Miao *et al.*, “4D printing smart biomedical scaffolds with novel soybean oil epoxidized acrylate,” *Sci Rep*, vol. 6, Jun. 2016, doi: 10.1038/srep27226.
[43] S. Hernandez and E. Vigueras, “Acrylated-Epoxidized Soybean Oil-Based Polymers and Their Use in the Generation of Electrically Conductive Polymer Composites,” in *Soybean - Bio-Active Compounds*, InTech, 2013. doi: 10.5772/52992.
[44] F. Li and R. C. Larock, “Novel Polymeric Materials from Biological Oils,” 2002.
[45] M. Rahmah, N. Mohd Nurazzi, A. R. F. Nordyana, and S. M. S. Anas, “Effect of epoxidised soybean oil loading as plasticiser on physical, mechanical and thermal properties of polyvinylchloride,” in *IOP Conference Series: Materials Science and Engineering*, Institute of Physics Publishing, Aug. 2017. doi: 10.1088/1757-899X/223/1/012048.
[46] A. Adhvaryu and S. Z. Erhan, “Epoxidized soybean oil as a potential source of high-temperature lubricants,” 2002. [Online]. Available: www.elsevier.com
[47] M. Lebedevaite, V. Talacka, and J. Ostrauskaite, “High biorenewable content acrylate photocurable resins for DLP 3D printing,” *J Appl Polym Sci*, vol. 138, no. 16, Apr. 2021, doi: 10.1002/app.50233.
[48] E. Skliutas *et al.*, “A Bio-Based Resin for a Multi-Scale Optical 3D Printing,” *Sci Rep*, vol. 10, no. 1, Dec. 2020, doi: 10.1038/s41598-020-66618-1.
[49] L. M. Bonnaillie, “Method for the fabrication of bio-based thermoset foam from acrylated epoxidized soybean oil Edible milk-based films View project Whey protein fractionation with sCO2 View project,” 2014. [Online]. Available: https://www.researchgate.net/publication/34979536
[50] M. Lebedevaite and J. Ostrauskaite, “Influence of photoinitiator and temperature on photocross-linking kinetics of acrylated epoxidized soybean oil and properties of the resulting polymers,” *Ind Crops Prod*, vol. 161, Mar. 2021, doi: 10.1016/j.indcrop.2020.113210.
[51] I. Gibson, D. Rosen, and B. Stucker, *Additive Manufacturing Technologies*. Springer New York, NY, 2015.
[52] Mohd. Javaid and A. Haleem, “Additive manufacturing applications in medical cases: A literature based review,” *Alexandria Journal of Medicine*, vol. 54, no. 4, pp. 411–422, Dec. 2018, doi: 10.1016/j.ajme.2017.09.003.
[53] R. Liu, Z. Wang, T. Sparks, F. Liou, and J. Newkirk, “Aerospace applications of laser additive manufacturing,” in *Laser Additive Manufacturing: Materials, Design, Technologies, and Applications*, Elsevier Inc., 2017, pp. 351–371. doi: 10.1016/B978-0-08-100433-3.00013-0.

[54] K. S. Prakash, T. Nancharaih, and V. V. S. Rao, “Additive Manufacturing Techniques in Manufacturing -An Overview,” in *Materials Today: Proceedings*, Elsevier Ltd, 2018, pp. 3873–3882. doi: 10.1016/j.matpr.2017.11.642.

[55] R. Raju *et al.*, “A Review of Challenges and Opportunities in Additive Manufacturing,” in *Recent Advances in Materials and Modern Manufacturing*, Springer, Singapore, 2022.

[56] J. ZHU, H. ZHOU, C. WANG, L. ZHOU, S. YUAN, and W. ZHANG, “A review of topology optimization for additive manufacturing: Status and challenges,” *Chinese Journal of Aeronautics*, vol. 34, no. 1. Chinese Journal of Aeronautics, pp. 91–110, Jan. 01, 2021. doi: 10.1016/j.cja.2020.09.020.

[57] C. W. Hull and C. Arcadia, “Apparatus for production of three-dimensional objects by stereolithography,” 4575330, Mar. 11, 1986

[58] Z. Liu, Q. Jiang, Y. Zhang, T. Li, and H.-C. Zhang, “SUSTAINABILITY OF 3D PRINTING: A CRITICAL REVIEW AND RECOMMENDATIONS,” 2016. [Online]. Available: http://asmedigitalcollection.asme.org/MSEC/proceedings-pdf/MSEC2016/49903/V002T05A004/4425601/v002t05a004-msec2016-8618.pdf

[59] T. Wohlers and T. Gornet, “History of Additive Manufacturing,” 2015.

[60] K. Haghsefat, L. Tingting, and A. professor, “FDM 3D Printing Technology and Its Fundemental Properties,” 2020. [Online]. Available: https://www.researchgate.net/publication/344768624

[61] J. Park, M. J. Tari, and H. T. Hahn, “Characterization of the laminated object manufacturing (LOM) process.” [Online]. Available: http://www.mcbup.com/research_registers/aa.asp

[62] A. Lindberg, J. Alfthan, H. Pettersson, G. Flodberg, and L. Yang, “Mechanical performance of polymer powder bed fused objects – FEM simulation and verification,” *Addit Manuf*, vol. 24, pp. 577–586, Dec. 2018, doi: 10.1016/j.addma.2018.10.009.

[63] D. T. Pham and R. S. Gault, “A comparison of rapid prototyping technologies,” 1998.

[64] ISO, “ISO/ASTM 52900:2015.” https://www.iso.org/standard/69669.html (accessed Feb. 16, 2023).

[65] J. Huang *et al.*, “A survey of design methods for material extrusion polymer 3D printing,” *Virtual and Physical Prototyping*, vol. 15, no. 2. Taylor and Francis Ltd., pp. 148–162, Apr. 02, 2020. doi: 10.1080/17452759.2019.1708027.

[66] C. A. Chatham, T. E. Long, and C. B. Williams, “A review of the process physics and material screening methods for polymer powder bed fusion additive manufacturing,” *Progress in Polymer Science*, vol. 93. Elsevier Ltd, pp. 68–95, Jun. 01, 2019. doi: 10.1016/j.progpolymsci.2019.03.003.

[67] S. L. Sing, C. F. Tey, J. H. K. Tan, S. Huang, and W. Y. Yeong, “3D printing of metals in rapid prototyping of biomaterials: Techniques in additive manufacturing,” in

Rapid Prototyping of Biomaterials: Techniques in Additive Manufacturing, Elsevier, 2019, pp. 17–40. doi: 10.1016/B978-0-08-102663-2.00002-2.

[68] D. G. Ahn, "Directed Energy Deposition (DED) Process: State of the Art," *International Journal of Precision Engineering and Manufacturing - Green Technology*, vol. 8, no. 2. Korean Society for Precision Engineeing, pp. 703–742, Mar. 01, 2021. doi: 10.1007/s40684-020-00302-7.

[69] N. K. Tolochko and O. V. Sokol, "Assessing the Economic Effectiveness of Additive Sheet Lamination," *Russian Engineering Research*, vol. 41, no. 1, pp. 5–9, Jan. 2021, doi: 10.3103/S1068798X2101024X.

[70] A. Unkovskiy, F. Schmidt, F. Beuer, P. Li, S. Spintzyk, and P. K. Fernandez, "Stereolithography vs. Direct light processing for rapid manufacturing of complete denture bases: An in vitro accuracy analysis," *J Clin Med*, vol. 10, no. 5, pp. 1–14, Mar. 2021, doi: 10.3390/jcm10051070.

[71] I. A. Tsolakis, W. Papaioannou, E. Papadopoulou, M. Dalampira, and A. I. Tsolakis, "Comparison in Terms of Accuracy between DLP and LCD Printing Technology for Dental Model Printing," *Dent J (Basel)*, vol. 10, no. 10, Oct. 2022, doi: 10.3390/dj10100181.

[72] O. Gülcan, K. Günaydın, and A. Tamer, "The state of the art of material jetting—a critical review," *Polymers*, vol. 13, no. 16. MDPI AG, Aug. 02, 2021. doi: 10.3390/polym13162829.

[73] A. Mostafaei *et al.*, "Binder jet 3D printing—Process parameters, materials, properties, modeling, and challenges," *Progress in Materials Science*, vol. 119. Elsevier Ltd, Jun. 01, 2021. doi: 10.1016/j.pmatsci.2020.100707.

[74] E. Feilden, F. Giuliani, L. Vandeperre, and E. Saiz, "Additive Manufacturing of Ceramics and Ceramic Composites via Robocasting."

[75] J. W. Stansbury and M. J. Idacavage, "3D printing with polymers: Challenges among expanding options and opportunities," in *Dental Materials*, Elsevier Inc., Jan. 2016, pp. 54–64. doi: 10.1016/j.dental.2015.09.018.

[76] R. J. Mondschein, A. Kanitkar, C. B. Williams, S. S. Verbridge, and T. E. Long, "Polymer structure-property requirements for stereolithographic 3D printing of soft tissue engineering scaffolds," *Biomaterials*, vol. 140. Elsevier Ltd, pp. 170–188, Sep. 01, 2017. doi: 10.1016/j.biomaterials.2017.06.005.

[77] P. J. Bártolo, "Stereolithographic process," in *Stereolithography*, P. J. Bártolo, Ed., New York: Springer, 2021, pp. 1–12.

[78] T. Grimm, *User's Guide to Rapid Prototyping*. Society of Manufacturing Engineers, 2004.

[79] W. Zha and S. Anand, "Geometric approaches to input file modification for part quality improvement in additive manufacturing," *J Manuf Process*, vol. 20, pp. 465–477, Oct. 2015, doi: 10.1016/j.jmapro.2015.06.021.

[80] S. Sikder, A. Barari, and H. A. Kishawy, “Effect of Adaptive Slicing on Surface Integrity in Additive Manufacturing,” ASME International, Aug. 2014. doi: 10.1115/detc2014-35559.

[81] J. Shah, B. Snider, T. Clarke, S. Kozutsky, M. Lacki, and A. Hosseini, “Large-scale 3D printers for additive manufacturing: design considerations and challenges,” *International Journal of Advanced Manufacturing Technology*, vol. 104, no. 9–12, pp. 3679–3693, Oct. 2019, doi: 10.1007/s00170-019-04074-6.

[82] W. Piedra-Cascón, V. R. Krishnamurthy, W. Att, and M. Revilla-León, “3D printing parameters, supporting structures, slicing, and post-processing procedures of vat-polymerization additive manufacturing technologies: A narrative review,” *Journal of Dentistry*, vol. 109. Elsevier Ltd, Jun. 01, 2021. doi: 10.1016/j.jdent.2021.103630.

[83] A. Vevers, A. Kromanis, E. Gerins, and J. Ozolins, “Additive Manufacturing and Casting Technology Comparison: Mechanical Properties, Productivity and Cost Benchmark,” *Latvian Journal of Physics and Technical Sciences*, vol. 55, no. 2, pp. 56–63, Apr. 2018, doi: 10.2478/lpts-2018-0013.

[84] T. Pereira, J. V. Kennedy, and J. Potgieter, “A comparison of traditional manufacturing vs additive manufacturing, the best method for the job,” in *Procedia Manufacturing*, Elsevier B.V., 2019, pp. 11–18. doi: 10.1016/j.promfg.2019.02.003.

[85] A. Kirchheim, H.-J. Dennig, and L. Zumofen, “Why Education and Training in the Field of Additive Manufacturing is a Necessity,” in *Industrializing Additive Manufacturing - Proceedings of Additive Manufacturing in Products and Applications - AMPA2017*, Springer International Publishing, 2018, pp. 329–336. doi: 10.1007/978-3-319-66866-6_31.

[86] S. K. Nithin Reddy, I. Ferguson, M. Frecker, T. W. Simpson, and C. J. Dickman, “TOPOLOGY OPTIMIZATION SOFTWARE FOR ADDITIVE MANUFACTURING: A REVIEW OF CURRENT CAPABILITIES AND A REAL-WORLD EXAMPLE,” 2016. [Online]. Available: http://asmedigitalcollection.asme.org/IDETC-CIE/proceedings-pdf/IDETC-CIE2016/50107/V02AT03A029/2471196/v02at03a029-detc2016-59718.pdf

[87] A. W. Gebisa and H. G. Lemu, “A case study on topology optimized design for additive manufacturing,” in *IOP Conference Series: Materials Science and Engineering*, Institute of Physics Publishing, Dec. 2017. doi: 10.1088/1757-899X/276/1/012026.

[88] S. Ford and M. Despeisse, “Additive manufacturing and sustainability: an exploratory study of the advantages and challenges,” *J Clean Prod*, vol. 137, pp. 1573–1587, Nov. 2016, doi: 10.1016/j.jclepro.2016.04.150.

[89] A. Al Rashid, W. Ahmed, M. Y. Khalid, and M. Koç, “Vat photopolymerization of polymers and polymer composites: Processes and applications,” *Additive*

Manufacturing, vol. 47. Elsevier B.V., Nov. 01, 2021. doi: 10.1016/j.addma.2021.102279.

[90] T. Billiet, M. Vandenhaute, J. Schelfhout, S. Van Vlierberghe, and P. Dubruel, "A review of trends and limitations in hydrogel-rapid prototyping for tissue engineering," *Biomaterials*, vol. 33, no. 26. pp. 6020–6041, Sep. 2012. doi: 10.1016/j.biomaterials.2012.04.050.

[91] H. Yao, J. Wang, and S. Mi, "Photo processing for biomedical hydrogels design and functionality: A review," *Polymers*, vol. 10, no. 1. MDPI, Jan. 01, 2018. doi: 10.3390/polym10010011.

[92] O. Santoliquido, P. Colombo, and A. Ortona, "Additive Manufacturing of ceramic components by Digital Light Processing: A comparison between the 'bottom-up' and the 'top-down' approaches," *J Eur Ceram Soc*, vol. 39, no. 6, pp. 2140–2148, Jun. 2019, doi: 10.1016/j.jeurceramsoc.2019.01.044.

[93] J.-P. Pascault and R. J. J. Williams, "28 THERMOSETTING POLYMERS," 2013.

[94] M. M. Prabhakar, A. K. Saravanan, A. H. Lenin, I. J. Leno, K. Mayandi, and P. S. Ramalingam, "A short review on 3D printing methods, process parameters and materials," in *Materials Today: Proceedings*, Elsevier Ltd, 2020, pp. 6108–6114. doi: 10.1016/j.matpr.2020.10.225.

[95] IEEE Electron Devices Society, Institute of Electrical and Electronics Engineers, and Vaigai College of Engineering, *Proceeding of the 2018 International Conference on Intelligent Computing and Control Systems (ICICCS) : June 14-15, 2018*.

[96] Y. Luo, G. Le Fer, D. Dean, and M. L. Becker, "3D Printing of Poly(propylene fumarate) Oligomers: Evaluation of Resin Viscosity, Printing Characteristics and Mechanical Properties," *Biomacromolecules*, vol. 20, no. 4, pp. 1699–1708, Apr. 2019, doi: 10.1021/acs.biomac.9b00076.

[97] A. Bagheri Saed, A. H. Behravesh, S. Hasannia, S. A. Alavinasab Ardebili, B. Akhoundi, and M. Pourghayoumi, "Functionalized poly L-lactic acid synthesis and optimization of process parameters for 3D printing of porous scaffolds via digital light processing (DLP) method," *J Manuf Process*, vol. 56, pp. 550–561, Aug. 2020, doi: 10.1016/j.jmapro.2020.04.076.

[98] D. Laumann, D. Spiehl, E. Dörsam, and A. Blaeser, "Interaction of printing speed and temperature settings on the build plate adhesion of 3D-printed polylactide acid parts," *Journal of Adhesion*, 2022, doi: 10.1080/00218464.2022.2093640.

[99] W. L. Ng *et al.*, "Vat polymerization-based bioprinting - process, materials, applications and regulatory challenges," *Biofabrication*, vol. 12, no. 2. Institute of Physics Publishing, 2020. doi: 10.1088/1758-5090/ab6034.

[100] J. Huang, Q. Qin, and J. Wang, "A review of stereolithography: Processes and systems," *Processes*, vol. 8, no. 9. MDPI AG, Sep. 01, 2020. doi: 10.3390/PR8091138.

[101] R. R. Paulsen and K. S. Pedersen, Eds., *Image Analysis*, vol. 9127. in Lecture Notes in Computer Science, vol. 9127. Cham: Springer International Publishing, 2015. doi: 10.1007/978-3-319-19665-7.

[102] G. B. Kim *et al.*, “Three-dimensional printing: Basic principles and applications in medicine and radiology,” *Korean Journal of Radiology*, vol. 17, no. 2. Korean Radiological Society, pp. 182–197, Mar. 01, 2016. doi: 10.3348/kjr.2016.17.2.182.

[103] W. Shan, Y. Chen, M. Hu, S. Qin, and P. Liu, “4D printing of shape memory polymer via liquid crystal display (LCD) stereolithographic 3D printing,” *Mater Res Express*, vol. 7, no. 10, Oct. 2020, doi: 10.1088/2053-1591/abbd05.

[104] Malas, Isakov, Couling, and Gibbons, “Fabrication of High Permittivity Resin Composite for Vat Photopolymerization 3D Printing: Morphology, Thermal, Dynamic Mechanical and Dielectric Properties,” *Materials*, vol. 12, no. 23, p. 3818, Nov. 2019, doi: 10.3390/ma12233818.

[105] H. Quan, T. Zhang, H. Xu, S. Luo, J. Nie, and X. Zhu, “Photo-curing 3D printing technique and its challenges,” *Bioactive Materials*, vol. 5, no. 1. KeAi Communications Co., pp. 110–115, Mar. 01, 2020. doi: 10.1016/j.bioactmat.2019.12.003.

[106] A. Lo Giudice, V. Ronsivalle, L. Rustico, K. Aboulazm, G. Isola, and G. Palazzo, “Evaluation of the accuracy of orthodontic models prototyped with entry-level LCD-based 3D printers: a study using surface-based superimposition and deviation analysis,” *Clin Oral Investig*, vol. 26, no. 1, pp. 303–312, Jan. 2022, doi: 10.1007/s00784-021-03999-1.

[107] T. Han, S. Kundu, A. Nag, and Y. Xu, “3D printed sensors for biomedical applications: A review,” *Sensors (Switzerland)*, vol. 19, no. 7. MDPI AG, Apr. 01, 2019. doi: 10.3390/s19071706.

[108] A. Unkovskiy, F. Schmidt, F. Beuer, P. Li, S. Spintzyk, and P. K. Fernandez, “Stereolithography vs. Direct light processing for rapid manufacturing of complete denture bases: An in vitro accuracy analysis,” *J Clin Med*, vol. 10, no. 5, pp. 1–14, Mar. 2021, doi: 10.3390/jcm10051070.

[109] M. Mao *et al.*, “The emerging frontiers and applications of high-resolution 3D printing,” *Micromachines*, vol. 8, no. 4. MDPI AG, Apr. 01, 2017. doi: 10.3390/mi8040113.

[110] W. Li, L. S. Mille, J. A. Robledo, T. Uribe, V. Huerta, and Y. S. Zhang, “Recent Advances in Formulating and Processing Biomaterial Inks for Vat Polymerization-Based 3D Printing,” *Advanced Healthcare Materials*, vol. 9, no. 15. Wiley-VCH Verlag, Aug. 01, 2020. doi: 10.1002/adhm.202000156.

[111] N. S. Allen, “Photoinitiators for UV and visible curing of coatings" mechanisms and properties,” 1996.

[112] K. O’ Driscoll, “Free Radical Polymerization Kinetic,” 1981.

[113] M. B. A. Tamez and I. Taha, “A review of additive manufacturing technologies and markets for thermosetting resins and their potential for carbon fiber integration,” *Additive Manufacturing*, vol. 37. Elsevier B.V., Jan. 01, 2021. doi: 10.1016/j.addma.2020.101748.

[114] D. Karalekas and A. Aggelopoulos, “Study of shrinkage strains in a stereolithography cured acrylic photopolymer resin,” *J Mater Process Technol*, vol. 136, no. 1–3, pp. 146–150, May 2003, doi: 10.1016/S0924-0136(03)00028-1.

[115] Ew. Andrzejewska, “Photoinitiators in Ionic Liquids,” in *Photopolymerisation Initiating Systems*, Royal Society of Chemistry, 2018, pp. 287–296.

[116] C. S. Sheppard and V. R. Kamath, “The Selection and Use of Free Radical Initiators.”

[117] “Photoinitiators and Photopolymerization.”

[118] M. Alsaadi *et al.*, “Liquid-Based 4D Printing of Shape Memory Nanocomposites: A Review,” *Journal of Manufacturing and Materials Processing*, vol. 7, no. 1. MDPI, Feb. 01, 2023. doi: 10.3390/jmmp7010035.

[119] A. Vyas, V. Garg, S. B. Ghosh, and S. Bandyopadhyay-Ghosh, “Photopolymerizable resin-based 3D printed biomedical composites: Factors affecting resin viscosity,” *Mater Today Proc*, vol. 62, pp. 1435–1439, Jan. 2022, doi: 10.1016/j.matpr.2022.01.172.

[120] R. G. Buchheit, “Corrosion Resistant Coatings and Paints,” in *Handbook of Environmental Degradation of Materials: Second Edition*, Elsevier Inc., 2012, pp. 539–568. doi: 10.1016/B978-1-4377-3455-3.00018-3.

[121] Y. Wang, C. Li, X. Tuo, Y. Gong, and J. Guo, “Polyethylene glycol modified epoxy acrylate UV curable 3D printing materials,” *J Appl Polym Sci*, vol. 138, no. 13, Apr. 2021, doi: 10.1002/app.50102.

[122] S. Li, D. Sun, A. Li, and Y. Cui, “Study on curing shrinkage and mechanism of DHOM-modified epoxy-acrylate-based UV-curing 3D printing materials,” *J Appl Polym Sci*, vol. 138, no. 7, Feb. 2021, doi: 10.1002/app.49859.

[123] C. Decker and A. D. Jenkins, “Kinetic Approach of 02 Inhibition in Ultraviolet-and Laser-Induced Polymerizations,” 1985. [Online]. Available: https://pubs.acs.org/sharingguidelines

[124] S. C. Ligon, B. Husár, H. Wutzel, R. Holman, and R. Liska, “Strategies to reduce oxygen inhibition in photoinduced polymerization,” *Chemical Reviews*, vol. 114, no. 1. pp. 577–589, Jan. 08, 2014. doi: 10.1021/cr3005197.

[125] F. A. Rueggeberg and D. H. Margeson, “The Effect of Oxygen Inhibition on an Unfilled/Filled Composite System,” *J Dent Res*, vol. 69, no. 10, pp. 1652–1658, 1990, doi: 10.1177/00220345900690100501.

[126] M. Khalina, M. H. Beheshty, and A. Salimi, “The effect of reactive diluent on mechanical properties and microstructure of epoxy resins,” *Polymer Bulletin*, vol. 76, no. 8, pp. 3905–3927, Aug. 2019, doi: 10.1007/s00289-018-2577-6.

[127] A. R. Jagtap and A. More, “Developments in reactive diluents: a review,” *Polymer Bulletin*, vol. 79, no. 8. Springer Science and Business Media Deutschland GmbH, pp. 5667–5708, Aug. 01, 2022. doi: 10.1007/s00289-021-03808-5.

[128] P. Boisaubert, N. Kébir, A. S. Schuller, and F. Burel, “Photo-crosslinked coatings from an acrylate terminated non-isocyanate polyurethane (NIPU) and reactive diluent,” *Eur Polym J*, vol. 138, Sep. 2020, doi: 10.1016/j.eurpolymj.2020.109961.

[129] A. Bagheri and J. Jin, “Photopolymerization in 3D Printing,” *ACS Applied Polymer Materials*, vol. 1, no. 4. American Chemical Society, pp. 593–611, Apr. 12, 2019. doi: 10.1021/acsapm.8b00165.

[130] J. V Crivello and J. L. Lee, “Photosensitized Cationic Polymerizations Using Dialkylphenacylsulfonium and Dialkyl(4-hydroxyphenyl)sulfonium Salt Photoinitiators.” [Online]. Available: https://pubs.acs.org/sharingguidelines

[131] M. A. Lago, A. Rodríguez-Bernaldo de Quirós, R. Sendón, J. Bustos, M. T. Nieto, and P. Paseiro, “Photoinitiators: a food safety review,” *Food Addit Contam Part A Chem Anal Control Expo Risk Assess*, vol. 32, no. 5, pp. 779–798, May 2015, doi: 10.1080/19440049.2015.1014866.

[132] M. S. Thompson, “Current status and future roles of additives in 3D printing—A perspective,” *Journal of Vinyl and Additive Technology*, vol. 28, no. 1, pp. 3–16, Feb. 2022, doi: 10.1002/vnl.21887.

[133] M. Gastaldi *et al.*, “Functional Dyes in Polymeric 3D Printing: Applications and Perspectives,” *ACS Materials Letters*, vol. 3, no. 1. American Chemical Society, pp. 1–17, Jan. 04, 2021. doi: 10.1021/acsmaterialslett.0c00455.

[134] A. Nanni and M. Messori, “Effect of the wine lees wastes as cost-advantage and natural fillers on the thermal and mechanical properties of poly(3-hydroxybutyrate-co-hydroxyhexanoate) (PHBH) and poly(3-hydroxybutyrate-co-hydroxyvalerate) (PHBV),” *J Appl Polym Sci*, vol. 137, no. 28, Jul. 2020, doi: 10.1002/app.48869.

[135] A. Giubilini, C. Sciancalepore, M. Messori, and F. Bondioli, “Valorization of oat hull fiber from agri-food industrial waste as filler for poly(3-hydroxybutyrate-co-3-hydroxyhexanoate),” *J Mater Cycles Waste Manag*, vol. 23, no. 1, pp. 402–408, Jan. 2021, doi: 10.1007/s10163-020-01104-4.

[136] T. A. Osswald and G. Menges, “Thermal Properties of Polymers,” in *Material Science of Polymers for Engineers*, 3rd ed.Munich: Carl Hanser Verlag, 2012, pp. 99–105.

[137] R. E. Zacharia and S. L. Simon, “Dynamic and Isothermal Thermogravimetric Analysis of a Polycyanurate Thermosetting System.”

[138] N. Al-Mutairi, “Some Methods for Measurements of Polymer Degradation: A Review,” 2021. [Online]. Available: https://www.researchgate.net/publication/357027920

[139] M. Nasrollahzadeh, M. Atarod, M. Sajjadi, S. M. Sajadi, and Z. Issaabadi, “Plant-Mediated Green Synthesis of Nanostructures: Mechanisms, Characterization, and Applications,” in *Interface Science and Technology*, Elsevier B.V., 2019, pp. 199–322. doi: 10.1016/B978-0-12-813586-0.00006-7.

[140] K. Kodre, S. Attarde, P. Yendhe, R. Patil, and V. Barge, “Research and Reviews: Journal of Pharmaceutical Analysis Differential Scanning Calorimetry: A Review.”

[141] “Standard Test Methods for Determination of Gel Content and Swell Ratio of Crosslinked Ethylene Plastics 1”, doi: 10.1520/D2765-16.

[142] A. Nimpaiboon, S. Amnuaypornsri, and J. Sakdapipanich, “Influence of gel content on the physical properties of unfilled and carbon black filled natural rubber vulcanizates,” *Polym Test*, vol. 32, no. 6, pp. 1135–1144, 2013, doi: 10.1016/j.polymertesting.2013.07.003.

[143] W. D. Callister and D. G. Rethwisch, “Characteristics, Applications, and Processing of Polymers,” in *Materials Science and Engineering: an introduction*, Wiley, 2018, pp. 512–515.

[144] S. K. M. Haque *et al.*, “Application and suitability of polymeric materials as insulators in electrical equipment,” *Energies*, vol. 14, no. 10. MDPI AG, May 02, 2021. doi: 10.3390/en14102758.

[145] M. Qi, Y. J. Xu, W. H. Rao, X. Luo, L. Chen, and Y. Z. Wang, “Epoxidized soybean oil cured with tannic acid for fully bio-based epoxy resin,” *RSC Adv*, vol. 8, no. 47, pp. 26948–26958, 2018, doi: 10.1039/c8ra03874k.

[146] J. R. Fried, “ Viscoelasticity and Rubber Elasticity ,” in *Polymer Science and Technology*, Pearson Education Limited, 2014, pp. 208–221.

[147] A. Dotan, “Biobased Thermosets,” in *Handbook of Thermoset Plastics*, Elsevier Inc., 2014, pp. 577–622. doi: 10.1016/B978-1-4557-3107-7.00015-4.

[148] F. Habib and M. Bajpai, “Chemistry SYNTHESIS AND CHARACTERIZATION OF ACRYLATED EPOXIDIZED SOYBEAN OIL FOR UV CURED COATINGS,” 2011. [Online]. Available: http://ena.lp.edu.ua

[149] Y. Xia and R. C. Larock, “Vegetable oil-based polymeric materials: Synthesis, properties, and applications,” *Green Chemistry*, vol. 12, no. 11, pp. 1893–1909, Nov. 2010, doi: 10.1039/c0gc00264j.

[150] M. Lebedevaite, J. Ostrauskaite, E. Skliutas, and M. Malinauskas, “Photoinitiator free resins composed of plant-derived monomers for the optical μ-3D printing of thermosets,” *Polymers (Basel)*, vol. 11, no. 1, Jan. 2019, doi: 10.3390/polym11010116.

[151] O. Llorente, A. Barquero, M. Paulis, and J. R. Leiza, “Challenges to incorporate high contents of bio-based isobornyl methacrylate (IBOMA) into waterborne coatings,” *Prog Org Coat*, vol. 172, Nov. 2022, doi: 10.1016/j.porgcoat.2022.107137.

[152] A. R. M. Martins, I. D. Silva, L. Machado-Santos, R. P. Vitti, M. A. C. Sinhoreti, and W. C. Brandt, “Isobornyl methacrylate as diluent co-monomer on physical-mechanical properties of dental resin composites,” *J Appl Polym Sci*, vol. 138, no. 21, Jun. 2021, doi: 10.1002/app.50498.

[153] F. Hajiali, A. Métafiot, L. Benitez-Ek, L. Alloune, and M. Marić, “Nitroxide mediated polymerization of sustainably sourced isobornyl methacrylate and tridecyl methacrylate with acrylonitrile co-monomer,” *J Polym Sci A Polym Chem*, vol. 56, no. 21, pp. 2422–2436, Nov. 2018, doi: 10.1002/pola.29216.

[154] H. Kim, S. Lee, and W. Won, “Economical process for the co-production of renewable polymers and value-added chemicals from lignocellulosic biomass,” *J Clean Prod*, vol. 276, Dec. 2020, doi: 10.1016/j.jclepro.2020.124237.

[155] M. Regalado Galvão, S. Godeiro Fernandes Rabelo Caldas, V. Salvador Bagnato, A. Nara de Souza Rastelli, and M. Ferrarezi de Andrade, “Evaluation of degree of conversion and hardness of dental composites photo-activated with different light guide tips.”

[156] I. D. Sideridou, M. M. Karabela, and E. C. Vouvoudi, “Physical properties of current dental nanohybrid and nanofill light-cured resin composites,” *Dental Materials*, vol. 27, no. 6, pp. 598–607, Jun. 2011, doi: 10.1016/j.dental.2011.02.015.

[157] J. L. Ferracane, “Resin-based composite performance: Are there some things we can’t predict?,” *Dental Materials*, vol. 29, no. 1, pp. 51–58, Jan. 2013, doi: 10.1016/j.dental.2012.06.013.

[158] W. Rutsch, K. Dietliker, D. Leppard, M. G. Rist C Photoinitiators Kiihler, and L. Misevb, “Recent developments in,” 1996.

[159] A. Kowalska, J. Sokolowski, and K. Bociong, “polymers The Photoinitiators Used in Resin Based Dental Composite-A Review and Future Perspectives,” 2021, doi: 10.3390/polym130.